Studies on Pyrolytic and Hydrothermal Conversion of Biomass and Lignite

劉, 天龍

Studies on Pyrolytic and Hydrothermal Conversion of Biomass and Lignite

By

Liu Tianlong

Department of Applied Science for Electronic and Materials

Interdisciplinary Graduate School of Engineering Sciences

Kyushu University

2020

ABSTRACT

The transition to a circular, bio-based economy is essential to reduce our current dependency on fossil resources and global environmental concerns. During the past decades, a growing scientific community is eagerly seeking for effective valorization approaches for lignocellulosic biomass, the world's most abundant and sustainable source of carbon and energy, with the targets of displacing petroleum in the production of commodity chemicals and liquid transportation fuels. While many different reactions and processes have been proposed in the literature, efficient and selective conversion of biomass are hampered to gain a firm foothold due to the complex and rigid structure. This thesis is thus organized to design and develop combined pyrolytic and hydrothermal pathways for efficient utilization of entire portion of biomass. First, most modern biorefineries are based on fractionation of biomass into individual constituents (cellulose, hemicellulose and lignin) using hydrothermal pretreatments with water, acidic water (for acid-catalyzed Saccharization) or alkaline water (for extracting lignin) prior to applying further conversion process. Tailoring the optimal carbohydrate valorization have produced a large quantity of lignin as a byproduct. Here, we proposed a particular type of pyrolysis for a *Klason* lignin, which recycles heavier portion of bio-oil (HO) entirely to pyrolysis by employing the parent lignin for their capture/recycling without any chemicals and catalysts. During nine sequential runs performed in a fix-bed pyrolyzer, HO was converted to char, water and lighter oil (LO) with once-through conversion of around 47%. It has been demonstrated that the proposed pyrolysis enables selective production of phenolic monomers (*e.g.*, catechols and guaiacols) with 100% HO recycling ratio. The recycled HO underwent not only self-pyrolysis/carbonization but also co-pyrolysis/carbonization with the lignin. Second, the processes of treating biomass or the constituents often produce aqueous by-product streams, the composition of which is more or less similar, containing a complex mixture of acids, ketones, phenols and other organic compounds. High total organic carbon (TOC) of those streams implies a chemical and energy loss of biomass and on the other hand, causes troubles before discharging to the environment. Catalytic hydrothermal gasification (CHTG) is a novel technology, well-suitable for processing highly wet feedstocks. We, in this study, developed a sequence of leaching and CHTG for treatment of an aqueous phase of pyrolytic bio-oil, enabling the reduction in TOC and energy recovery in the form of CH_4 and H_2. The

aqueous phase was subjected to leaching char and then CHTG with a ruthenium/activated-charcoal catalyst (4.5 wt% loading) in a continuous flow reactor at 350°C, 20 MPa. A major portion of alkali and alkaline earth metal species (AAEMs) was leached from the char following a pseudo-second-order model while some non-acidic compounds such as ketones and alcohols had negative effects on the leaching. The uptake of organic compounds by char, in particular, those with a larger molecular mass and the concentration of AAEMs in the aqueous phase contributed to maintenance of high catalytic activity for 280 min by suppressing coke formation and also metal particle growth during CHTG. The cold gasification efficiency achieves as high as 104%. Third, according to the BP static review of world energy, coal continues as an important energy resource in the near future due to the abundant reserves worldwide. We, for the first time, demonstrated a sequence of degradation, dissolution and CHTG of lignite in alkaline water, aiming at sufficiently high dissolution rates of the lignite and then low-temperature conversion into CH_4-rich gases. Sequential hydrothermal treatment and oxidation were successfully developed towards solubilizing a 95% portion of Victorian lignite in an aqueous solution of NaOH. The solubilized lignite, with a number-average molecular mass no greater than 770, was converted by CHTG in a continuous flow reactor at 350°C, 20 MPa, employing a ruthenium/activated-charcoal catalyst (16 wt% loading). The initial carbon conversion to gas was as high as 98% while slowly decreased to 83% in 10 h. The heavier portion (molecular mass > 1,000) was responsible for the coke formation and accumulation that caused the catalyst deactivation.

CHAPTER I

GENERAL INTRODUCTION

1.1. Current energy scenario

This century has seen a rapid growth of global energy consumption with the increasingly faster pace of population, urbanization and industrialization. As of 2018, the fuel consumption reached 13865 million tons of oil equivalent, increased by 48% with an annual rate of 2.7% (**Figure 1.1**). [1] The primary energy resources include coal, oil, natural gas, nuclear energy and renewables. According to the BP statistical review of world energy, currently 85% of world's primary energy comes from fossil fuels which have detrimental environmental impacts and contribute to greenhouse gas emission, resulting in adverse climate change. It is estimated that until 2030, fossil fuels will dominate near 90% of the total energy consumption if no breakthrough innovation would like to occur. Energy security is becoming a serious issue as fossil fuels are non-renewable and will deplete eventually in near future. This has boosted the efforts for developing advanced technologies and finding alternative, clean and renewable resources of energy. Natural sources such as solar, wind, biomass and hydroelectricity are now attracting considerable attention as these are abundant and have the potential to fulfill the energy gaps with zero emission of greenhouse gases. The International Energy Agency forecasted that the renewable electricity generation will increase from the current level of 6800 TWh in 2018 to 26065 TWh by 2040, which represents two-thirds of global electricity generation. [2]

Among renewable resources, biomass is the only sustainable source of energy and carbon available on earth and is a promising substitute for petroleum-based chemicals, fuels and materials in a wide array of applications. It currently contributes to 10% of the world's primary energy demand and is regarded as the fourth largest source after coal, oil, and natural gas. One fundamental feature of biomass is the closed cycle of carbon. This means that CO_2 generated in the transformation or/and burning of biomass is recaptured by plants *via* photosynthesis during their growth. On the other hand, the production of liquid transportation fuels from biomass would reduce our reliance on fossil fuels. At present, first-generation biofuels (*i.e.*, starch-derived biodiesel and ethanol) produced from food crops (*e.g.*, corn, cane sugar and vegetable oils) have been successfully implemented in the transportation sector and share 3% of transportation energy consumption. The biofuel production increased 10 billion liters in 2018 to reach a record of 154 billion liters, and 3% annual gain is expected over the next five years. [3] However, consumption of edible biomass yields competition with food for land use. The so-called food-*versus*-fuel debate

emerged in many countries as a response to the sharp increase in food prices during 2007 and 2008. These issues have driven to process non-edible biomass (*i.e.*, lignocellulose) for the production of 'second-generation fuels' without affecting food supplies.

Lignocellulosic biomass, which composes cellulose, hemicellulose and lignin, is abundant in the form of agricultural residues (*e.g.*, corn stover and wheat straw), waste streams (*e.g.*, pulp and paper mill and food waste) and aquatic plant (*e.g.*, algae and seaweeds), etc. [4] Bioenergy can be produced from biomass *via* biochemical/biological and thermochemical processes. The later shows higher efficiencies than the former that usually takes several days, weeks or even longer, and the superior ability to destroy most of the organic compounds. For example, lignin materials are typically non-fermentable and thus cannot be completely decomposed via biological approaches, whereas they are decomposable *via* thermochemical approaches. The following part will provide an overview of thermochemical conversion.

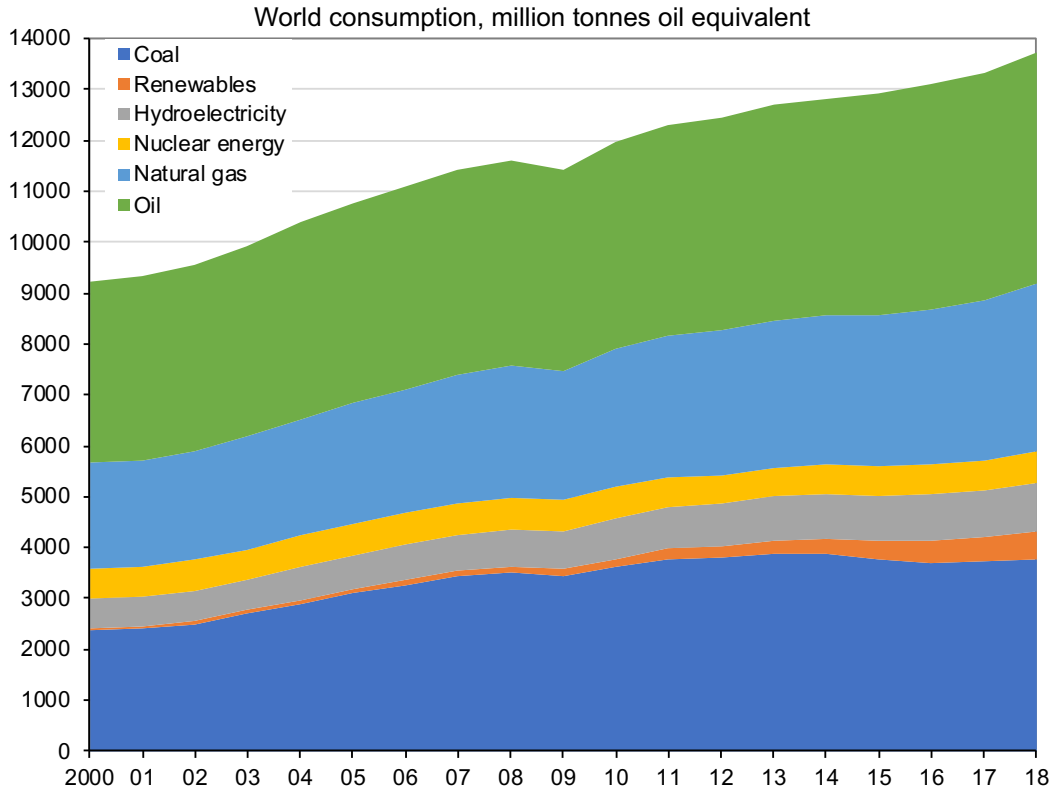

Figure 1.1. *World primary energy consumption in years 2000–2018. Adapted from the BP Statistical Review of World Energy, accessed 2019, 68th edition.*

1.2. Thermochemical conversion

Thermochemical conversion is a high-temperature chemical process that breaks apart the bonds of organic matter and reforms these intermediates into solid, liquid or gaseous forms

for the production of electric power, heat, chemicals and fuels. The benefits of the process, as is the case for biomass, are advantageous over biochemical ones in terms of reaction time, flexibility and capability of handling a variety of carbonaceous resources and blends. Direct combustion, gasification, pyrolysis and liquefaction are the most relevant technologies that have witnessed significant developments over the past decades through fundamental research and pilot-scale demonstrations. A flow diagram of the branches of thermochemical conversion is presented in **Figure 1.2**.

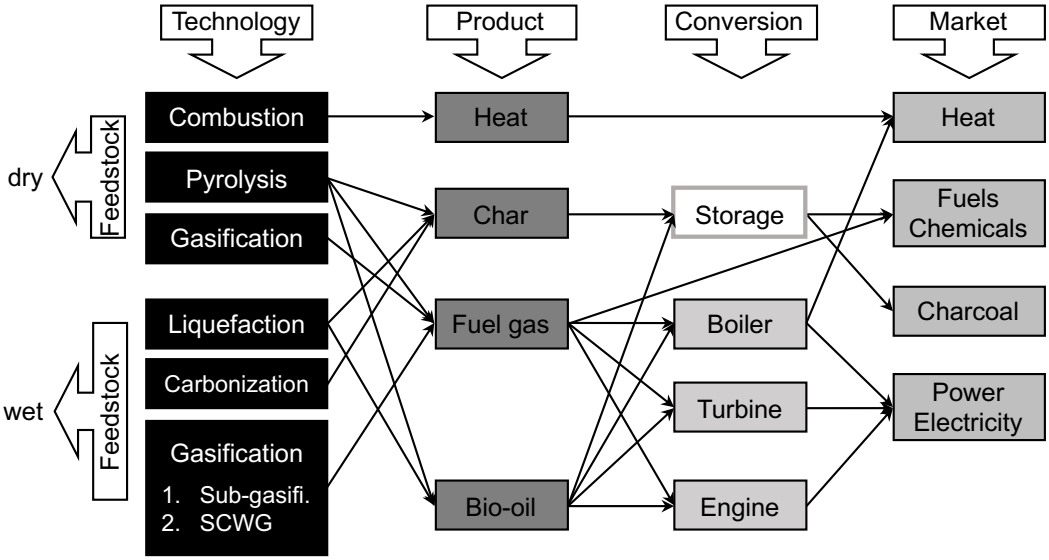

Figure 1.2. *Schematic diagram of thermochemical conversion for dry and wet feedstocks.*

Combustion is a well-established technology with applications in most industrialized and developing countries. The process takes place in excess air, which is an exothermic reaction between oxygen and hydrocarbon contained in solid fuels. It produces CO_2 and steam as the ultimate products with overall energy efficiency at 20–40% and heat transfer loss as high as 90%. The technology is widely used for treating forestry, agricultural and industrial wastes while technical problems remain challenges concerning aerosol emissions, deposit formation, corrosion and ash utilization/disposal.

Gasification is one of the most promising options to convert carbonaceous solids into gases, such as H_2, CO and CH_4, for power generation and chemical production. Many state-of-art technologies of the gasification, in particular, that of coal, are based on partial combustion at temperatures well above 1000°C and generally carried out under oxygen-deficient conditions in the presence of a gasifying carrier, such as air, oxygen, steam or

carbon dioxide. The principal reactions of gasification are endothermic, consisting of three major stages as below.

(1) pyrolysis (endothermic stage): feedstock → fuel gas + char

(2) oxidation (exothermic stage): fuel gas + oxygen → flue gas + heat

(3) reduction (endothermic stage): fuel gas + char + heat → syngas

The final step (so-called reduction stage) is slowest and often governs overall gasification reaction rate. Under the reducing atmosphere, a number of high-temperature chemical reactions occur, transforming sensible heat of the fuel gas and char into chemical energy of the syngas. According to Hayashi et al. [5] the significance of gasification is its versatility of accommodating a variety of carbon resources into a simplified set of producer gas as above, *i.e.*, syngas. The gasification integrates thermal and chemical energies into chemical energy of syngas, recuperating the former energy in terms of exergy rate. Current gasification relies greatly on the partial oxidation that grants necessary energy for occurrence of the above reactions but at its expense, causes a significant loss of chemical energy of the feedstock. van der Meijden et al. [6] evaluated gross cold gas efficiency, which is defined by the heating value of cold producer gas per that of the feedstock, as 53–71% on a higher heating value basis for CH_4 production from woody biomass by conventional gasification combined with methanation of syngas. The energy loss is mainly attributed to exothermic reactions that are associated with the consumption of oxygen. To improve the energy efficiency of the gasification, it is, therefore, needed to reduce this consumption and instead, increase that of steam or CO_2, which causes endothermic reactions.

Pyrolysis is a fundamental thermochemical process that represents the preliminary step of both combustion and gasification of solid fuels while occurring in the absence of oxygen and at relatively low temperatures (500–800°C). Slow pyrolysis, also termed carbonization, produces charcoal as the target product while always accompanied by liquid and gas products although these are rarely recovered. Such thermal decomposition proceeds under moderate temperatures (~ 400°C) and a very low heating rate with long vapor residence time that allows for secondary polymerization to maximize the solid yield. On the other hand, fast pyrolysis involves high heating rates (10–200 °C/s) and short residence time (typically < 2 s). The main product, well-known as pyrolysis oil, is obtained in yields of up to 75 wt% on a dry-feed basis together with char and gas by-products that can be used within the process for heat supply so that there are no waste streams other than flue gas and ash. The pyrolysis

oil gives the flexibility of storage and transportation over a long distance, and has been successfully tested in boilers, gas turbines, and diesel engines for heat and power applications or upgraded *via* a catalytic process into useful hydrocarbon fuels, albeit at a presently unacceptable energetic and financial cost. Typical drawbacks of the oil, as summarized in the literature, [7–9] are high viscosity, low heating value, incomplete volatility and chemical instability. More research is still needed in the field of fast pyrolysis and pyrolysis oil upgrading to address those issues and develop economic applications.

A major disadvantage, common to those thermochemical processes, is the necessity of feeding dry solid with less than 10 wt% moisture. A high moisture content is no longer favored for the process feasibility because of energy penalty arisen from enormous latent heat of water. Unfortunately, wet biomass and coal containing initial moisture frequently up to 80 wt% represent a very large portion of the available resources. Hydrothermal conversion, in other words, a process in hot and pressurized water, opens up opportunities to convert wet solid or even organic wastewaters with a natural water content. This is a novel thermochemical process based on the idea of turning the water included in feedstocks into an advantage rather than a disadvantage as water is needed in the process as a reactant and reaction medium.

1.3. Hydrothermal conversion

Hydrothermal conversion is broadly defined as chemical and physical transformations carried out in high-temperature (200–600°C) and high-pressure (5–40 MPa) liquid or sub/supercritical water. One of the most important features is that this conversion requires no energy-intensive dewatering and drying steps, as in the case of pyrolysis. On the other hand, hot-compressed water near its thermodynamic critical point (374°C, 22.1 MPa) behaves very differently from either extreme state of the gas phase or the liquid phase in some respects pertained to the ionic product, density, dielectric constant and viscosity. Due to these unique properties, other advantages have been reported: reduced interphase mass transfer resistance, minimized char/coke formation, enhanced reaction rates and efficient separations, etc. [4,10] As a result, hydrothermal processing of wet or ‘green’ biomass has gained prominence in recent decades. A review in *Science* [11] suggested that supercritical fluids are well-suited in the processing of renewable bioresources. Tekin et al. [12] reported that hydrothermal process is more efficient and environment-friendly than many other treatments, which can be deemed as a first step for the utilization of lignocellulose. Peterson

et al. [13] criticized that hydrothermal technologies offer many potential benefits over conventional ones of converting biomass to useful fuels although these technologies have not been widely commercialized today. Depending on the reaction temperature and pressure, hydrothermal processes can be classified into (1) hydrothermal carbonization (180–250°C) for hydrochar purpose (2) hydrothermal liquefaction (about 200–370°C with pressures of 4–22 MPa) for oil production and (3) hydrothermal gasification (near-critical temperatures up to about 500°C) to produce H_2/CH_4-rich gas. The pressure-temperature phase diagram of water is drawn in **Figure 1.3** to highlight the hydrothermal conversion options under different condition ranges.

Hydrothermal carbonization is a combination of dehydration and decarboxylation, which lowers both the oxygen and hydrogen contents of biomass and achieves a higher calorific value. This is generally realized by applying relatively low temperatures in a suspension of biomass and water at saturated pressures for serval hours. With this conversion, a coal-like solid fraction (*i.e.*, hydrochar) with well-defined properties is obtained. A comprehensive review of the carbonization of biomass on chemical mechanisms is reported elsewhere. [14] Currently, a wide variety of biomass has been carbonized hydrothermally, such as cellulose, lignin, microalgae, sewage sludge and waste streams. [15–17] Lignite and sub-bituminous coal have ever been reported to be successfully carbonized, nonetheless, with higher temperatures. [18,19] The produced hydrochar containing a large number of attractive function groups is amendable to environmental and energy-related applications such as a precursor of carbonaceous functional materials, an adsorbent for harmful pollutants and a soil amendment.

As process parameters are further intensified from the hydrothermal carbonization, liquefaction takes place. The process, also known as hydrous pyrolysis, was first convinced as a technology for coal conversion into liquids but in recent years has shown a dramatic increase in the research works for biomass, especially algae. Typical operating conditions range 200–370°C and 4–22 MPa, often with catalyst present and sometimes with reducing gases such as H_2. The lower operating temperature, higher energy efficiency and less char formation compared to pyrolysis add to the attractiveness of this technology. Although the mechanism of liquefaction has not been well elucidated, it is widely accepted that the pathway comprises three major steps: depolymerization of biomass, decomposition of biomass monomers by cleavage, dehydration, decarboxylation and deoxygenation, and then

rearrangement of reactive fragments. [20] Products from these steps are an oily phase namely biocrude, an aqueous phase of light organics and a gas phase rich in CO_2, of which the distributions and properties are controlled by the type of biomass, processing conditions and catalyst. [21] The major product, biocrude, as comparison to its counterpart in fast pyrolysis, has less oxygen (10–20%), higher heating value (30–35 MJ kg^{-1}) and lower moisture content as a result of the relatively lower polarity. [4] Furthermore, most of recent studies reported a beneficial effect of using catalysts on the yield and properties of biocrude. A variety of common catalysts have been tested such as Na_2CO_3, Pd/C, Pt/C, Ru/C, Ni/SiO_2–Al_2O_3 and CoMo/γ–Al_2O_3. [22] On the other hand, undesirable properties also exist in biocrude as high viscosity, corrosiveness and poor stability, which render it directly unusable as liquid fuels. The biocrude can be further upgraded into useful biofuels by subsequent hydrotreatment such as hydrodeoxygenation. Duan and Savage [23–25] studied the reforming of a crude algal biocrude over Pt, Pd or Mo supported carbon in supercritical water at 400°C and pressurized H_2, and demonstrated a reduction in S, N and O contents as well as an improvement in higher heating value of the bio-crude by about 10%.

Hydrothermal oxidation is, in fact, a combustion in water, where the miscibility with an oxidant allows for organic compounds to be easily oxidized and degraded. It can be classified into wet oxidation, which is carried out under subcritical conditions, and supercritical water oxidation, that under supercritical conditions. Commonly used oxidants are air and molecular oxygen, including also ozone and hydrogen peroxide. Wet oxidation has been used as an economical and environmental-friendly process to dispose of wastewaters, especially sewage sludge or refractory organic pollutants in toxic industrial wastewater. [26,27] Under elevated temperatures(150–320°C) and pressures (5–20 MPa) using the least expensive air or pure oxygen as the oxidant, the organics are either partially oxidized into biodegradable intermediates or mineralized to carbon dioxide, water and innocuous end products. On the other hand, the wet oxidation has been proposed to produce valuable chemicals such as small molecule carboxylic acids from lignin and low-rank coal, which essentially represents a degradative process. The studies mainly include the flowing three: hydrogen peroxide oxidation, [28–30] oxidative acid oxidation, [31] and oxygen oxidation. [32–34] Of these attempts, oxidation by oxygen in an alkaline water is most promising, typically at 200–260°C under a pressure of 4.0–7.5 MPa. Carbon conversion to water-soluble carboxylic acids reached 0.36 (base on carbon) under the operating conditions. [34] Supercritical water oxidation was developed since some compounds (*e.g.*, acetic acid or

methanol) were not efficiently treated using wet oxidation. The technology is particularly suited to destruction of such molecules and promotes fast reaction rates along with rapid and complete oxidation. [35,36] Unlike conventional thermal incineration, the formation of additional pollutants, such as SO_x or NO_x gases, is minimized by wet oxidation or supercritical water oxidation.

When hydrothermal reactions occur without oxidant but using higher temperatures above 350°C, the process is referred to as hydrothermal gasification. The objective of the process, rather than heat or liquid oil, is a synthetic fuel gas rich in CH_4 or H_2 depending on the operating temperature ranges. An overview of this novel gasification will be more extensively presented in the following paragraphs.

1.4. Hydrothermal gasification

The pioneering works of Modell, appearing in the 1970s, were the first to describe hydrothermal gasification. [37–39] Those studies examined the feasibility of such a process to decompose biomass into useful gaseous products in supercritical water. One advantage they reported was the direct and rapid route that was mildly exothermic and inhibited char formation to yield gases including H_2, CO, CO_2, CH_4 and light hydrocarbons. Soon after, substantial efforts were devoted to this novel gasification. Over the last fifty years, studies of this field have fallen into the general categories based on desired products: subcritical catalytic gasification to mainly CH_4 and supercritical water gasification (SCWG) with or without a catalyst to mainly H_2. Comprehensive reviews of catalytic and noncatalytic hydrothermal gasification are available. [13,40–43]

1.4.1. The reaction medium

The basic idea of hydrothermal gasification originates from the unique properties of highly compressed water as a solvent and also a reaction partner. **Figure 1.3** illustrates the physicochemical properties of water as a function of temperature. [44] Under a constant pressure of 25 MPa, water density decreases as temperature increases and the most drastic decrease occurs around the critical temperature (274°C, 22 MPa). As the density becomes lower, water molecules separate further from each other, and hydrogen bonds are broken. Consequently, the dielectric constant, that is, the polarity of water, decreases substantially.

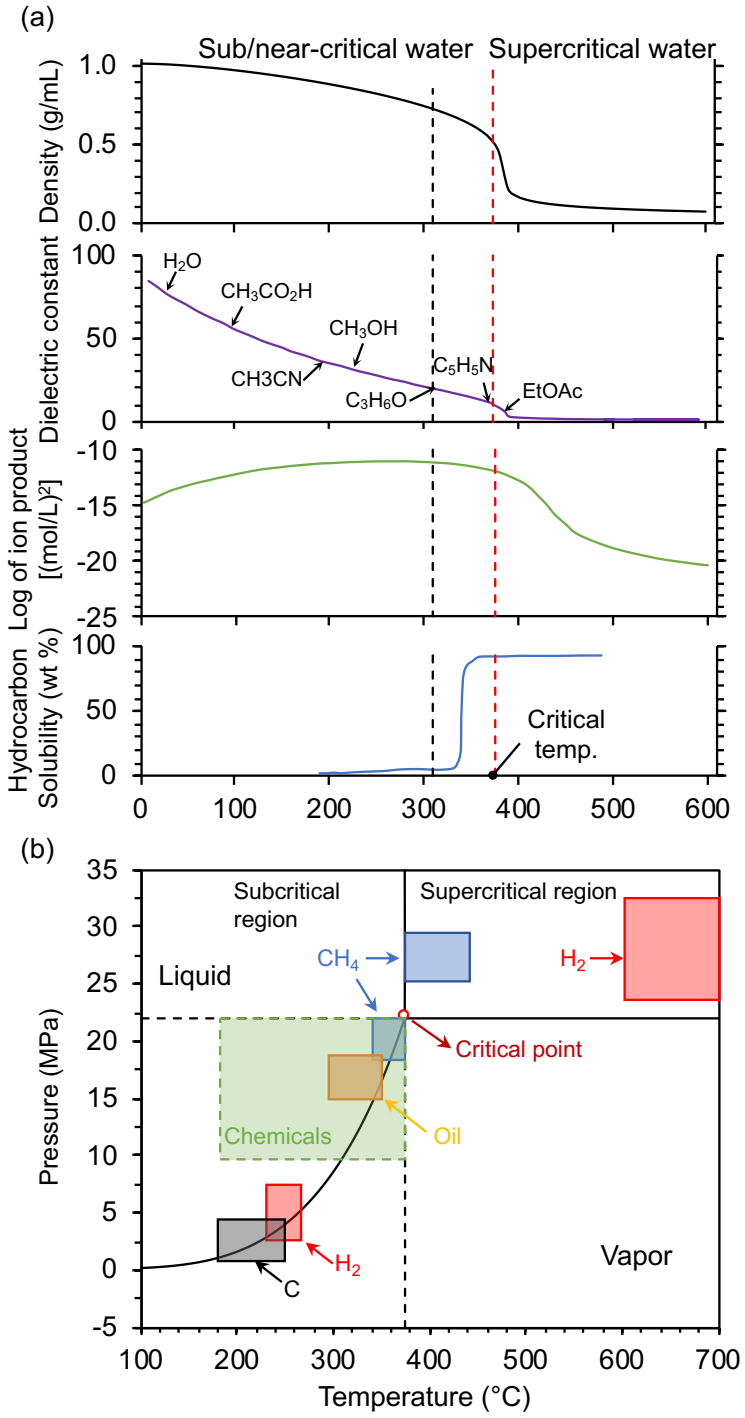

Figure 1.3. *(a) Physical properties of water at 25 MPa and (b) pressure-temperature regimes for hydrothermal conversion options.*

A lower dielectric constant reflects a higher solubility of organic compounds but a lower solubility of inorganics. The subcritical water at 220 and 300°C has a similar dielectric constant with methanol and acetone (under normal conditions), respectively. In the supercritical region, the dielectric constant decreases to a very low level and water performs

similarly to nonpolar organic compound that becomes completely miscible with many organic compounds and gases. This provides a single-phase environment for homogenous reactions that would otherwise take place in a multiphase system under conventional conditions. The advantage of a single-phase reaction medium is the eliminated interphase mass transfer resistance that aggravates reaction rates. It is as well possible to conduct convenient post-reaction separation of water and products by simply changing the operating temperature and pressure.

On the other hand, the ionic product, also termed self-ionization product, is the product of the concentrations of H_3O^+ and OH^- of water, K_w = [H_3O^+][OH^-], in a unit of $(mol/L)^2$. As depicted in **Figure 1.3**, the K_w rises from 10^{-14} at ambient temperature to 10^{-11} at about 300°C and then decreases by eight orders of magnitude or more above 500°C. Under subcritical conditions, water acts as not only a reaction medium but also acid/base catalysts because of the high concentrations of H_3O^+ and OH^-. Some acid- and base-catalyzed ionic reactions, such as hydrolysis, are thus reinforced. Whereas, free-radical reaction mechanism dominates over that of ionic reactions in supercritical water due to the extremely low self-dissociation of water. Hydroxyl radical, known as the most effective oxidant, is very important in supercritical water oxidation.

1.4.2. Supercritical water gasification

High-temperature SCWG is carried out at temperatures above 600°C and a H_2-rich gas can be produced with near-complete conversion rates. Studies of this field have been systematically conducted by means of model compounds such as hemicellulose, cellulose (including its hydrolysis product, glucose and other carbohydrates), lignin (including aromatic rings) and a variety of real biomass resources. The results are not identical but always prove: (i) Temperatures above 600°C are required for thermodynamic reasons to obtain a high H_2 yield, whereas at lower temperatures, CH_4 is the preferred product. (ii) In contrast to the pressure, the reaction temperature has a stronger effect on gas composition and gasification efficiency. (iii) The process can be conducted with or without a catalyst; common catalysts include activated carbon and alkali. Early studies by Antal et al. examined SCWG of glucose and real biomass feedstocks. Noncatalytic gasification of glucose (0.2 M, 600°C, 34.5 MPa, 34 s residence time and tubular flow reactor) showed at least 82% of carbon conversion into gases with no tar or char formation but the gas yields were far from the equilibrium predictions. [45] Their later works with carbon catalysts achieved complete

gasification of concentrated glucose (22 wt%) or real biomass (~15 wt%) into a H_2-rich gas. [46–48] Schmieder et al. [49] and Kruse et al. [50] also demonstrated complete gasification to primarily H_2 in catalytic SCWG of biomass model compounds (glucose, catechol and vanillin glycine) at 600°C and 25 MPa. They reported that the alkali catalysts (KOH and K_2CO_3) promoted the water-gas shift reaction and drastically increased H_2 yield. D'Jesús et al. [51] studied the SCWG of corn starch using a continuous flow reactor and found that the potassium catalyst increased the gas yield from 0.82 to 0.92 (based on carbon) at 700°C and 25 MPa. Gasification of low-rank coal in supercritical water has been recently investigated by several research groups. It was found that noncatalytic process is difficult to achieve a desired gasification efficiency even at 800°C because of the recalcitrant nature of coal. [52] Guo et al. [53,54] employed alkali catalysts including NaOH, K_2CO_3 and $Ca(OH)_2$ that improved the gasification efficiency significantly but the reaction temperature is very high.

At moderate temperatures (below 500°C), active heterogeneous catalysts are necessary to allow an accepted gasification rate. The roles are not only to reduce char formation and promote gasification reactions (activity) but also to steer the product distribution toward a desired one (selectivity). Because the catalysts will not influence the chemical equilibrium composition, increasing the gasification rate with a catalyst is useful only if thermodynamics are favorable. Reviews by Davda et al. [55] and Azadi et al. [56] provide a detailed discussion of catalysts for the production of H_2/CH_4 from biomass. The widely studied ones include supported noble metals such as Ru, Rh Pt (low loadings), supported Ni (high loadings: ~45 wt%) and unsupported noble metal oxides (*e.g.*, RuO_2). If a suitable catalyst is used, it is possible to convert solid lignocellulose completely into gases at temperatures below 500°C, much lower than conventional gas-solid gasification. Yoshida et al. [57] gasified cellulose, lignin and their mixture in an unstirred stainless batch reactor with 60% Ni/SiO_2–Al_2O_3 under supercritical conditions (400°C, 25 MPa, 25 min residence time). The carbon conversion to gas reached a maximum value of 0.90 for cellulose and the mixture of lignin resulted in lower gas yields. Osada et al. [58] gasified organosolv-lignin completely into CH_4-rich gases with supported Ru catalysts at 400°C and a reaction time of 180 min in a batch reactor. TiO_2-supported Ru catalyst was found to be most stable while metal crystal growth, ruthenium leaching, and phase transition occurred in carbon/Al_2O_3-supported catalysts. Yu et al. [59] prepared a Ru/CeO_2–ZrO_2 catalyst for SCWG of a lignite and achieved 86% carbon gasification efficiency at 500°C with a 21-fold enhancement of H_2 yield compared to that in the noncatalytic case.

1.4.3. Subcritical catalytic gasification

While supercritical water has been identified as an important operating medium, later work shows that the subscribe water can also be useful for highly effective gasification with an active catalyst. Since the rate of hydrolysis in subcritical water is slower than that in supercritical water, [60] it is difficult to gasify high-molecular-weight biomass and its constituents such as cellulose and lignin, and therefore, the organics to be gasified should be dissolved in an aqueous medium prior to the catalytic gasification. The gasification at such low temperatures is advantageous because of the low energy input and most importantly, 100% theoretical recovery of chemical energy, resulting from the endothermic formation of H_2/CO and its exothermic conversion into CH_4. Based on existing studies, the calculated energy efficiencies of different approaches and process designs for SCWG are in the range of 44–65%. [61–64]

The catalyst is a key parameter in the low-temperature gasification. In order for catalysis to be an effective adduct for hydrothermal gasification, materials with long-term stability in hot-compressed water need to be identified and utilized in catalyst formulations. Elliott et al., [65–67] at the Pacific Northwest National Laboratory in the early 1990s, demonstrated that subcritical water gasification using active catalysts had the economic potential to convert biomass to CH_4. Studies focused on the development of long-term stable catalysts identified Ni, Ru and Rh as stable/active metals and monoclinic ZrO_2, rutile TiO_2, a–Al_2O_3, and carbon as stable supports under subcritical conditions (~350°C, 20 MPa). In general, the product gas consisted of > 50 vol.% CH_4, 40–50 vol% CO_2, < 10 vol% H_2 and trace levels of light hydrocarbons. Miura's group at Kyoto university prepared a nickel supported carbon catalyst with a high metal loading (~45 wt%) by impregnating an ion-exchange resin with a nickel precursor and then carbonizing the resin in an inert atmosphere at 500°C. The catalyst was used at 350°C and 20 MPa to gasify organics leached from coal and those dissolved in wastewater. [68–70] Their results showed a high catalytic activity and durability of at least 100 h with no sintering observed. Dumesic et al. [71] reported that platinum is an active metal for H_2 production with minimal methane from biomass-derived oxygenates, including glucose, glycerol or methanol at low feedstock concentrations (1–2 wt%) and temperatures (225–265°C). In the gasification of ethylene glycol, a model compound of glucose, over SiO_2-supported Ni, Ru, Pd, Pt and Rh catalysts at 210–225°C and 2.2 MPa, they claimed that the activity for gaseous production was in the order of Ru > Rh, Pt > Ni, Pd. [72] Among

these metals, Rh, Ru and Ni showed a low selectivity for H_2 and a high selectivity for alkane production, whereas the opposite trend was found for Pt and Pd. Waldner and Vogel [73] reported the gasification of a real biomass (wood sawdust: 10–30 wt%) that was operated using a Raney Ni catalyst in a closed batch apparatus (300–410°C and 12–34 MPa). A maximum methane yield of 0.33 g/g-wood was obtained while a slight coke deposited on the catalyst surface.

Catalytic effect of homogeneous catalysts/additives such as KOH, NaOH, K_2CO_3 and Na_2CO_3 has been confirmed in many studies. Main characteristics of this kind of catalyst are to enhance decomposition of biomass into gasifiable intermediates and promote the water-gas shift reaction towards H_2 formation. Xu et al. [74] used glycine and glycerol as the model compounds of protein and fattiness, respectively, for the gasification operated in a continuous tubular-flow reactor at 380–500°C, 25 MPa. They found that Na_2CO_3 increased H_2 yield and COD (*i.e.*, chemical oxygen demand) destruction efficiency. Williams and Onwudili [75] conducted gasification by partial oxidation of glucose in a closed batch reactor under subcritical water conditions of 330°C, 13.5 MPa, and reported the following order in relation to H_2 yield: NaOH > KOH > $Ca(OH)_2$ > K_2CO_3 > Na_2CO_3 > $NaHCO_3$. Their further activities under the same conditions studied influence of the combination of Ni/SiO_2 or Ni/Al_2O_3 catalyst with NaOH on the gasification performance. Both Ni catalysts slightly increased H_2 production and decreased the amount of deposited coke but sintering of the Ni/Al_2O_3 due to the reaction of sodium hydroxide with alumina was observed. The catalytic gasification under alkaline water was previously investigated by Elliott et al. [76] It was confirmed that the conversion of phenolic and carboxylic compounds was much lower than that in acidic media because of the stability of phenolate and carboxylate and other reasons such as the deactivation of catalyst (Ni/Al_2O_3) although the change in its structural property was not shown. Kudo et al. [77] used a carbon-supported ruthenium catalyst for the gasification of lignin in an aqueous alkaline medium (500°C, 25 MPa). The catalyst maintained 98% conversion of the lignin and was stable for more than 10 h. The superior stability of activated carbon enables its extensive application as a catalyst support in a hydrothermal environment.

1.5. Scope and outline of this study

As stated above, growing interest in utilizing more renewable and sustainable lignocellulose feedstocks is spurring intensive research efforts devoted to developing

biorefinery technologies for the production of useful fuels, chemicals and materials. The primary objective of this study is thus the design and development of combined pyrolytic and hydrothermal processes for efficient utilization of entire potion of biomass, as drawn in **Figure 1.4**.

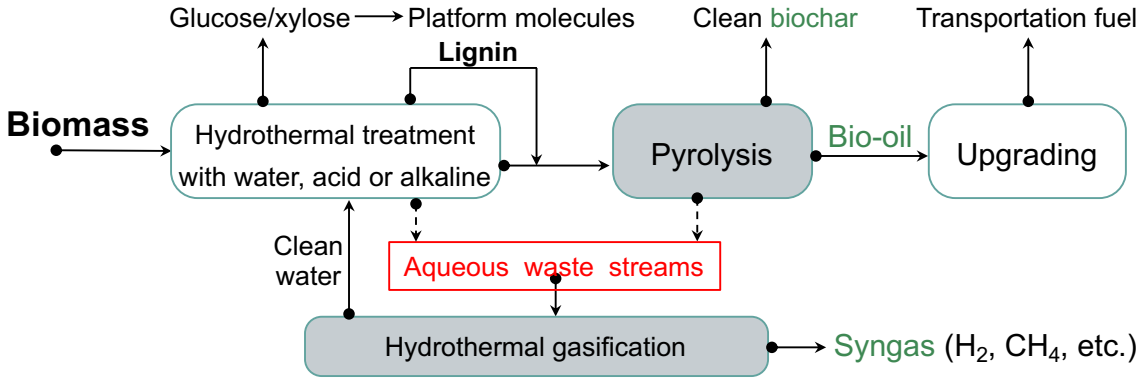

Figure 1.4. *A design of biomass conversion system that integrates hydrothermal treatment, pyrolysis, upgrading and hydrothermal gasification.*

First, the robust structure of biomass, composed of different chemical components (cellulose, hemicellulose and lignin), impedes an effective valorization of that and therefore, fractionation of the biomass into individual components is frequently applied in modern biorefinery such as the pulp and emerged *2nd* ethanol industries. To data, various pretreatment technologies have been developed including alkaline-based methods (*e.g.*, *Kraft* pulping, sulfate pulping) and acid-catalyzed Saccharization (*e.g.*, organosolv pulping, concentrated acid hydrolysis, subcritical water hydrolysis), in which the lignin fraction is isolated as a typical by-product. [78] Lignin though embodies the largest source of bio-aromatics, and the utilization of this feedstock for aromatic chemicals has come into the spotlight. However, the condensed structure renders the isolated lignin a difficult value-added use but mostly as a cheap energy source. [79] We recognize that amongst the above-mentioned thermochemical technologies, pyrolysis is the simplest way for lignin utilization. The conversion of a *Klason* lignin by a proposed pyrolysis process was thus investigated, the results of which are presented in **Chapter 2**. Second, biomass-derived aqueous stream in modern biorefinery is another by-product with very limited applications, which otherwise must then be treated before discharging to the environment. The aqueous phase of bio-oil from pyrolysis is a representative waste stream, the composition of which is more or less similar to that of effluent water from hydrothermal treatment of biomass. This type of by-products mainly contains water and lots of organic compounds such as phenolic compounds,

alcohols and carboxylic acids, etc. Treatment of the waste streams by hydrothermal gasification not only reduces its total organic content but also enables energy recovery in the form of CH_4/H_2 fuel gases, which are the main driving force for **Chapter 3**. Regardless of the hazardous properties, the pyrolytic aqueous phase is highly acidic and thus shows great promise as an alternative of mineral acids for leaching alkali and alkaline earth metal species (AAEMs) from biochar, which could mitigate ash-related issues during char-related applications. The leaching of char with the aqueous phase was in-detail investigated in **Chapter 4**. Third, as a promising method to process highly wet feedstocks, hydrothermal gasification was further applied to lignite-to-syngas conversion (**Chapter 5**).

Five chapters including the detailed works and a general summary are involved here.

- **Chapter 1** gives a general overview of the core topic of the present work. The importance of biomass as an energy source is presented, along with the technologies for its energetic exploitation. The focus is then moved to hydrothermal processes and, in particular, hydrothermal gasification. After presenting the most relevant physical and chemical properties of hot-compressed water, the state of the art for the gasification is drawn. Finally, the objectives of the present work are stated.
- **Chapter 2** describes a particular type of pyrolysis that recycles the heavier portion of bio-oil (HO) entirely to pyrolysis, employing the parent feedstock for their capturing or/and recycling. Continuous pyrolysis of a cedar lignin with HO recycling was simulated by repeating fix-bed pyrolysis of HO-loaded lignin up to nine times, and demonstrated the steady state of yields of gas, water, char and light oil (LO) that consisted solely of monomers and furans and lower acids, with neither discharge of HO from the system nor accumulation therein. Theoretical yields of the products were compared with the experimental values, which confirmed the HO–lignin interactions. The recycled HO underwent not only self-pyrolysis/carbonization but also co-pyrolysis/carbonization with the lignin, resulting in the char formation and degradation into LO, in particular, phenolic monomers such as catechol, guaiacol and their derivates.
- **Chapter 3** proposes a sequential conversion of biomass into syngas and clean biochar, without the use of external chemicals. Aqueous pyrolytic phase of bio-oil was used as a useful agent to leach alkali and alkaline earth metallic species from the char, and then was subjected to hydrothermal gasification in a continuous flow reactor at 350°C

for 280 min, employing a 4.6 wt% ruthenium/activated-charcoal catalyst. The leaching transforms 92% of K form the char to the solution and the resultant carbon conversion by the subsequent HTG was 99% while a CH_4-rich fuel gas and clean water abundance in K were produced.

- **Chapter 4** in-detail investigated repeated leaching of char with pyrolytic aqueous phase at ambient temperature in a batch mode. The leaching of AAEMs is initially rapid and followed by a slower rate towards equilibrium, which can be broadly described by a pseudo-second order model. In terms of the leaching kinetics of K, Mg and Ca, the leaching almost reaches equilibrium within 1 h, with near-steady removal rates of 65, 55 and 74%, respectively. Repeated leaching of biochar with the aqueous phase up to 18 times enables the internal recycling of the pyrolytic products.
- **Chapter 5** demonstrated a sequence of degradation, dissolution and catalytic hydrothermal gasification of lignite in alkaline water. A Victorian lignite was subjected to hydrothermal treatment (HT) in an aqueous solution of NaOH at 250°C, and then oxidation with pressurized O_2 at 100°C. The sequential HT and oxidation near-completely solubilized the lignite. The resulting solution was successfully converted by gasification in a flow reactor at 350°C for 10 h, employing a 16 wt% ruthenium/activated-charcoal catalyst. The initial carbon conversion to gas was as high as 98% while CH_4, CO_2 and H_2 were produced. The catalyst deactivation was in detail discussed and caused mainly by the coke deposition that is related to the heavier portion (molecular mass >1,000) of the solubilized lignite.
- **Chapter 6** summarizes the general conclusions, perspectives and recommendations based on the finding in the preceding chapters.

1.6. References

[1] Dudley B. BP statistical review of world energy. *BP Statistical Review of World Energy*, London, accessed June **2019**.

[2] International Energy Agency. *World Energy Outlook 2019*, IEA, Paris. Available from: https://www.iea.org/reports/world-energy-outlook-2019

[3] International Energy Agency. *Renewables 2019*, IEA, Paris. Available from: https://www.iea.org/reports/renewables-2019

[4] Hornung A., Transformation of biomass: Theory to practice; Chapter 8. Hydrothermal liquefaction-upgrading. *John Wiley & Sons* **2014**.

[5] Hayashi J-i., Kudo S., Kim H. S., Norinaga K., Matsuoka K., Hosokai S. Low-temperature gasification of biomass and lignite: Consideration of key thermochemical phenomena, rearrangement of reactions, and reactor configuration. *Energy & Fuels* **2014,** 28, 4–21.

[6] van der Meijden C. M., Veringa H. J., Rabou L. P. The production of synthetic natural gas (SNG): A comparison of three wood gasification systems for energy balance and overall efficiency. *Biomass and Bioenergy* **2010,** 34, 302–311.

[7] Czernik S., Bridgwater A. Overview of applications of biomass fast pyrolysis oil. *Energy & Fuels* **2004**, 18, 590–598.

[8] Mohan D., Pittman Jr C. U., Steele P. H. Pyrolysis of wood/biomass for bio-oil: A critical review. *Energy & Fuels* **2006**, 20, 848–889.

[9] Kan T., Strezov V., Evans T. J. Lignocellulosic biomass pyrolysis: A review of product properties and effects of pyrolysis parameters. *Renewable Sustainable Energy Review* **2016**, 57, 1126–1140.

[10] Kang S., Li X., Fan J., Chang J. Hydrothermal conversion of lignin: a review. *Renewable and sustainable Energy Reviews* **2013,** 27, 546–558.

[11] Ragauskas A. J., Williams C. K., Davison B. H., Britovsek G., Cairney J., Eckert C. A., Frederick W. J., Hallett J. P., Leak D. J., Liotta C. L. The path forward for biofuels and biomaterials. *Science* **2006,** 311, 484–489.

[12] Tekin K., Karagöz S., Bektaş S. A review of hydrothermal biomass processing. *Renewable and sustainable Energy Reviews* **2014,** 40, 673–687.

[13] Peterson A. A., Vogel F., Lachance R. P., Fröling M., Antal J. M. J., Tester J. W. Thermochemical biofuel production in hydrothermal media: A review of sub- and supercritical water technologies. *Energy & Environmental Science* **2008,** 1, 32.

[14] Funke A., Ziegler F. Hydrothermal carbonization of biomass: A summary and discussion of chemical mechanisms for process engineering. *Biofuels, Bioproducts and Biorefining* **2010,** 4, 160–177.

[15] Sevilla M., Fuertes A. B. The production of carbon materials by hydrothermal carbonization of cellulose. *Carbon* **2009,** 47, 2281–2289.

[16] He C., Giannis A., Wang J. Y. Conversion of sewage sludge to clean solid fuel using hydrothermal carbonization: Hydrochar fuel characteristics and combustion behavior. *Applied Energy* **2013,** 111, 257–266.

[17] Berge N. D., Ro K. S., Mao J., Flora J. R., Chappell M. A., Bae S. Hydrothermal carbonization of municipal waste streams. *Environmental Science & Technology* **2011,** 45, 5696–5703.

[18] Liu P., Wang L., Zhou Y., Pan T., Lu X., Zhang D. Effect of hydrothermal treatment on the structure and pyrolysis product distribution of Xiaolongtan lignite. *Fuel* **2016,** 164, 110–118.

[19] Nakagawa H., Namba A., Böhlmann M., Miura K. Hydrothermal dewatering of brown coal and catalytic hydrothermal gasification of the organic compounds dissolving in the water using a novel Ni/carbon catalyst. *Fuel* **2004,** 83, 719–725.

[20] Demirbaş A. Mechanisms of liquefaction and pyrolysis reactions of biomass. *Energy Conversion and Management* **2000,** 41, 633–646.

[21] Dimitriadis A., Bezergianni S. Hydrothermal liquefaction of various biomass and waste feedstocks for biocrude production: A state of the art review. *Renewable and sustainable Energy Reviews* **2017,** 68, 113–125.

[22] Yeh h. M., Dickinson J. G., Franck A., Linic S., Jr L. T. T., Savage P. E. Hydrothermal catalytic production of fuels and chemicals from aquatic biomass. *J Chem Technol Biotechnol* **2013,** 88, 13–24.

[23] Duan P., Savage P. E. Catalytic hydrotreatment of crude algal bio-oil in supercritical water. *Applied Catalysis B: Environmental* **2011,** 104, 136–143.

[24] Duan P., Savage P. E. Upgrading of crude algal bio-oil in supercritical water. *Bioresource Technology* **2011,** 102, 1899–1906.

[25] Duan P., Savage P. E. Catalytic treatment of crude algal bio-oil in supercritical water: optimization studies. *Energy & Environmental Science* **2011,** 4, 1447–1456.

[26] Khan Y., Anderson G., Elliott D. Wet oxidation of activated sludge. *Water Research* **1999,** 33, 1681–1687.

[27] Kim K. H., Ihm S. K. Heterogeneous catalytic wet air oxidation of refractory organic pollutants in industrial wastewaters: A review. *Journal of Hazardous Materials* **2011,** 186, 16–34.

[28] Hasegawa I., Inoue Y., Muranaka Y., Yasukawa T., Mae K. Selective production of organic acids and depolymerization of lignin by hydrothermal oxidation with diluted hydrogen peroxide. *Energy & Fuels* **2011,** 25, 791–796.

[29] Doskočil L., Grasset L., Válková D., Pekař M. Hydrogen peroxide oxidation of humic acids and lignite. *Fuel* **2014,** 134, 406–413.

[30] Mae K., Shindo H., Miura K. A new two-step oxidative degradation method for producing valuable chemicals from low rank coals under mild conditions. *Energy & Fuels* **2001,** 15, 611–617.

[31] Liu F. J., Wei X. Y., Zhu Y., Wang Y. G., Li P., Fan X., Zhao Y. P., Zong Z. M., Zhao W., Wei Y. B. Oxidation of Shengli lignite with aqueous sodium hypochlorite promoted by pretreatment with aqueous hydrogen peroxide. *Fuel* **2013,** 111, 211–215.

[32] Wang W., Hou Y., Wu W., Niu M., Liu W. Production of Benzene Polycarboxylic Acids from Lignite by Alkali-Oxygen Oxidation. *Industrial & Engineering Chemistry Research* **2012,** 51, 14994–15003.

[33] Li W., Hou Y., Yang F., Wu W. Production of benzene carboxylic acids and small-molecule fatty acids from lignite by two-stage alkali-oxygen oxidation. *Industrial & Engineering Chemistry Research* **2017,** 56, 1971–1978.

[34] Hayashi J-i., Matsuo Y., Kusakabe K., Morooka S. Depolymerization of lower rank coals by low-temperature O_2 oxidation. *Energy & Fuels* **1997,** 11, 227–235.

[35] Anitescu G., Zhang Z., Tavlarides L. L. A kinetic study of methanol oxidation in supercritical water. *Industrial & Engineering Chemistry Research* **1999,** 38, 2231–2237.

[36] Hong G., Spritzer M. Supercritical water partial oxidation, Proceedings of the 2002 US DOE Hydrogen Program Review. NREL/CP–610–32405, **2002**.

[37] Amin S., Reid R., Modell M. Reforming and decomposition of glucose in an aqueous phase. *Intersociety Conference on Environmental Systems* **1975**.

[38] Modell M., Reid R. C., Amin S. I. Gasification process. U.S. Patent 4,113,446, **1978.**

[39] Modell M., Gasification and liquefaction of forest products in supercritical water. In Fundamentals of thermochemical biomass conversion, *Springer* **1985**, 95–119.

[40] Elliott D. C. Catalytic hydrothermal gasification of biomass. *Biofuels, Bioproducts and Biorefining* **2008,** 2, 254–265.

[41] Kruse A. Supercritical water gasification. *Biofuels, Bioproducts and Biorefining* **2008,** 2, 415–437.

[42] Guo Y., Wang S. Z., Xu D. H., Gong Y. M., Ma H. H., Tang X. Y. Review of catalytic supercritical water gasification for hydrogen production from biomass. *Renewable and sustainable Energy Reviews* **2010,** 14, 334–343.

[43] He C., Chen C. L., Giannis A., Yang Y., Wang J. Y. Hydrothermal gasification of sewage sludge and model compounds for renewable hydrogen production A review. *Renewable and sustainable Energy Reviews* **2014,** 39 1127–1142.

[44] Machmudah S., Kanda H., Goto M., Hydrolysis of biopolymers in near-critical and subcritical water. In *Water Extraction of Bioactive Compounds*, Elsevier: 2017; pp 69–107.

[45] Yu D., Aihara M., Antal Jr M. J. Hydrogen production by steam reforming glucose in supercritical water. *Energy & Fuels* **1993,** 7, 574–577.

[46] Xu X., Matsumura Y., Stenberg J., Antal M. J. Carbon-catalyzed gasification of organic feedstocks in supercritical water. *Industrial & Engineering Chemistry Research* **1996,** 35, 2522–2530.

[47] Xu X., Antal Jr M. J. Gasification of sewage sludge and other biomass for hydrogen production in supercritical water. *Environmental Progress* **1998,** 17, 215–220.

[48] Antal Jr M. J., Allen S. G., Schulman D., Xu X., Divilio R. J. Biomass gasification in supercritical water. *Industrial & Engineering Chemistry Research* **2000,** 39, 4040–4053.

[49] Schmieder H., Abeln J., Boukis N., Dinjus E., Kruse A., Kluth M., Petrich G., Sadri E., Schacht M. Hydrothermal gasification of biomass and organic wastes. *The Journal of Supercritical Fluids* **2000,** 17, 145–153.

[50] Kruse A., Meier D., Rimbrecht P., Schacht M. Gasification of pyrocatechol in supercritical water in the presence of potassium hydroxide. *Industrial & Engineering Chemistry Research* **2000,** 39, 4842–4848.

[51] D'Jesús P., Boukis N., Kraushaar-Czarnetzki B., Dinjus E. Gasification of corn and clover grass in supercritical water. *Fuel* **2006,** 85, 1032–1038.

[52] Yamaguchi D., Sanderson P. J., Lim S., Aye L. Supercritical water gasification of Victorian brown coal: Experimental characterisation. *International Journal of Hydrogen Energy* **2009,** 34, 3342–3350.

[53] Ge Z., Jin H., Guo L. Hydrogen production by catalytic gasification of coal in supercritical water with alkaline catalysts: Explore the way to complete gasification of coal. *International Journal of Hydrogen Energy* **2014,** 39, 19583–19592.

[54] Lan R., Jin H., Guo L., Ge Z., Guo S., Zhang X. Hydrogen production by catalytic gasification of coal in supercritical water. *Energy & Fuels* **2014,** 28, 6911–6917.

[55] Davda R., Shabaker J., Huber G., Cortright R., Dumesic J. A. A review of catalytic issues and process conditions for renewable hydrogen and alkanes by aqueous-phase reforming of oxygenated hydrocarbons over supported metal catalysts. *Applied Catalysis B: Environmental* **2005,** 56, 171–186.

[56] Azadi P., Farnood R. Review of heterogeneous catalysts for sub- and supercritical water gasification of biomass and wastes. *International Journal of Hydrogen Energy* **2011,** 36, 9529–9541.

[57] Yoshida T., Oshima Y., Matsumura Y. Gasification of biomass model compounds and real biomass in supercritical water. *Biomass and Bioenergy* **2004,** 26, 71–78.

[58] Osada M., Sato O., Arai K., Shirai M. Stability of supported ruthenium catalysts for lignin gasification in supercritical water. *Energy & Fuels* **2006,** 20, 2337–2343.

[59] Yu J., Lu X., Shi Y., Chen Q., Guan Q., Ning P., Tian S., Gu J. Catalytic gasification of lignite in supercritical water with Ru/CeO_2–ZrO_2. *International Journal of Hydrogen Energy* **2016,** 41, 4579–4591.

[60] Sasaki M., Adschiri T., Arai K. Kinetics of cellulose conversion at 25 MPa in sub- and supercritical water. *AIChE Journal* **2004,** 50, 192–202.

[61] Lu Y., Guo L., Zhang X., Yan Q. Thermodynamic modeling and analysis of biomass gasification for hydrogen production in supercritical water. *Chemical Engineering Journal* **2007,** 131, 233–244.

[62] Calzavara Y., Joussot-Dubien C., Boissonnet G., Sarrade S. Evaluation of biomass gasification in supercritical water process for hydrogen production. *Energy Conversion and Management* **2005,** 46, 615–631.

[63] Matsumura Y. Evaluation of supercritical water gasification and biomethanation for wet biomass utilization in Japan. *Energy Conversion and Management* **2002,** 43, 1301–1310.

[64] Feng W., Van Der Kooi H. J., de Swaan Arons J. Biomass conversions in subcritical and supercritical water: driving force, phase equilibria, and thermodynamic analysis. *Chemical Engineering and Processing: Process Intensification* **2004,** 43, 1459–1467.

[65] Elliott D. C., Sealock Jr L. J., Baker E. G. Chemical processing in high-pressure aqueous environments. 2. Development of catalysts for gasification. *Industrial & Engineering Chemistry Research* **1993,** 32, 1542–1548.

[66] Elliott D. C., Phelps M., Sealock Jr L. J., Baker E. G. Chemical processing in high-pressure aqueous environments. 4. Continuous-flow reactor process development experiments for organics destruction. *Industrial & Engineering Chemistry Research* **1994,** 33, 566–574.

[67] Elliott D. C., Hart T. R., Neuenschwander G. G. Chemical processing in high-pressure aqueous environments. 8. Improved catalysts for hydrothermal gasification. *Industrial & Engineering Chemistry Research* **2006,** 45, 3776–3781.

[68] Miura K., Shimada M., Mae K., Sock H. Y. Extraction of coal below 350°C in flowing non-polar solvent. *Fuel* **2001,** 80, 1573–1582.

[69] Sharma A., Nakagawa H., Miura K. Uniform dispersion of Ni nano particles in a carbon based catalyst for increasing catalytic activity for CH_4 and H_2 production by hydrothermal gasification. *Fuel* **2006,** 85, 2396–2401.

[70] Sharma A., Nakagawa H., Miura K. A novel nickel/carbon catalyst for CH_4 and H_2 production from organic compounds dissolved in wastewater by catalytic hydrothermal gasification. *Fuel* **2006,** 85, 179–184.

[71] Cortright R. D., Davda R. R., Dumesic J. A. Hydrogen from catalytic reforming of biomass-derived hydrocarbons in liquid water. *Nature* **2002,** 418, 964–967.

[72] Davda R., Shabaker J., Huber G., Cortright R., Dumesic J. A. Aqueous-phase reforming of ethylene glycol on silica-supported metal catalysts. *Applied Catalysis B: Environmental* **2003,** 43, 13–26.

[73] H M., Waldner, Vogel F. Renewable production of methane from woody biomass by catalytic hydrothermal gasification. *Industrial & Engineering Chemistry Research* **2005,** 44, 4543–4551.

[74] Xu D., Wang S., Hu X., Chen C., Zhang Q., Gong Y. Catalytic gasification of glycine and glycerol in supercritical water. *International Journal of Hydrogen Energy* **2009,** 34, 5357–5364.

[75] Muangrat R., Onwudili J. A., Williams P. T. Influence of alkali catalysts on the production of hydrogen-rich gas from the hydrothermal gasification of food processing waste. *Applied Catalysis B: Environmental* **2010,** 100, 440–449.

[76] Elliott D. C., Sealock L. J. J., Baker E. G. Chemical processing in high-pressure aqueous environments. 3. Batch reactor process development experiments for organics destruction. *Industrial & Engineering Chemistry Research* **1994,** 33, 558–565.

[77] Kudo S., Hachiyama Y., Takashima Y., Tahara J., Idesh S., Norinaga K., Hayashi J-i. Catalytic hydrothermal reforming of lignin in aqueous alkaline medium. *Energy & Fuels* **2014,** 28, 76–85.

[78] Kumar P., Barrett D. M., Delwiche M. J., Stroeve P. Methods for pretreatment of lignocellulosic biomass for efficient hydrolysis and biofuel production. *Industrial & Engineering Chemistry Research* **2009,** 48, 3713–3729.

[79] Renders T., Van den Bosch S., Koelewijn S. F., Schutyser W., Sels B. Lignin-first biomass fractionation: the advent of active stabilisation strategies. *Energy & Environmental Science* **2017,** 10, 1551–1557.

CHAPTER 2

PYROLYSIS OF LIGNIN WITH FULL RECYCLING OF HEAVY OIL

2.1. Introduction

Lignin, the richest aromatic resource in nature, is a major component of renewable lignocellulose (15–30% by weight, up to 40% by energy) and its valorization plays important roles in modern biorefinery. [1–3] The structure of lignin is robust, consisting of aromatic rings highly linked *via* C-O and C-C bonds. [4] Owing to the recalcitrant nature, lignin serves mostly as a source of heat and power in the pulp industry, leading to serious environmental concerns. In the past few years, the production of value-added chemicals and fuels from lignin has been an active area of research. Substantial works, as summarized by Li et al., [3] have demonstrated great improvements in lignin conversion through various thermochemical strategies, such as hydrolysis and hydrotreatment (*e.g.*, hydrogenation and hydrogenolysis). However, most of those approaches, which involve costly external solvents, catalysts and pressurized H_2, are limited to the laboratory scale.

As an alternative, efficient conversion of lignin with sufficiently high recoveries might be a solution to the above-mentioned issues. Pyrolysis is thus far the technically simplest technology and feasible in large industrial plants. It decomposes lignin under anoxic conditions into liquid bio-oil, gases and carbonized solid, that is, biochar at moderate temperatures, but without any external chemical reagents. The biochar has a variety of applications including the precursor of functional materials, sorbent, soil amendment, and reductant in metallurgical and power industries. [5,6] For these reasons, a higher char yield is the primary target in most instances. Lignin has a higher fixed carbon content than the entire part of biomass that is suitable for char production. Several attempts have been made for the biochar purpose by lowering the peak temperature or raising the gaseous pressure within the pyrolyzer. [7–9] However, the lower temperature and the higher pressure imply a high volatile matter (VM) content of biochar and additional facility and operation cost, respectively. Therefore, the present technology for such a purpose is not necessarily well-developed.

Bio-oil is another energy intermediate of lignin, the yield of which depends on the heating rate, temperature and other operating variables. [10] It is a mixture of organics rich in phenolic substances that can be further upgraded to petroleum-alternative chemicals and fuels. However, there is still a challenge associated with the nature of bio-oil, that is, the presence of considerable heavy oil (HO). The HO is non-volatile, viscous and highly reactive, containing phenolic oligomers with molecular mass (MM) up to 2,500 or even more. [11]

These compounds are hardly transformed into useful products and often induce catalyst deactivation and reactor plugging in the downstream upgrading process. [12] Although the mechanism of formation of such oligomers remains debatable, it is more plausible that a significant portion of the oligomers originated from re-oligomerization of small phenolic molecules in the vapor phase and random condensation of primary products during storage. [13,14]

Pyrolysis with a catalyst is considered as a promising method to yield liquid with improved quality. The main pathway represents thermal decomposition of carbonaceous solid into VM that is subsequently deoxygenated to hydrocarbons. [15] The mostly used catalysts are zeolites, in particular, ZSM-5. Jackson et al. [16] and Yu et al. [17] screened several zeolites for the pyrolysis of a black liquor-derived lignin and reported that ZSM-5 was the optimal one for the production of aromatics. Zhao et al. [18] pyrolyzed a rice husk-derived lignin with ZSM-5 and found that the carbon-based yield and selectivity to aromatic hydrocarbons were 39 and 85%, respectively. Zhou et al. [19] studied the catalytic pyrolysis of another type of lignin from wheat straw over ZSM-5 and produced an organic liquid containing 70% aromatics and only 4 wt% total oxygen. Meanwhile, extensive coke/char formation is a major and common problem that causes rapid catalyst deactivation.

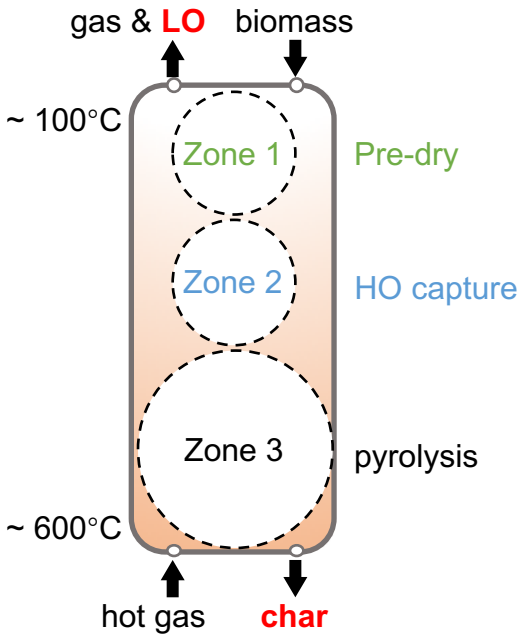

Scheme 2.1. *Concept diagram for an updraft moving-bed reactor containing pre-dry, capturing, and pyrolysis zones.*

The present authors previously proposed an updraft moving-bed reactor that enabled HO to be sorbed by the parent biomass and then be re-pyrolyzed with the biomass in a capturing and pyrolysis zone, respectively. [20] The conceptual diagram of the system is presented in **Scheme 2.1**. The proposed process improved the volatility of bio-oil much by pyrolysis with internal HO recycling, in other words, selectivity for light oil (LO). In consideration of the unique aromatic structure, this proposal, if applied to the utilization of lignin, hopefully enables removal of HO and simultaneous production of LO consisting mainly of phenolic monomers without either separated upgrading process or use of an external chemical reagent/catalyst. On the other hand, the recycling of HO contributes to the production of char. It has been reported that the co-pyrolysis of bio-oil and biomass or *in situ* contact of volatiles with the biomass increased the char yield, whereas it had little impact on its properties such as microporosity and heating value. [21,22]

With the aim of cost-effective use of lignin, this study, therefore, investigated the pyrolysis of a type of softwood lignin with full and internal recycling of HO. The pyrolysis employing a fixed bed reactor was repeated up to nine times to experimentally simulate the continuous pyrolysis with HO recycling. The results are reported with detailed product distributions and quality and discussed focusing on the technical feasibility of this process.

2.2. Experimental Section

2.2.1. Preparation of lignin sample

Lignin sample was prepared from chipped Japanese cedar by a conventional *Klason* method. The details are described elsewhere. [23] The as-prepared lignin was pulverized, sieved to sizes of < 106, 106–150 and 150–213 μm, and vacuum-dried at 50°C before use. The lignin sample had an ash content of 0.07 wt%-dry and C, H, N, O and S contents of 64.8, 5.4, 0.2, 29.5 and < 0.1 wt% on a dry-ash-free basis, respectively. It was confirmed from preliminary pyrolysis runs that the product distributions were little influenced by the particle size and initial mass of the starting lignin (**Figure 2.1**). We then chose a particle size range of 106–150 μm and 1.0 g as the mass of the lignin for pyrolysis.

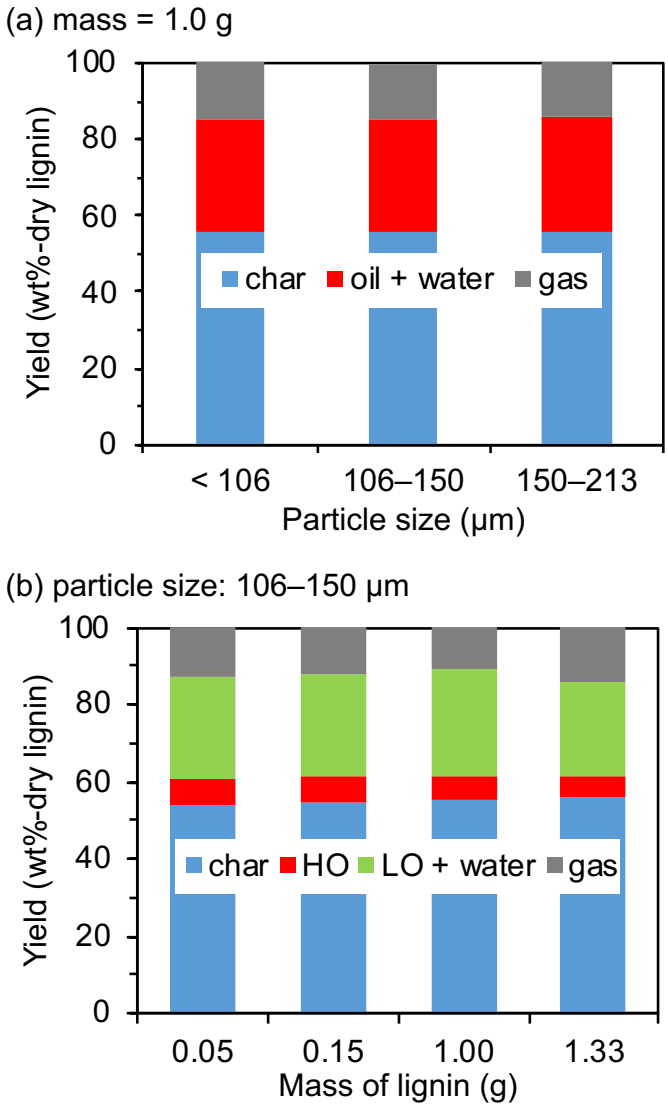

***Figure 2.1**. Yields of pyrolytic products as a function of (a) particle size and (b) mass of as-prepared lignin.*

2.2.2. Experimental apparatus and procedure

The pyrolysis of the lignin was performed in a fix-bed reactor. **Figure 2.2** schematically shows the experimental system for the pyrolysis, consisting of an electric furnace, a horizontal quartz-made reactor tube (i.d.; 25 mm, length; 300 mm), an aerosol filter, two condensers and others. The lignin (1.0 g) was put in a quartz boat in the form of a thin bed and placed within the isothermal zone of the reactor. The tip of the thermocouple was inserted into the bed for monitoring the temperature. The fixed bed was heated to 600°C at a rate of 5 °C min^{-1} under a continuous flow of carrier gas (nitrogen, purity > 99.9999 vol%) at a rate of 100 mL (STP) min^{-1}.

The VM was swept *in-situ* away from the reactor through the necked end (i.d.; 6 mm, length; 100 mm), which was designed for minimizing the vapor residence time in the hot zone. The vapor of the heavier portion of bio-oil, that is, HO, tended to form aerosol immediately after escaping from the reactor. The HO was trapped completely by the silica-fiber-made thimble filter (No. 88R, Advantec Co., Ltd.). The VM was then sent to the two condensers in series, which were packed with glass beads (diameter; 2 mm). The lighter portion of the bio-oil, that is, LO, and pyrolytic water were completely collected in the condensers. The non-condensable gases such as H_2, CO_2, and C_1–C_4 hydrocarbons were collected in a gasbag and analyzed with gas chromatographs (Shimadzu, GC-8A and GC-14B) equipped with a thermal conductivity detector and a flame ionization detector. During the pyrolysis run, the end of the reactor and the thimble filter were heated independently at 230 and 130°C, respectively, for avoiding the condensation of LO, in other words, for condensing the entire portion of HO. After cooling down, LO and water were carefully recovered from the condensers by dissolving them in a known amount of acetone. The water content of the solution was determined by Karl-Fischer titrimetry with an MKS-520 model of Kyoto Electric Manufacturing Co., Ltd. The yields of char, HO and LO/water (as total) were determined gravimetrically as the mass of the product normalized by that of the dry lignin (without the loaded HO). Further analysis of HO and LO will be reported later.

The first to ninth pyrolysis runs were performed in sequence, simulating the HO recycling. In the first run, the entire portion of HO was dissolved in acetone. A very small fraction of

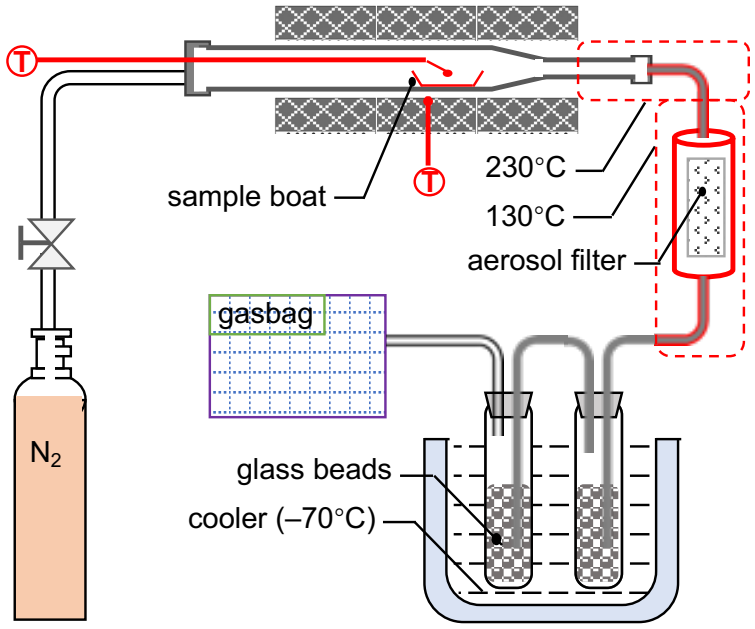

Figure 2.2. *Experimental apparatus for pyrolysis. T, thermocouple.*

the HO solution was subjected to analysis. One gram of lignin (to be used for the second run) was immersed in the HO solution, and then the acetone was removed by rotary evaporation. The HO-loaded lignin was thus prepared and pyrolyzed in the second run. Likewise, the third and later runs were carried out. In each run, the HO loading was defined by the mass of HO divided by that of the lignin and the product yields were calculated as stated above. As demonstrated later, the total number of pyrolysis runs, nine, was enough to simulate the steady states of product yields.

2.2.3. Product analysis and characterization

LO/water from every run of pyrolysis was analyzed using gas chromatography-mass spectrometry (GC/MS) on a Perkin Elmer model (Clarus SQ 8) that was equipped with a TC-1701 column (GL Science Inc., i.d.; 0.25 mm, length; 600 mm). The conditions were as follows: carrier gas; helium (purity > 99.9999 vol%), carrier gas flow rate; 1.0 mL (STP) min^{-1}, temperatures of split injector and ion source; 250 and 230°C, respectively, temperature program; holding at 40°C for 5 min, heating at 4 °C min^{-1} to 270°C, holding at 270°C for 20 min, and then cooling. Among the identified compounds, major ones were quantified by using individual standard compounds.

LO/water and HO were also subjected to gel permeation chromatography (GPC) for measuring the MM distribution. GPC was performed on a Shimazu LC-20 prominence liquid chromatography system, which was equipped with a refractive index detector and three polystyrene gel packed columns in series (Tosoh TSK-gel G1000H_{XL}, G2000H_{XL} and G3000H_{XL}). Tetrahydrofuran was used as the mobile phase. For all analyses, the flowrate of

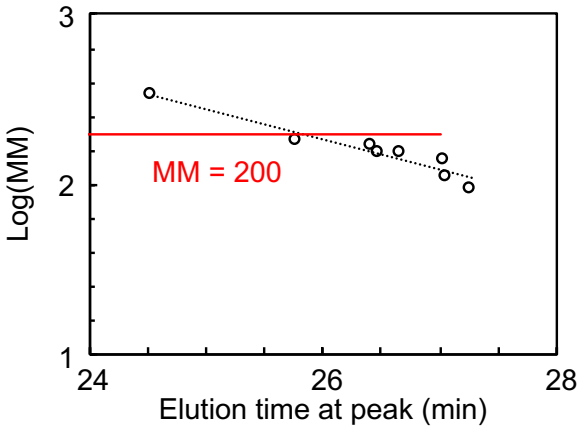

Figure 2.3. *Relationships between elution time and molecular mass of the eight model compounds.*

the solvent and the temperature were 1.0 mL min^{-1} and 40°C, respectively. It was found in a preliminary investigation that polystyrenes were inappropriate for the calibration of bio-oils between MM and elution time. Instead, eight phenolic compounds were employed as the standard compounds. Those were phenol (94), *o*-cresol (108), creosol (138), 4-ethylguaiacol (152), vanillin (152), acetovanillone (166), guaiacylacetone (180) and 1-(3,4-dimethoxyphenyl)-2-(2-methoxyphenoxy)-1,3-propanediol (334). The calibration curve is available in **Figure 2.3**.

VM of the char was determined by thermogravimetric analysis (TGA), by employing a Hitachi STA 7200 Thermal Analysis System. The sample (5–7 mg) was heated at a rate of 5 °C min^{-1} in a flow of nitrogen (purity > 99.9999 vol%) up to 950°C and was maintained for 30 min before cooling. Ultimate analysis of the char was carried out on a Perkin Elmer 2400 series II CHON/S analyzer. Higher heating value (HHV) of the char was approximated by the Dulong's formula. [24]

$$Q\ [\mathrm{MJ\ kg^{-1}}] = 0.3383C + 1.442\ (H - 0.125O) \quad (1)$$

where C, H and O are the contents of carbon, hydrogen and oxygen on a mass basis, respectively.

2.3. Results and Discussion

2.3.1. Experimental simulation of recycling pyrolysis

Thermal behaviors of the lignin were investigated by TGA. According to the mass fraction as a function of temperature in **Figure 2.4**, the mass release occurs over a wide temperature interval up to 700°C. The total VM yield seems to reach 50% at 600°C, whereas further heating to 700°C gave only 3% additional mass release. According to Yang et al., [25] a temperature of 600°C is high enough to complete the evolution of VM and prepare tar-free biochar (residual VM < 0.01 wt%). The peak temperature for the present pyrolysis was thus decided to be 600°C.

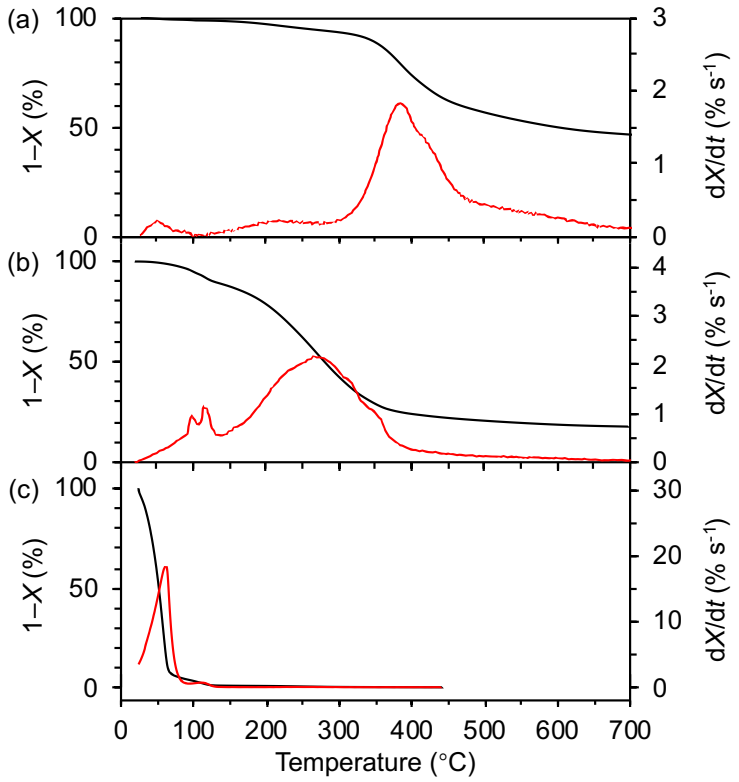

Figure 2.4. *TGA and differential thermogravimetric curves for (a) lignin, (b) HO, and (c) LO/water. Heating rate, 5 °C min^{-1}; carrier gas (N_2) flow rate, 200 mL (STP) min^{-1}. The mass release curve, presented by 1 − X (X; mass-based conversion, black line), was transformed to the differential thermogravimetric profile (= dX/dt, red line). The LO/water in the run with a packed bed of lignin was directly subjected to TGA, whereas the HO was from a run equivalent to the first run of nine runs in series. The HO was recovered from the thimble filter by dissolution in acetone, evaporative removal of acetone, and redissolution in tetrahydrofuran and then analyzed by TGA.*

The HO recycling pyrolysis is technically feasible in the industrial practice assuming that the parent lignin has capabilities of HO capturing in terms of kinetics of condensation/sorption and holding capacity. In a previously reported continuous pyrolysis of lignocellulosic biomass with HO recycling, it was completely condensed into and/or sorbed to the feedstock in a fixed bed, and successfully recycled to pyrolysis. [26] In this regard, the experimental simulation of HO recycling was preliminarily performed by inserting a fixed-bed of lignin (mass; 1 g, temperature; 130°C) between the pyrolyzer and the thimble filter. The complete capture of HO by the lignin fixed bed enables negligible HO (< 0.1 wt%-dry lignin) deposited onto the filter. It is also apparent from the fact that the inner surface of the filter shows almost no changes in the color (**Figure 2.5**). The yield of HO

captured by the lignin was 4.9 wt%. When the pyrolysis of lignin was performed without the lignin fixed bed, HO was deposited on the inner surface of the filter as a brown colored half solid, which accounted for 4.5 wt%-dry lignin. These results clearly demonstrated that the parent lignin had a good ability for holding aerosol-forming HO. It was found after unloading the spent fixed bed that only a portion of lignin (upstream side of the bed) was loaded with HO. This evidenced a high capacity of the lignin as a HO retainer. However, such a capacity made it difficult to load HO directly to the lignin homogenously. It was therefore decided to collect the entire portion of HO with the thimble filter and then load the lignin with acetone.

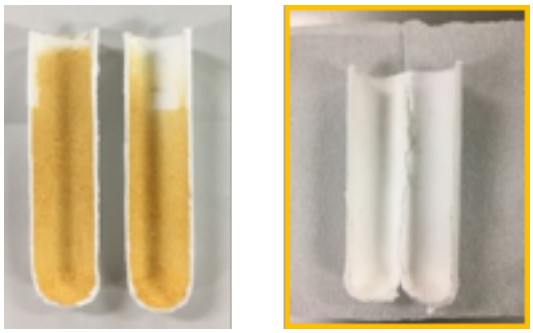

Figure 2.5. *Photographs of spent thimble filters. Left: after a pyrolysis run with the parent lignin as the feedstock. In the run, the filter was set at the reactor downstream and heated at 130°C. The brown colored solid was deposit of HO. Right: after another run with a fixed bed of the parent lignin between the reactor and the thimble filter. No color change occurred on the inner surface of the filter due to complete capture of HO by the lignin fixed bed.*

Such a property was also revealed by GPC. As shown in **Figure 2.6**, HO had a very wide molecular mass distribution far beyond 200. It appears that HO contains compounds with a molecular mass lower than 200, but GC/MS detected no compounds in HO (*i.e.*, no peaks, **Figure S2.1**). This indicates the limitation of determining the range of molecular mass by GPC. Recent advances in bio-oil characterization have revealed that high-molecular-mass compounds (> 200 Da) are essentially those containing two or more phenolic structural units. [13] The presence of such oligomeric compounds renders the bio-oil chemically and thermally unstable and therefore leads to coke/char formation during storage or handling. Because these compounds were captured by the packed bed of lignin, the recovered liquid is rich in monomers with a MM below 200. The monomers are valuable for producing commodity chemicals and biofuels. The internal and full recycling of HO with the parent

lignin as a medium (HO carrier) therefore demonstrates the selective production of LO having very little residue after evaporation.

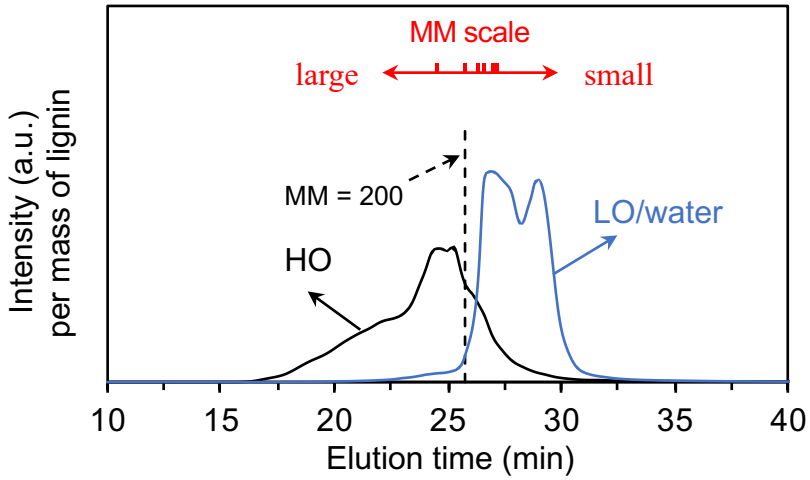

Figure 2.6. *GPC chromatograms LO/water and HO. The intensity was normalized to per mass of lignin. The LO/water from the run with the lignin fixed bed was recovered from the condensers by dissolution in tetrahydrofuran and then analyzed by GPC. The HO was from a run equivalent to the first run of nine runs in series. The HO was recovered from the thimble filter by dissolution in acetone, evaporative removal of acetone, redissolution in tetrahydrofuran, and then analyzed by GPC.*

2.3.2. Product distribution

Figure 2.7 presents the variation in the HO yield as a function of the run number, *n*. The HO yield is indicated on the basis of mass of the parent lignin. The HO yield increases from 5.3 to 11–12 wt% until sixth run, and levels off there. This trend is possible only when the recycled HO is converted to other products by pyrolysis. Higher once-through conversion of the recycled HO results in sooner and lower steady yield. On the other hand, in practice, very low once-through conversion increases the HO yield over the HO-holding capacity of the lignin. It was difficult to estimate the maximum capacity of a given lignin feedstock from its physical/chemical properties, but necessary to experimentally know the capacity under a certain condition. **Figure 2.8** indicates that the HO loading became steady at 11–12 wt%. The corresponding HO loading was far below the reported biomass capacity for retaining the entire or heavier portions of bio-oil. [21,26] It was confirmed that HO-loaded lignin with such loading was dry without forming agglomerates.

Variation in the HO yield is given by the following equation.

$$Y_{HO} \text{ for } n+1 \text{ th run} = Y_{HO,0} + (1 - X_{HO}) \times (\text{HO loading in } n\text{th run}) \quad (2)$$

where Y_{HO}, $Y_{HO,0}$ and X_{HO} are the HO yields in the $(n + 1)$th run and in the first run and once-through conversion of the recycled HO, respectively. This equation is a simplification of eq. (3) based on the material balance with respect to the HO and assuming that the once-through conversion of the recycled HO is independent of the formation of HO from the parent lignin.

$$(Y_{HO} \text{ for } n+1 \text{ th run}) \times A_{n+1} = Y_{HO,0} \times A_{n+1} + (1 - X_{HO}) \times (Y_{HO} \text{ for } n\text{th run})\, A_n \quad (3)$$

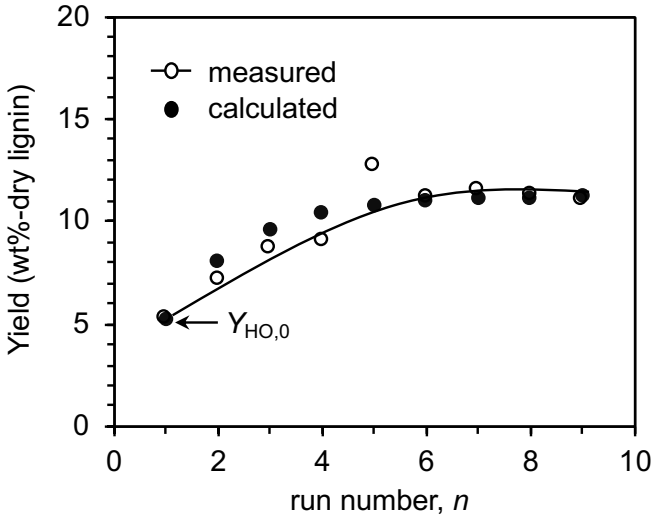

Figure 2.7. *HO yields as a function of the run number. The line has been drawn to indicate the trend. Closed symbols indicate yields calculated by eq 2, assuming steady once-through conversion of recycled HO (X_{HO}) at 47%.*

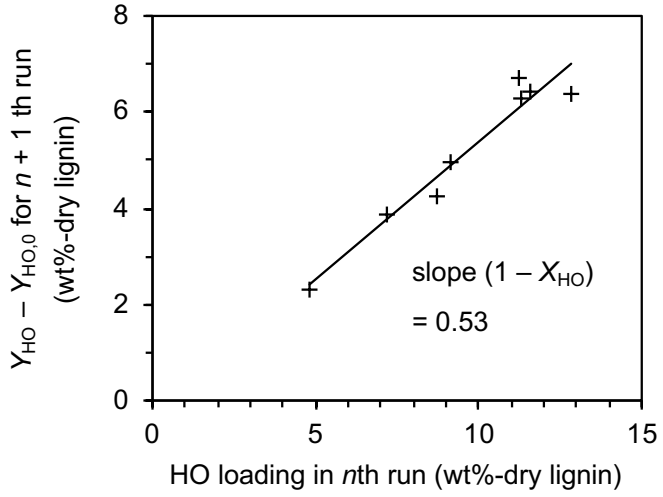

Figure 2.8. *Relationship between $Y_{HO} - Y_{HO,0}$ and HO loading for runs of 2−9. X_{HO} is the once-through conversion of the recycled HO, i.e., the total conversion of the recycled HO into char, LO, and non-condensable gas, which is definable for each run of pyrolysis.*

where A_n and A_{n+1} are the mass of lignin feedstock in the nth and $(n + 1)$th runs, respectively. The same amounts of parent lignin were used for the pyrolysis and HO loading in all runs, that is, $A_{n+1} = A_n$. It is thus possible to transform the HO yield directly to HO loading. The closed keys in **Figure 2.7** indicate the HO yield calculated by eq. (2), assuming $X_{HO} = 47\%$ regardless of the run number. This assumption seems to explain the measured trend well, though there was no necessity of steady X_{HO}. Thus, it is safely concluded that a substantial portion of the recycled HO was converted by pyrolysis with the parent lignin. **Figure 2.8** shows the basis of the above assumption of X_{HO}, plotting $Y_{HO} - Y_{HO,0}$ against HO loading for runs of 2–9. X_{HO} depends on the run to more or less degree, but the slope of 0.53 (corresponding to $X_{HO} = 47\%$) is reasonably obtained by the linear regression analysis.

Run of pyrolysis was carried out with HO alone under the same conditions as those for runs of 1–9. As seen in **Table 2.1**, the conversion of HO, in the absence of parent lignin, was 42%, and lower than that in its presence by 5%. This was indicative of chemical interactions between the lignin and HO in contact with each other, which promoted the HO conversion. The yields of the other products, char, LO, water and gas, are mentioned and discussed in the next section.

Figure 2.9 provides the yields of char, water, LO and non-condensable gas, showing some important trends. First, the char yield increases in runs of 2–5, whereas it is near steady in those of 6–9, where the average yield, 58.9 wt%, is greater than that at the first run (55.6 wt%) by a factor of 1.1. Such an increase is primarily due to the conversion of HO into the char. As shown in **Table 2.1**, the pyrolysis of HO alone formed char with a yield of 21%. Taken together with the average HO yield (11.3 wt%) at runs of 6–9, the char yield was calculated as 58.0 wt% (= 55.6 + 11.3 × 0.21) assuming no chemical interactions between the lignin and HO. Comparing this char yield with the measured value, it was believed that the lignin and HO underwent co-carbonization. Assuming that the increased char yield was fully contributed by that from HO, its conversion into the char was 29%.

Table 2.1. *Product yield (wt %-dry HO) in pyrolysis of HO*

char	HO	LO	water	gas
20.9	57.9	6.9	11.6	2.7

Second, the increase in the water yield, 4.1 wt%, over runs of 1–9, was greater than that calculated in the same way as above, only 1.3 wt%. The difference, +2.8 wt%, corresponded to as much as 25 wt% of the loaded HO (runs of 6–9). The HO–lignin interaction thus promoted the water formation probably by dehydration condensation among hydrogen-bonded -OH groups. [27,28] This result is consistent with the above-mentioned increase in the char yield because dehydration condensation formed cross-links. Huang et al. [26] investigated the pyrolysis of a woody biomass (Japanese cedar) with HO recycling in a way similar to the present study, and achieved a steady state of HO yield as high as 40 wt%-biomass and also *ca*. 40% once-through conversion of HO. They found a slight increase in the char yield by the HO recycling but concluded that such an increase was mainly due to self-charring of the HO rather than co-carbonization with the parent biomass. It was also reported that the water yield was increased but insignificantly by the HO recycling. HO from the biomass was rich in cellulose- and hemicellulose-derived compounds, which was involved minimally in water-forming cross-linking and resulting co-carbonization.

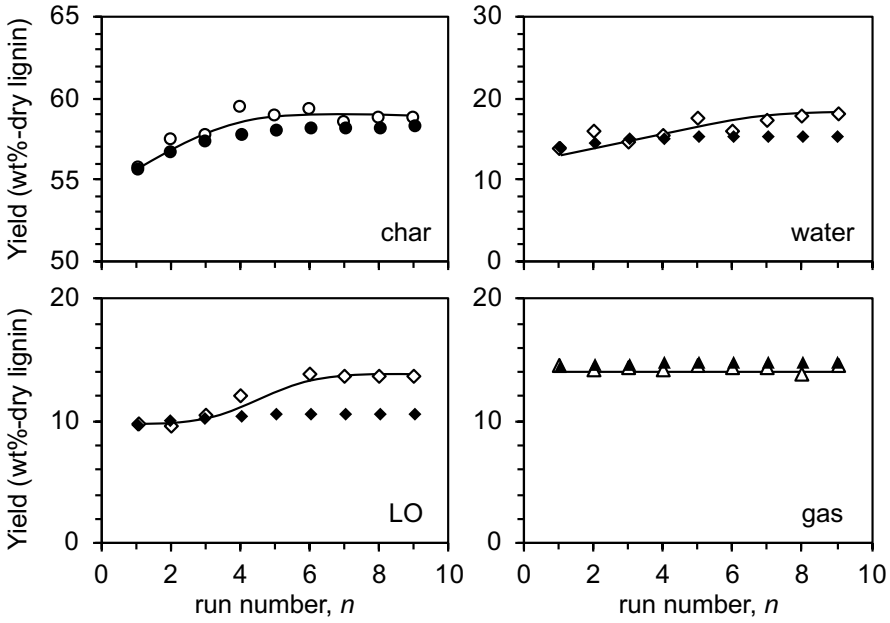

Figure 2.9. *Yields of char, water, LO, and gas as a function of the run number. Open and closed symbols indicate measured and calculated yields, respectively. The lines have been drawn only for showing the trends. Calculated yields have been given by assuming no interaction between HO and parent lignin during pyrolysis.*

Third, in contrast to the water yield, that of gas was almost steady through runs of 1–9 at 14.2–14.7 wt%. There was, if any, a very little synergistic effect from HO–lignin interaction on the formation of gases such as CH_4, CO, CO_2 and H_2. Fourth, the synergistic effect was evident for LO. It increased from 9.7 to 13.6 wt%, which was greater by 3.0 wt% (corresponding to 26 wt% of HO loading). Thus, the interaction between HO and lignin promoted co-carbonization (*i.e.*, char formation) and LO formation simultaneously. Although the mechanism of LO formation is not in-depth studied, it was sufficiently possible that the HO–lignin interaction suppressed the evaporation of HO, inducing its degradation to LO and polymerization to char.

2.3.3. Composition of liquid and gaseous products

The LOs in runs of 1–9 were analyzed by GC/MS. The individual chromatograms are shown and compared in **Figure S2.2**. All identified compounds for the first run, of which area% was over a range of 0.01–14.7%, are listed in **Table S2.1**. GC/MS identified 137 organic compounds. Among them, 81 phenolic compounds are with carbon numbers ≤12, originating primarily from guaiacyl units that are the major aromatic units of Japanese cedar-derived lignin. [29] Most of the phenolic compounds were typical ones are found in the literature. [30,31] Other types of compounds were alcohols, acids, furans and ketones.

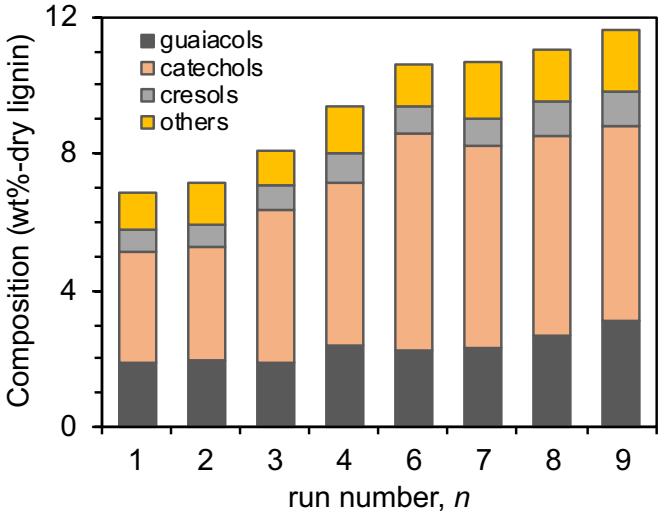

Figure 2.10. *Composition of the major compounds of LOs. Guaiacols: guaiacol, 4-ethylguaiacol, creosol, vanillin, and apocynin; Catechols: catechol, 3-methylcatechol, and 4-methylcatechol; Cresols: phenol, cresol, xylenol, and 4-ethylphenol; Others: methanol, acetic acid, toluene, and xylene.*

Figure 2.10 depicts the composition of 17 major compounds on the basis of mass of the lignin. The individual yields for each product category are available in **Table S2.2**. The total yields of these compounds increased with the run number from 7.0 to 10.7 wt% (sixth run) and finally to 11.8 wt% (ninth run), which accounted for 87% of the LO. The HO recycling also increased the cumulative yield of the 13 phenolic compounds from 5.8 to 9.8 wt%, that is, by a factor of 1.7. The production of phenolic compounds as lignin monomers has been improved by tuning the operating variables such as the peak temperature but not so much. [32,33] On the other hand, the HO recycling greatly increased the monomer yield without external chemicals or catalysts. A particular feature of the LO composition is the abundance of catechols and guaiacols. The sum of catechols and guaiacols was 8.0 wt% (average for runs of 6–9), accounting for 58% of the LO. The yield of catechols was near steady at runs of 6–9 with an average of 6.0 wt%, constituting 42% of the LO. It was believed that catechols were formed mainly by methoxy-to-hydroxyl conversion (*i.e.*, -OCH_3 to -OH) of corresponding guaiacols and that such reactions would be promoted by the interaction between the pyrolyzing lignin and the recycled HO. The HO consisting mainly of oligomers (abundant in both Ph-OCH3 and Ph-OH) was pyrolyzed while recycling. Ph-OCH_3 groups were relatively labile, definitely much more labile than Ph-OH, and therefore converted to Ph-OH groups through several types of reactions in competition as below.

(a) Ph-OCH_3 + H_2O = Ph-OH + CH_3OH

(b) Ph-OCH_3 + 2H (active hydrogen) = Ph-OH + CH_4

(c) Ph-OCH_3 = Ph-OH + C (char) + 2H (active hydrogen)

The reaction (a) produces a catechol and methanol from a guaiacol unit in the oligomer. The methanol yield in fact increased by the HO recycling but only slightly, at most *ca.* 0.03 wt%, whereas the total yield of catechol, 3-methyl catechol and 4-methyl catechol was as much as 2.6 wt%. Considering the molecular weights of methyl-catechol (124) and methanol (32), the above-mentioned 2.6 wt% corresponds to 0.68 wt% increase in the methanol yield. It was then believed that the reaction (a) contributed to the formation of catechols, if any, to a very limited degree. The reaction (b) is associated with formation of CH_4 but its yield remained unchanged as shown in **Figure 2.11**. It was difficult to examine the importance of the reaction (c). It was, however, speculated from the significant HO conversion to char that this type of reaction played a major role in promoting the formation of catechols. In other words, catechols were formed at the expense of -OCH_3 groups.

The non-condensable gases comprised H_2, CO, CO_2 and CH_4, and very minor compounds such as C_2-C_3 hydrocarbons and acetaldehyde. As presented in **Figure 2.11**, the gas composition remained almost unchanged through the sequential runs. This was reasonably understood because the HO recycling hardly affected the gas yield, more exactly, increased it. The total concentration of CO, CO_2 and CH_4 was around 90 vol% on a N_2-free and dry basis, whereas those of H_2 and C_{2+} were as low as 7–8 vol% and 2–3 vol%, respectively. The HHV of the gas was within a range of 20.3–20.9 MJ Nm^{-3} on the same basis as above.

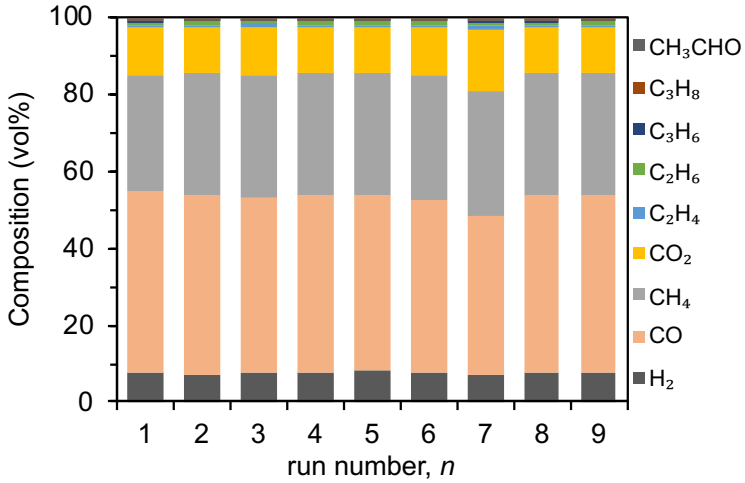

Figure 2.11. *Composition of non-condensable gas.*

2.3.4. Properties of char

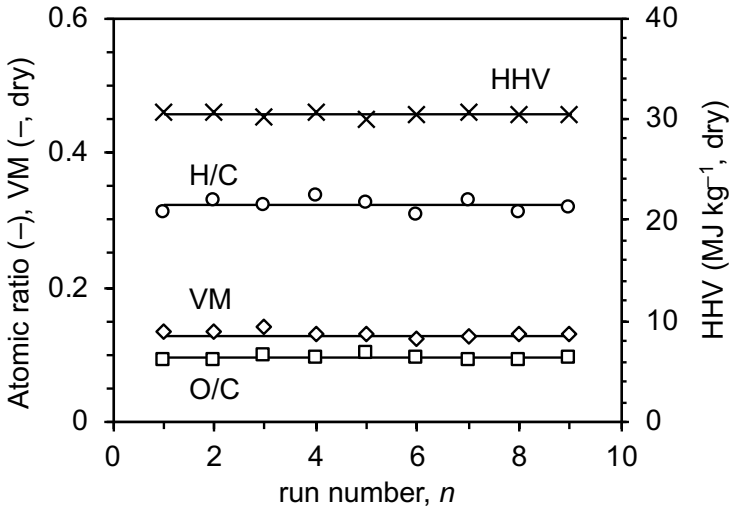

Figure 2.12. *H/C and O/C atomic ratios, VM, and HHV of char. The lines have been drawn for showing the trends.*

Figure 2.12 shows the properties of char, that is, H/C and O/C atomic ratios, VM and HHV, as functions of the run number. The yield of char was increased by the HO loading but its properties remained unchanged. Thus, the recycling of HO hardly affected the char properties. This result is reasonably interpreted as that the char properties were determined virtually by the peak temperature of pyrolysis. [34,35] HHV of the char, which was in a narrow range, 30.1–30.7 MJ kg^{-1}, was clearly higher than that of the parent lignin, 24.4 MJ kg^{-1}. Production of smoke-free biochar with a high HHV is a feature of the present pyrolysis.

2.4. Conclusions

The pyrolysis of *Klason* lignin from Japanese cedar was investigated experimentally by simulating the full recycling of HO with lignin as its carrier and the pyrolysis promoter. Lignin played the role of capturing HO completely and retaining it. The HO retained by the lignin was pyrolyzed and converted into char, water, LO and gas with average X_{HO} of 47%. Such high once-trough conversion realized steady HO loading to the lignin (11.3 wt%-lignin). The recycled HO underwent not only the self-pyrolysis/carbonization but also the co-pyrolysis/carbonization with the lignin. The HO–lignin interaction enhanced water-forming cross-linking, resulting in the char formation but also degradation into LO, in particular, phenolic monomers such as catechol, guaiacol and their derivatives. The HO recycling increased the char yield but maintained its properties such as elemental composition, VM and HHV. The present study has proven the concept of lignin pyrolysis with 100% HO recycling ratio.

2.5. References

[1] Ragauskas A. J., Beckham G. T., Biddy M. J., Chandra R., Chen F., Davis M. F., Davison B. H., Dixon R. A., Gilna P., Keller M. Lignin valorization: Improving lignin processing in the biorefinery. *Science* **2014,** 344, 1246843.

[2] Zakzeski J., Bruijnincx P. C., Jongerius A. L., Weckhuysen B. M. The catalytic valorization of lignin for the production of renewable chemicals. *Chemical Reviews* **2010,** 110, 3552–3599.

[3] Li C., Zhao X., Wang A., Huber G. W., Zhang T. Catalytic transformation of lignin for the production of chemicals and fuels. *Chemical Reviews* **2015,** 115, 11559–11624.

[4] Crestini C., Lange H., Sette M., Argyropoulos D. S. On the structure of softwood kraft lignin. *Green Chemistry* **2017,** 19, 4104–4121.

[5] Liu W. J., Jiang H., Yu H. Q. Thermochemical conversion of lignin to functional materials: A review and future directions. *Green Chemistry* **2015,** 17, 4888–4907.

[6] Boateng A. Characterization and thermal conversion of charcoal derived from fluidized-bed fast pyrolysis oil production of switchgrass. *Industrial & Engineering Chemistry Research* **2007,** 46, 8857–8862.

[7] Katyal S., Thambimuthu K., Valix M. Carbonisation of bagasse in a fixed bed reactor: influence of process variables on char yield and characteristics. *Renewable Energy* **2003,** 28, 713–725.

[8] Antal M. J., Croiset E., Dai X., DeAlmeida C., Mok W. S. L., Norberg N., Richard J. R., Al Majthoub M. High-yield biomass charcoal. *Energy & Fuels* **1996,** 10, 652–658.

[9] Recari J., Berrueco C., Abelló S., Montané D., Farriol X. Effect of temperature and pressure on characteristics and reactivity of biomass-derived chars. *Bioresource Technology* **2014,** 170, 204–210.

[10] Carpenter D., Westover T. L., Czernik S., Jablonski W. Biomass feedstocks for renewable fuel production: a review of the impacts of feedstock and pretreatment on the yield and product distribution of fast pyrolysis bio-oils and vapors. *Green Chemistry* **2014,** 16, 384–406.

[11] Scholze B., Hanser C., Meier D. Characterization of the water-insoluble fraction from fast pyrolysis liquids (pyrolytic lignin): Part II. GPC, carbonyl goups, and ^{13}C-NMR. *Journal of Analytical and Applied Pyrolysis* **2001,** 58, 387–400.

[12] Czernik S., Bridgwater A. Overview of applications of biomass fast pyrolysis oil. *Energy & Fuels* **2004,** 18, 590–598.

[13] Patwardhan P. R., Brown R. C., Shanks B. H. Understanding the fast pyrolysis of lignin. *ChemSusChem* **2011,** 4, 1629–1636.

[14] Bai X., Kim K. H., Brown R. C., Dalluge E., Hutchinson C., Lee Y. J., Dalluge D. Formation of phenolic oligomers during fast pyrolysis of lignin. *Fuel* **2014,** 128, 170–179.

[15] Liu T. L., Cao J. P., Zhao X. Y., Wang J. X., Ren X. Y., Fan X., Zhao Y. P., Wei X. Y. *In situ* upgrading of Shengli lignite pyrolysis vapors over metal-loaded HZSM-5 catalyst. *Fuel Processing Technology* **2017,** 160, 19–26.

[16] Jackson M. A., Compton D. L., Boateng A. A. Screening heterogeneous catalysts for the pyrolysis of lignin. *Journal of Analytical and Applied Pyrolysis* **2009,** 85, 226–230.

[17] Yu Y., Li X., Su L., Zhang Y., Wang Y., Zhang H. The role of shape selectivity in catalytic fast pyrolysis of lignin with zeolite catalysts. *Applied Catalysis A: General* **2012,** 447, 115–123.

[18] Zhao Y., Deng L., Liao B., Fu Y., Guo Q. X. Aromatics production via catalytic pyrolysis of pyrolytic lignins from bio-oil. *Energy & Fuels* **2010,** 24, 5735–5740.

[19] Zhou G., Jensen P. A., Le D. M., Knudsen N. O., Jensen A. D. Direct upgrading of fast pyrolysis lignin vapor over the HZSM-5 catalyst. *Green Chemistry* **2016,** 18, 1965–1975.

[20] Huang Y., Kudo S., Masek O., Norinaga K., Hayashi J-i. Simultaneous maximization of the char yield and volatility of oil from biomass pyrolysis. *Energy & Fuels* **2013,** 27, 247–254.

[21] Veksha A., McLaughlin H., Layzell D. B., Hill J. M. Pyrolysis of wood to biochar: Increasing yield while maintaining microporosity. *Bioresource Technology* **2014,** 153, 173–179.

[22] Phounglamcheik A., Wretborn T., Umeki K. Increasing efficiency of charcoal production with bio-oil recycling. *Energy & Fuels* **2018,** 32, 9650–9658.

[23] Sluiter A., Hames B., Ruiz R., Scarlata C., Sluiter J., Templeton D., Crocker D. Determination of structural carbohydrates and lignin in biomass NREL/TP–510–42618. *National Renewable Energy Laboratory, Golden, Colorado* **2008**.

[24] Idesh S., Kudo S., Norinaga K., Hayashi J-i. Catalytic hydrothermal reforming of Jatropha oil in subcritical water for the production of green fuels: Characteristics of reactions over Pt and Ni catalysts. *Energy & Fuels* **2013,** 27, 4796–4803.

[25] Yang H., Kudo S., Hazeyama S., Norinaga K., Masek O., Hayashi J-i. Detailed analysis of residual volatiles in chars from the pyrolysis of biomass and lignite. *Energy & Fuels* **2013,** 27, 3209–3223.

[26] Huang Y., Kudo S., Norinaga K., Amaike M., Hayashi J-i. Selective production of light oil by biomass pyrolysis with feedstock-mediated recycling of heavy oil. *Energy & Fuels* **2011,** 26, 256–264.

[27] Asadullah M., Zhang S., Li C. Z. Evaluation of structural features of chars from pyrolysis of biomass of different particle sizes. *Fuel Processing Technology* **2010,** 91, 877–881.

[28] Chaiwat W., Hasegawa I., Tani T., Sunagawa K., Mae K. Analysis of cross-linking behavior during pyrolysis of cellulose for elucidating reaction pathway. *Energy & Fuels* **2009,** 23, 5765–5772.

[29] Jin F., Application of hydrothermal reactions to biomass conversion. Chapter 12: Coronella C. J., Lynam J. G., Reza M. T., Uddin M. H. Hydrothermal carbonization of lignocellulosic biomass. *Springer* **2014**, 275−311.

[30] Wang S., Ru B., Lin H., Sun W., Luo Z. Pyrolysis behaviors of four lignin polymers isolated from the same pine wood. *Bioresource Technology* **2015,** 182, 120–127.

[31] [31] Chang G., Huang Y., Xie J., Yang H., Liu H., Yin X., Wu C. The lignin pyrolysis composition and pyrolysis products of palm kernel shell, wheat straw, and pine sawdust. *Energy Conversion and Management* **2016,** 124, 587–597.

[32] Jiang G., Nowakowski D. J., Bridgwater A. V. Effect of the temperature on the composition of lignin pyrolysis products. *Energy & Fuels* **2010,** 24, 4470–4475.

[33] Liaw S. S., Wang Z., Ndegwa P., Frear C., Ha S., Li C. Z., Garcia Perez M. Effect of pyrolysis temperature on the yield and properties of bio-oils obtained from the auger pyrolysis of Douglas Fir wood. *Journal of Analytical and Applied Pyrolysis* **2012,** 93, 52–62.

[34] Garcia Perez M., Wang X. S., Shen J., Rhodes M. J., Tian F., Lee W. J., Wu H., Li C. Z. Fast pyrolysis of oil mallee woody biomass: Effect of temperature on the yield and quality of pyrolysis products. *Industrial & Engineering Chemistry Research* **2008,** 47, 1846–1854.

[35] Wang X., Kersten S. R., Prins W., van Swaaij W. P. Biomass pyrolysis in a fluidized bed reactor. Part 2: Experimental validation of model results. *Industrial & Engineering Chemistry Research* **2005,** 44, 8786–8795.

Supporting Information

Table S2.1. *List of compounds identified by GC/MS analysis of LO in the first run.*

Number	Time (min)	Compound/ Formula	Mw	Area%
1	5.465	methanol/ CH_4O	32	3.81
2	7.384	*iso*-butyraldehyde/ C_4H_8O	72	0.04
3	7.494	1,1-dimethoxyethane/ $C_4H_{10}O_2$	90	0.05
4	8.264	allyl alcohol/ C_3H_6O	58	0.05
5	8.569	butenone/ C_4H_6O	70	0.10
6	8.689	2,3-butanedione/ $C_4H_6O_2$	86	0.06
7	8.744	2-butanone/ C_4H_8O	72	0.18
8	9.009	methyl propionate/ $C_4H_8O_2$	88	0.02
9	9.569	benzene/ C_6H_6	86	0.12
10	10.365	pentanal/ $C_5H_{10}O$	86	0.05
11	10.835	2,5-dimethylfuran/ C_6H_8O	96	0.04
12	11.205	crotonaldehyde/ C_4H_6O	70	0.05
13	11.785	acetic acid/ $C_2H_4O_2$	60	3.66
14	13.386	acetol/ $C_3H_6O_2$	74	0.06
15	13.751	toluene/ C_7H_8	92	0.56
16	15.017	3-penten-2-one/ C_5H_8O	84	0.02
17	16.172	propanoic acid/ $C_3H_6O_2$	94	0.16
18	17.608	cyclopentanone/ C_5H_8O	84	0.02
19	17.993	*m*-xylene/ C_8H_{10}	106	0.03
20	18.328	*o*-xylene/ C_8H_{10}	106	0.31
21	19.639	*p*-xylene/ C_8H_{10}	106	0.04
22	20.519	furfural/ $C_5H_4O_2$	96	0.45
23	21.799	anisole/ C_7H_8O	108	0.03
24	22.37	2-furanmethanol/ $C_5H_6O_2$	98	0.06
25	22.66	1,2,3-trimethylbenzene/ C_9H_{12}	120	0.04
26	22.98	2-methyl-5-ethylfuran/ C_6H_8O	110	0.11
27	23.605	2-ethyl-5-methylfuran/ $C_7H_{10}O$	110	0.02
28	23.925	mesitylene/ C_9H_{12}	120	0.05
29	25.361	2-methylanisole/ $C_8H_{10}O$	122	0.05
30	25.446	benzofuran/ C_8H_6O	118	0.08
31	26.131	3-methylanisole/ $C_8H_{10}O$	122	0.15
32	26.321	5-methylfurfural/ $C_6H_6O_2$	110	0.05
33	27.026	3-methyl-2-cyclopenten-1-one/ C_6H_8O	96	0.08
34	27.131	4-ethynyltoluene/ C_9H_8	116	0.04
35	27.477	2(5H)-furanone/ $C_4H_4O_2$	84	0.06
36	28.037	5-methyl-2(5H)-furanone/ $C_5H_6O_2$	98	0.03
37	29.162	2-ethyl-6-methylphenol/ $C_9H_{12}O$	136	0.05
38	29.267	2,3-dimethylanisole/ $C_9H_{12}O$	136	0.29
39	29.723	7-methylbenzofuran/ C_9H_8O	132	0.12
40	29.873	2-methylbenzofuran/ C_9H_8O	132	0.05
41	30.008	3,5-dimethylanisole/ $C_9H_{12}O$	136	0.06
42	30.218	phenol/ C_6H_6O	94	2.28
43	31.098	guaiacol/ C_7H_8O2	124	10.93

44	31.603	3-methyl-1H-indene/ $C_{10}H_{10}$	130	0.02
45	32.013	*o*-cresol/ C_7H_8O	108	2.42
46	32.239	1,2-dimethoxybenzene/ $C_8H_{10}O_2$	138	0.12
47	32.649	2,6-dimethylphenol/ $C_8H_{10}O$	122	0.46
48	33.279	*p*-cresol/ C_7H_8O	108	1.64
49	33.344	*m*-cresol/ C_7H_8O	108	1.42
50	33.644	2-methoxy-6-methylphenol/ $C_8H_{10}O_2$	138	2.03
51	33.819	4,7-dimethylbenzofuran/ $C_{10}H_{10}O$	146	0.11
52	34.389	2-methoxy-5-methylphenol/ $C_8H_{10}O_2$	138	1.01
53	34.519	levoglucosenone/ $C_6H_6O_3$	126	0.22
54	34.83	creosol/ $C_8H_{10}O_2$	138	14.71
55	34.965	2,5-dimethylphenol/ $C_8H_{10}O$	122	2.06
56	35.16	2-ethyl-6-methylphenol/ $C_9H_{12}O$	136	0.06
57	35.425	3,4-dimethoxytoluene/ $C_9H_{12}O_2$	152	0.48
58	35.515	4,6-dimethyl-2-α-pyrone/ $C_7H_8O_2$	124	0.04
59	35.735	2,4,6-trimethylphenol/ $C_9H_{12}O$	136	0.27
60	36.23	3,5-dimethylphenol/ $C_8H_{10}O$	122	0.43
61	36.36	4-ethylphenol/ $C_8H_{10}O$	122	0.48
62	36.44	3-ethylphenol/ $C_8H_{10}O$	122	0.08
63	36.64	6-ethyl-2-methyl-decane/ $C_{13}H_{28}$	184	0.01
64	36.845	estragole/ $C_{10}H_{12}O$	148	0.19
65	36.99	3,4-dimethoxytoluene/ $C_9H_{12}O_2$	152	2.48
66	37.181	1-ethylidene-1H-indene/ $C_{11}H_{10}$	142	0.07
67	37.251	3,4-dimethylphenol/ $C_8H_{10}O$	122	0.13
68	37.396	2-isopropylphenol/ $C_9H_{12}O$	136	0.04
69	37.671	4-ethylguaiacol/ $C_9H_{12}O_2$	152	3.80
70	37.856	2-ethyl-5-methylphenol/ $C_9H_{12}O$	136	0.34
71	37.951	3-ethyl-5-methylphenol/ $C_9H_{12}O$	136	0.07
72	38.186	4-ethyl-1,2-dimethoxybenzene/ $C_{10}H_{14}O_2$	166	0.07
73	38.561	2,3,4,6-tetramethylphenol/ $C_{10}H_{14}O$	150	0.05
74	38.611	2-(1-methylethylidene)-cyclohexanone/ $C_9H_{14}O$	138	0.04
75	38.751	3,4,5-trimethylphenol/ $C_9H_{12}O_2$	136	0.10
76	38.856	2,5-dimethoxytoluene/ $C_9H_{12}O_2$	152	1.19
77	38.931	2,3,5-trimethylphenol/ $C_9H_{12}O$	136	0.11
78	39.066	3-ethyl-5-methylphenol/ $C_9H_{12}O$	136	0.05
79	39.181	2,5-dimethoxyethylbenzene/ $C_{10}H_{14}O_2$	166	0.06
80	39.331	3-methoxy-2,4,5-trimethylphenol/ $C_{10}H_{14}O_2$	166	0.40
81	39.541	2-methoxy-4-vinylphenol/ $C_9H_{10}O_2$	150	1.21
82	39.616	2,5-diol-p-cymene/ $C_{10}H_{14}O_2$	166	0.76
83	39.952	2-isopropoxyphenol/ $C_9H_{12}O_2$	152	0.08
84	40.077	4-hydroxybenzylideneacetone/ $C_{10}H_{10}O_2$	162	0.35
85	40.197	4-ethenyl-1,2-dimethoxybenzene/ $C_{10}H_{12}O_2$	164	0.09
86	40.242	2,7-dimethyl-3(2H)-benzofuranone/ $C_{10}H_{10}O_2$	162	0.05
87	40.332	eugenol/ $C_{10}H_{12}O_2$	164	0.32
88	40.437	2-methoxy-4-propylphenol/ $C_{10}H_{14}O_2$	166	0.52
89	40.587	2-methyl-6-propylphenol/ $C_{10}H_{14}O$	150	0.05
90	40.907	catechol/ $C_6H_6O_2$	110	9.53
91	41.177	syringol/ $C_9H_{12}O_4$	184	0.46
92	41.527	dihydrojasmone/ $C_{11}H_{18}O$	166	0.09

93	41.662	2-methoxy-5-[(*E*)-1-propenyl]-phenol/ $C_{10}H_{12}O_2$	164	0.24
94	42.102	3-methylcatechol/ $C_7H_8O_2$	124	5.23
95	42.288	3-methoxy-5-methylphenol/ $C_8H_{10}O_2$	138	0.52
96	42.733	3-hydroxybenzenemethanol / $C_7H_8O_2$	124	0.25
97	42.853	2-methyl-1,4-benzenediol/ $C_7H_8O_2$	124	0.05
98	43.323	4-methylcatechol/ $C_7H_8O_2$	124	5.08
99	43.718	*cis*-isoeugenol/ $C_{10}H_{12}O_2$	164	1.78
100	44.018	isoeugenol/ $C_{10}H_{12}O_2$	164	0.50
101	44.508	vanillin/ $C_8H_8O_3$	152	2.41
102	44.814	5-methoxy-2,3-dimethylphenol/ $C_9H_{12}O_2$	152	0.09
103	44.904	2,5-dimethyl-1,3-benzenediol/ $C_8H_{10}O_2$	138	0.19
104	45.219	4-hydroxybenzylideneacetone/ $C_{10}H_{10}O_2$	162	0.19
105	45.519	4-ethyl-1,3-benzenediol/ $C_8H_{10}O_2$	138	0.10
106	45.609	2-methoxy-4-methyl-6-[(1E)-1-propenyl]-phenol/ $C_{11}H_{14}O_2$	178	0.21
107	45.709	3,3,4,7-tetramethyl-2-benzofuran-1(3H)-one/ $C_{12}H_{14}O_2$	190	0.10
108	45.794	4,5-dimethyl-1,3-benzenediol/ $C_8H_{10}O_2$	138	0.07
109	46.429	4-(3-aminobutyl)-2-methoxyphenol/ $C_{11}H_{17}NO_2$	195	0.18
110	46.704	methyl vanillate/ $C_9H_{10}O_4$	182	0.87
111	46.904	acetovanillone/ $C_9H_{10}O_3$	166	1.78
112	46.974	5-methoxy-2,3,4-trimethylphenol/ $C_{10}H_{14}O_2$	166	0.06
113	47.114	3,3,4,6-tetramethyl-1-benzofuran-2(3H)-one/ $C_{12}H_{14}O_2$	190	0.05
114	47.18	4-(2,6,6-trimethyl-1-cyclohexen-1-yl)-2-butanone/ $C_{13}H_{22}O$	194	0.09
115	47.43	4-(but-2-oxy)-benzaldehyde/ $C_{11}H_{14}O_2$	178	0.07
116	47.685	methyl p-tolyl-sulfoxide/ $C_8H_{10}OS$	154	0.06
117	47.87	1-(2-methoxyphenyl)-3-buten-1-ol/ $C_{11}H_{14}O_2$	178	0.05
118	48.005	2,4-dimethoxyacetophenone/ $C_{10}H_{12}O_3$	180	0.17
119	48.31	methyl vanillyl ketone/ $C_{10}H_{12}O_3$	180	1.48
120	48.455	4-methoxy-2-[(3E)-3-penten-2-yl]-phenol/ $C_{12}H_{16}O_2$	192	0.03
121	48.575	methyl (4-hydroxy-3-methoxyphenyl)-acetate/ $C_{10}H_{12}O_4$	196	0.25
122	48.94	1-naphthalenol/ $C_{11}H_{16}O_2$	144	0.22
123	49.22	1-(2-hydroxy-4-methoxyphenyl)-1-propanone/ $C_{10}H_{12}O_3$	180	0.66
124	49.33	3-methoxy-2,5,6-trimethylphenol/ $C_{10}H_{14}O_2$	166	0.11
125	49.49	3-phenylfuran/ $C_{10}H_8O$	144	0.05
126	49.731	4-butyl-1,2-dimethoxybenzene/ $C_{12}H_{18}O_2$	194	0.09
127	49.836	butyrovanillone/ $C_{11}H_{14}O_3$	194	0.93
128	49.971	5-hydroxy-6-methoxy-1-benzofuran-3(2H)-one/ $C_9H_8O_4$	180	0.03
129	50.246	2-ethyl-4,5-dimethylphenol/ $C_{10}H_{14}O$	150	0.07
130	50.541	1,2-dimethoxy-4-(1-methoxyvinyl)-benzene/ $C_{11}H_{14}O_3$	194	0.05
131	50.716	2-tert-butyl-1,4-dimethoxybenzene/ $C_{12}H_{18}O_2$	194	0.06
132	51.086	1-(3,4-dimethoxyphenyl)-propan-1-one/	194	0.03

		$C_{11}H_{14}O_3$		
133	51.231	3-acetyl-2-methoxybenzo[b]furan/ $C_{11}H_{10}O_3$	190	0.01
134	51.321	3-methoxy-2-naphthalenol/ $C_{11}H_{10}O_2$	174	0.17
135	51.401	butyrovanillone/ $C_{11}H_{14}O_3$	194	0.04
136	51.496	4-(3-hydroxy-2-methoxyphenyl)-2-butanone/ $C_{11}H_{14}O_3$	194	0.04
137	51.611	7-hydroxy-6-methoxy-1-benzofuran-3(2H)-one/ $C_9H_8O_4$	180	0.03

***Table S2.2**. Yield of major compounds of LOs quantified in runs of 1–9 (wt%-dry lignin).*

compounds	run 1	run 2	run 3	run 4	run 6	run 7	run 8	run 9
methanol	0.19	0.21	0.20	0.19	0.21	0.22	0.21	0.22
acetic acid	0.86	0.95	0.77	1.10	0.95	1.39	1.29	1.50
toluene	0.03	0.03	0.03	0.04	0.03	0.03	0.05	0.03
xylene	0.02	0.02	0.03	0.02	0.02	0.02	0.03	0.02
phenol	0.16	0.16	0.17	0.21	0.19	0.19	0.24	0.25
guaiacol	0.52	0.56	0.57	0.73	0.64	0.75	0.81	0.92
creosol	0.68	0.70	0.71	0.90	0.76	0.70	0.97	1.13
cresol	0.30	0.29	0.34	0.41	0.35	0.35	0.46	0.47
xylenol	0.18	0.18	0.18	0.23	0.21	0.22	0.26	0.29
4-ethylphenol	0.01	0.01	0.01	0.01	0.01	0.01	0.01	0.02
4-ethylguaiacol	0.25	0.27	0.25	0.31	0.28	0.35	0.34	0.40
catechol	1.20	1.13	1.27	1.43	1.80	1.95	1.95	1.97
syringol	0.05	0.03	0.03	0.06	0.07	0.06	0.08	0.07
3-methylcatechol	0.74	0.71	1.18	1.17	1.51	1.53	1.57	1.12
4-methylcatechol	1.29	1.50	2.01	2.15	3.06	2.41	2.35	2.58
vanillin	0.24	0.22	0.19	0.23	0.22	0.25	0.24	0.34
apocynin	0.14	0.16	0.14	0.18	0.26	0.24	0.21	0.26
total	6.97	7.25	8.17	9.50	10.72	10.87	11.22	11.78

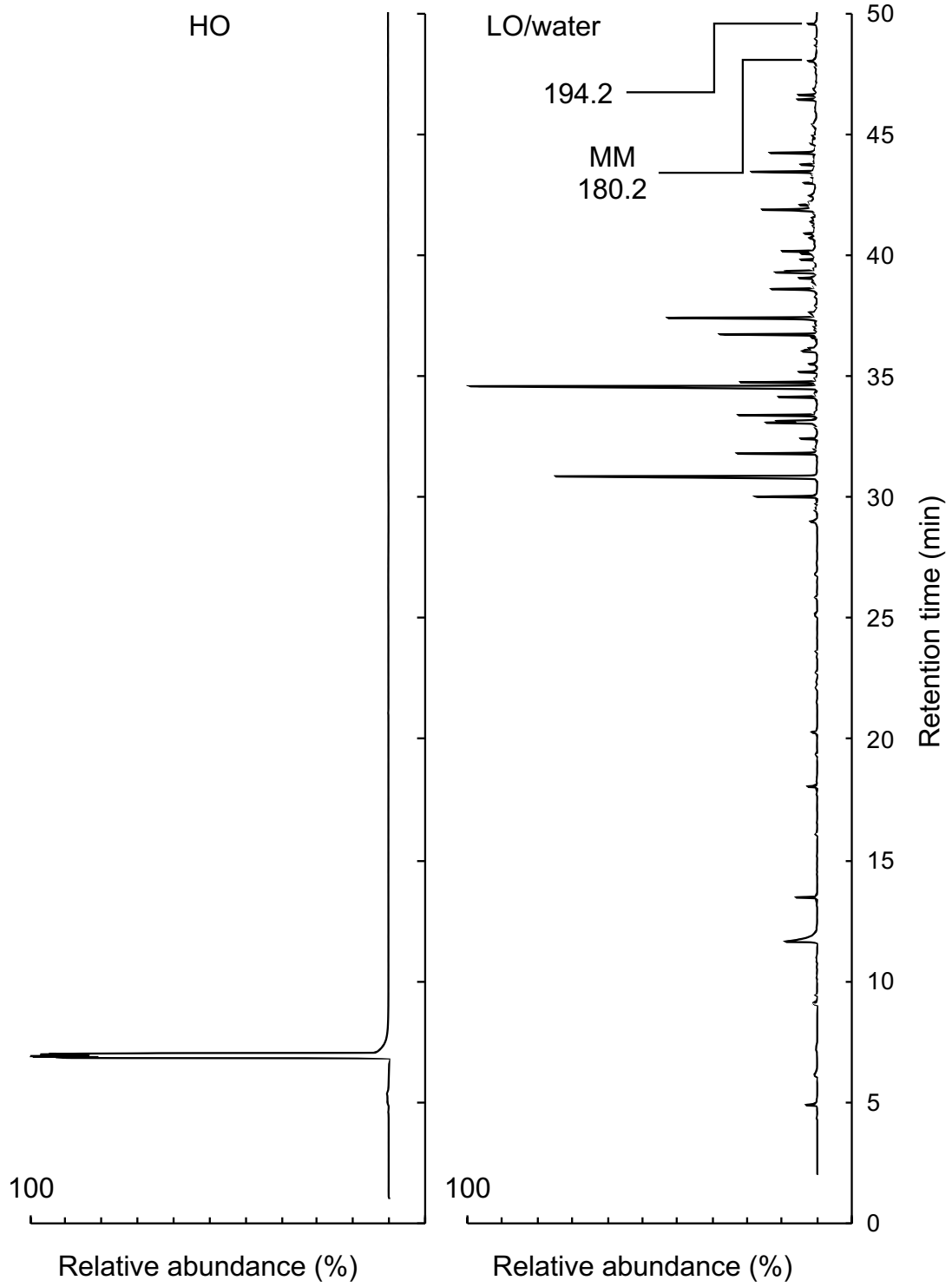

Figure S2.1. Typical GC/MS chromatograms of LO/water and HO. The LO/water was collected in the condensers from the run with the lignin fixed bed while the HO was from a run equivalent to the first run of nine runs in series. No peaks were found for HO. Only compounds at molecular mass < 200 were detected in LO.

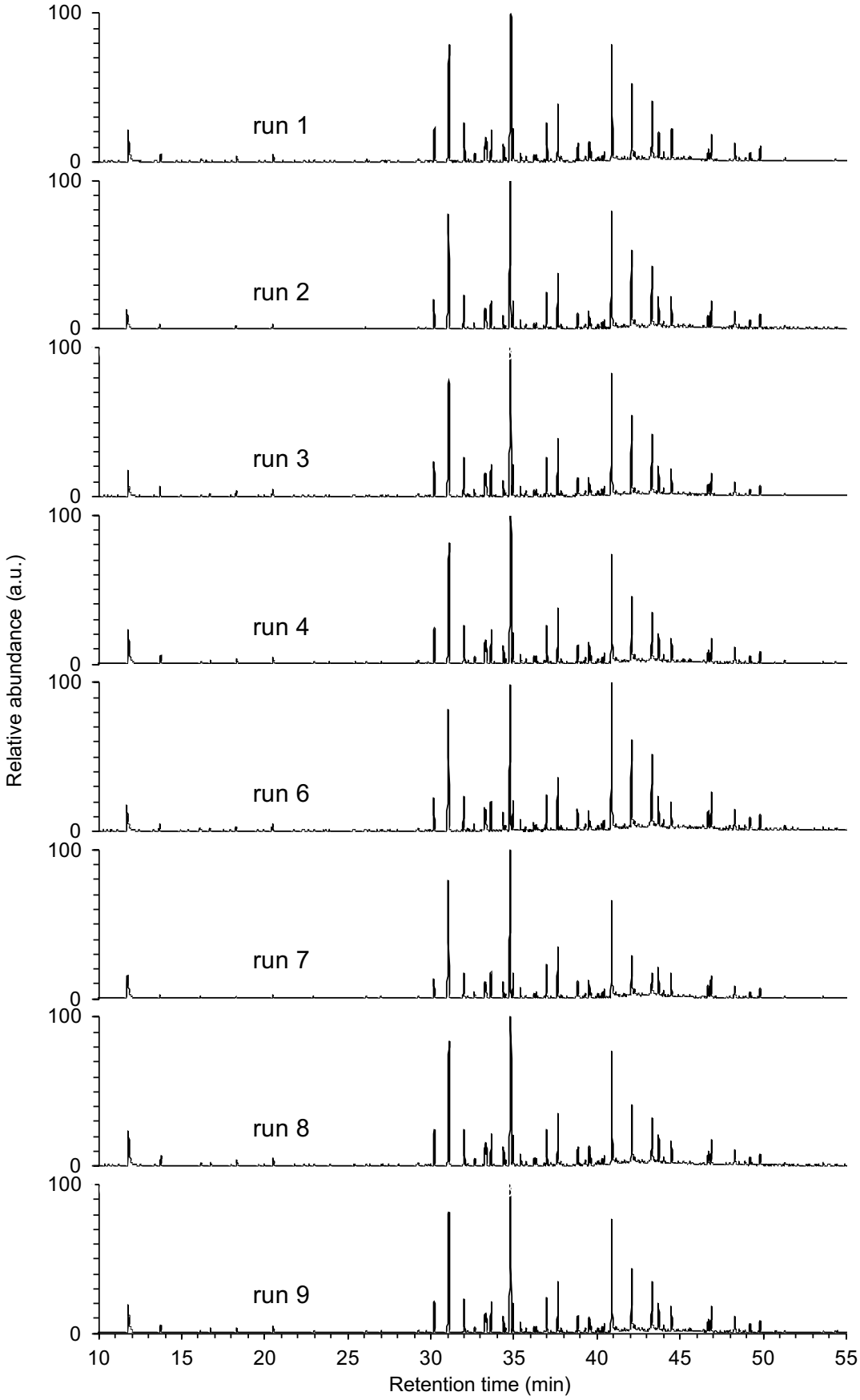

Figure S2.2. Total ion chromatograms of LOs in runs of 1–9.

CHAPTER 3

SEQUENTIAL BIOMASS CONVERSION TO SYNGAS AND CLEAN BIOCHAR

3.1. Introduction

Renewable biofuels from biomass have shown great promise toward diversifying global fuel supplies and delivering significant environmental benefits. The replacement of petroleum-derived fuels by biofuels is one of the important keys to building a sustainable economy. Over the past few decades, the cost-effective production of biofuel has already become an active area of research. Fast pyrolysis, which rapidly decomposes biomass at moderate temperatures and in the absence of oxygen, emerges as the most feasible technology. The liquid product, often termed pyrolysis oil or bio-oil, is today the cheapest biofuel that contains up to 75% of dry biomass weight and initial biomass energy. [1] However, the properties of bio-oil render it directly unusable as a transportation fuel substitute in a diesel engine. The gloss heating value is only about half of that of petroleum due to the high contents of oxygen (35–40 wt%) and water (up to 50 wt%). [2] Other drawbacks, as described in the literature, [1,2] are foremost poor volatility, instability and high viscosity and corrosiveness.

A simple and primary way of upgrading bio-oil is to remove its aqueous phase through fractional condensation of initial pyrolytic volatiles or phase separation of the bio-oil by the addition of water. [3] The aqueous phase (APB) of the bio-oil, containing a mixture of acids, phenols, ketones, saccharides and other organic compounds, [1] is normally considered as a stream of byproduct with very limited applications. Hydro-deoxygenation offers another viable option to remove oxygen and upgrading the bio-oil using pressurized molecular hydrogen and bifunctional catalysts. Numerous studies [4,5] revealed the benefits of this approach such as high heating value of the desired liquid product. The disadvantage of the process is the consumption of hydrogen that serves as an essential agent for the deoxygenation. The process also produces much water as byproduct, the composition of which is similar to that of APB. Catalytic hydrothermal gasification (CHTG) is a developing technology worth devoting great attention, particularly suitable for processing water-rich byproduct streams. CHTG is a process that occurs in sub- or super-critical water, converting organics into versatile syngas that can be later directed into fuels and chemicals *via* Fisher–Tropsch synthesis. Despite the high capital cost of the reactor and facilities, many advantages of CHTG have been claimed over hydro-deoxygenation or conventional catalytic steam reforming; low temperature, high reaction rate, clean effluent water, formation of less coke and no need for H_2 and energy-intensive water evaporation. [6,7]

Since the first publication of Model, [8] substantial research and development activities have applied CHTG to the conversion of specific model compounds or even real biomass. Elliot et al. [9, 10] systematically examined CHTG of phenol and *o*/*p*-cresol as wastewater organics, and evidenced CHTG to be effective in both batch and continuous flow reactors with active metal catalysts including Ru, Ni and Rh. Guan et al. [11] reported complete conversion of microalga by CHTG with excessive Ru/C in a batch reactor at 410°C. From a practical perspective, the liquid bio-oils are more suitable than the real biomass for continuous feeding into a highly pressurized reactor. Nevertheless, there have been a very limited number of reports on CHTG of bio-oil. Vispute and Huber [12] investigated the reforming of hydrotreated APB (carbon content; 2 wt%) with a $Pt/SiO_2–Al_2O_3$ catalyst in a tubular flow reactor at 260°C and 5.2 MPa. The carbon conversion to gas was only 35% but with alkane selectivity of 45%. Behnia et al. [13] reported the gasification of APB containing 2.98 wt% carbon under supercritical conditions (700°C, 27.5 MPa) and obtained a H_2-rich gas and 89% carbon conversion in the presence of $Ni\text{-}Ru/Al_2O_3$. Idesh et al. [14] developed several Ni supported carbon catalysts (Ni loading; 47 wt%) that enabled near-complete reforming of water solubles from biomass pyrolysis. Chakinala et al. [15] screened a range of metal catalysts (Pt, Pd, Ru, Rh and Ni) for CHTG of APB in a batch reactor and found that a Ru catalyst showed the best activity for not only the gasification efficiency but also selectivity to CH_4.

The above-mentioned studies, except that reported by Idesh et al. [14], generally regarded APB as a wastewater that must be treated before disposal. The present study proposes a new scheme to apply APB or other biomass-derived liquid streams as a useful agent for leaching *i.e.*, removal of metallic species from biomass or char, prior to CHTG, as illustrated in **Scheme 3.1**. The process uses APB from the pyrolysis and thus there is no need for additional chemicals (*e.g.*, mineral acids). It is known that APB is abundant in AcOH and other organic acids, and has the potential of leaching alkali and alkaline earth metallic species (AAEMs, including K, Na, Mg and Ca) from biomass and char. The reduced content of AAEMs, in particular that of K, can mitigate ash-related issues in operating combustion or/and gasification, such as agglomeration, slagging and fouling. [16] These issues are not necessarily present in hydrothermal environments because the AAEMs leached by the bio-oil are mainly in forms of carboxylates. [17] On the other hand, it has been stated that the alkaline additives such as NaOH, $Ca(OH)_2$ and CaO facilitate carbon gasification efficiencies by enhancing the decomposition of biomass as well as inhibiting char/coke

formation. [18,19] Azadi et al. [20] reported that the addition of alkali promotors (Na, K and Cs) improved CH_4 yield and carbon conversion of glucose over a nickel catalyst for the supercritical gasification of glucose at 380°C. The leaching proposed in **Scheme 3.1** is thus expected to play a role in the CHTG, to a more or less extent, because of not only changes in the chemical composition of APB but also the introduction of AAEMs. Unfortunately, so far barely any research has been performed on leaching biomass/char with bio-oil prior to CHTG.

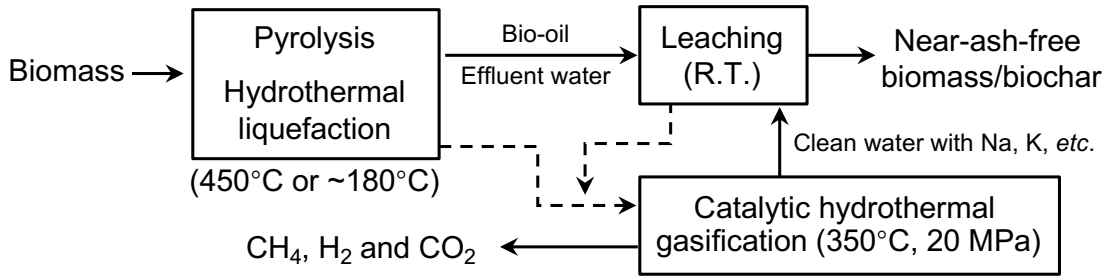

Scheme 3.1. *Conceptual diagram for combined leaching and CHTG for conversion of biomass into syngas and clear char.*

Two recent reviews [21,22] well summarized the heterogeneous catalysts for CHTG in terms mainly of activity and stability. Activated carbon is a widely used support with superior stability and high degree of metal dispersion, and ruthenium is highlighted as a catalytically active/stable metal under hydrothermal conditions. Hence, in this study, a carbon-supported ruthenium catalyst was chosen but with a low metal loading (< 5 wt% RuO_2) considering the economy. The main target is to demonstrate complete conversion of APB after leaching biomass/char in a continuous flow reactor.

3.2. Experimental Section

3.2.1. Preparation of aqueous phase of bio-oil

A type of rice straw (RS) was pyrolyzed in a horizontal screw-conveyer pyrolyzer that had dimensions of 50 mm inner diameter and 150 mm effective length. Particles of as-prepared biomass ranged 1.8–2.5 mm in length and had the composition of C, 46.3; H, 6.0; N, 0.9; O, 46.8 wt%-d.a.f and ash, 14.4 wt%-dry. The rice straw, that had been dried at 105°C prior to the pyrolysis and thereafter, was continuously fed into the pyrolyzer at a rate of 3.3 g min^{-1}. The temperature at the center of the pyrolyzer was 450°C. The heating rate of biomass that moved to the center calculated as *ca.* 320 °C min^{-1} assuming a sufficiently

high heat exchange between the wall of pyrolyze tube and the pyrolyzing solid. The pyrolytic volatiles were condensed in a thimble filter at 150°C and a train of three cooled traps at 0, –40, and –70°C, respectively. The total product recovery was around 102% on the basis of the dry biomass mass. **Table 3.1** lists the product yields. The description of the apparatus and procedures are described elsewhere in more detail. [23]

The 0°C condensate, a multicomponent mixture of lighter oil, water and heavier oil, was used to prepare feedstocks for leaching and also CHTG. Upon collection, the condendsate was centrifugated at 8000 rpm for 30 min until complete phase separation. The aqueous phase (*i.e.*, APB) was then separated from the oil phase (at bottom) by careful decantation. The APB was dark brown in color, and it had a Karl–Fischer moisture content of 62.3 wt% and constituted 92.4 wt% of the condensates. The proportion of carbon in the solution amounted to 12.6% of carbon of the pyrolyzed rice straw. The solution was diluted by 7 times in volume by adding deionized water, followed by centrifugation, phase separation and filtration (pore size; 0.45 mm). The resulting transparent solution, hereafter termed LO, primarily contains lighter water-solubles. **Table 3.1** gives C, H, O, and N contents of 45.6, 7.1, 47.3, and < 0.01 wt % on a water-free basis, respectively. The LO was finally stored in an airtight glass bottle at 5°C to minimize aging, and later employed for leaching tests that were performed within two weeks since the preparation.

Table 3.1. *Product yields in biomass pyrolysis and element composition of APB and LO.*

		condensable (°C for traps)				
char	gas	150	0	–40	–60	balance
37.4	19.6	9.9	28.8	1.9	4.4	102.0
		element composition (wt%, on a water-free basis)				
		C	H	N	O[a]	HHV[b]
APB		50.8	7.73	0.18	41.3	20.9
LO		45.6	7.08	< 0.01	47.3	17.1

[a] calculated by difference. [b] high heating value, MJ kg^{-1}; calculated by the Dulong's formula.

3.2.2. Biomass and char leaching

The leaching was performed in a batch system at room temperature. The biomass or char was preliminarily ground to sizes below 150 μm for minimizing mass transfer limitation effect. Typically, 10 g-dry solid and 80 mL LO were charged in an airtight bottle and gently stirred with a magnetic stirrer for 48 h to ensure an equilibrium (no further changes in both

the organic and inorganic compositions). The mixture was then filtered with a hydrophilic PTFE-membrane filter (pore size; 0.45 μm). The solid left over the filter was washed with deionized water and then vacuum-dried at 60°C. The solution was recovered as LRS or LCR for leaching RS or char, respectively, and kept at 5°C before further use. Additionally, a HCl-washed char (HC) was prepared separately through stirring 10 g-dry char together with 200 mL aqueous solution of HCl (0.1 M) for 24 h. The solid, HC, was rinsed with deionized water until no Cl^- was detected by ion chromatography, and after the drying was leached with LO to prepare a solution free from AAEMs, that is, LHC. Every leaching run was done at least in duplicate. The four different types of LOs, *i.e.*, LO, LRS, LCR and LHC, were characterized for pH, total organic carbon (TOC) and AAEM content. The chemical composition of LOs was identified by gas chromatography/mass spectrometry (GC/MS) and further quantified by gas chromatography. Anions of organic acids (mainly formate and acetate) were quantified by high performance liquid chromatography (HPLC). Molecular weight distribution of LOs was analyzed by gel-permeation chromatography (GPC). More detailed information on the equipment and analysis procedures are found in a previous publication. [24]

AAEMs in the solid were quantified following a previously reported method [25] that involves sequential ashing, acid-digestion and dissolution. Briefly, about 10 mg of pulverized sample was loaded in a platinum crucible (diameter; 5.2 mm, height; 5.0 mm). The sample was heated to 600°C at a rate as low as 1 °C min^{-1} for avoiding ignition upon heating. The resulting ash was completely digested in an equivolume mixture of HF/HNO_3 (1:1; mol/mol) that was then evaporated. The dry solid was dissolved in a known volume of methanesulfonic acid (2 mM). The analysis was carried out on a Shimadzu LC-10A liquid chromatograph coupled with a conductivity detector Model CDD-10Avp. Individual AAEMs (Na, K, Mg and Ca) were separated in a Shim-pack IC-C4 column protected by an IC-GC4 guard using an aqueous solution of methanesulfonic acid (conditions; 2mM, 1.0 mL min^{-1} and 40°C) as the mobile phase.

3.2.3. Catalyst preparation and characterization

A ruthenium on carbon (Ru/C) catalyst was prepared by an incipient wetness impregnation method. All the chemicals used were purchased from Wako Pure Chemical Industry, Inc. The support, activated charcoal, was sieved to a fraction of 0.7–1.0 mm, sonicated to remove fines and then dried. 10 g of the support was impregnated with 50 mL

acetone solution of ruthenium (III) chloride (80 mM). The metal thus attains a nominal loading of 5.0 wt% in the form of RuO_2. After the Ru loading, the solid was dried and then calcined at 400°C for 3 h in a flow of equivolume mixture of H_2 and N_2. The metal loading, 4.6 wt% (as RuO_2), was finally determined gravimetrically by simple combustion in air at 800°C for 1 h.

The Burnauer–Emmett–Teller surface area (S_{BET}) and total pore volume (V_p) of fresh and spent Ru/C catalysts were determined by analyzing N_2 adsorption/desorption isotherms at 77 K that were measure with a Quantachrome, NOVA 3200e. Before measurement, the catalyst was outgassed at 200°C for 3 h. X-ray diffraction (XRD) patterns were recorded on a Rigaku TTR-III X-ray diffractometer with Cu Kα radiation at a voltage of 50 kV and a current of 300 mA. Diffractograms were obtained at 2θ = 10–80° with a scanning speed of 1° min^{-1}. Transmission field emission transmission electron microscopy (TEM) imaging was performed on a JEOL JEM-2100F electron microscope operating at an accelerating voltage of 200 kV. A small amount of sample powder was suspended in ethanol, sonicated and deposited on a Cu-made grid with a perforated carbon membrane.

3.2.4. Catalytic hydrothermal gasification

CHTG was performed in a continuous flow reactor under subcritical hydrothermal conditions (350°C, 20 MPa). The apparatus was illustrated in **Figure 3.1**. In brief, it consisted of an HPLC pump, a SUS316-made tubular reactor (inner diameter; 10.9 mm, length; 42 mm), a backpressure regulator and a gas-liquid separator. Typically, 1.0 g of as-prepared catalyst was charged and fixed in the reactor. Either of LO, LRS, LCR and LHC

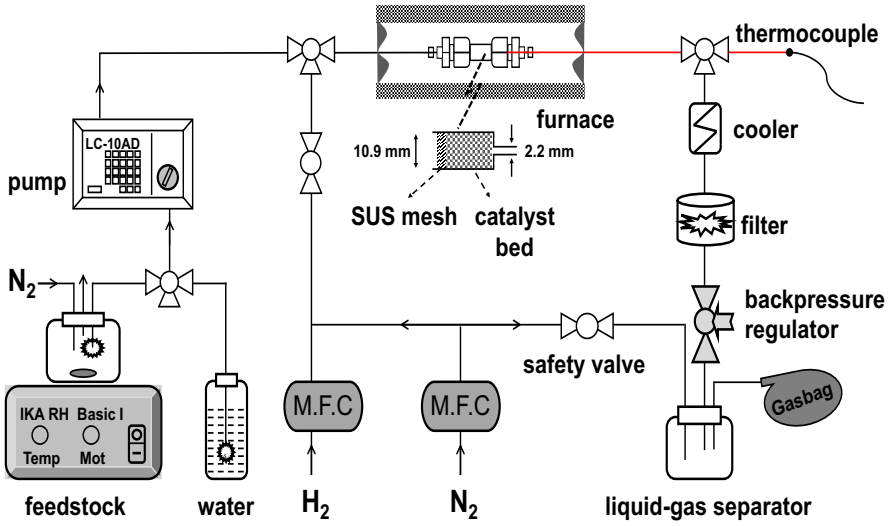

Figure 3.1. *Schematic diagram of the experimental setup for CHTG.*

was used as the feedstocks, unless otherwise stated. The degassed water was first supplied from the pump to the reactor with 20 MPa at a rate of 0.5 mL min^{-1}. After the temperature reached 350°C (heating rate; 10 °C min^{-1}), the water flow was kept for 40 min and then replaced by that of feedstock to start CHTG. In a typical run, the feeding rate and time were 0.5 mL min^{-1} and 40 min, respectively. The flow rate corresponded to weight hourly space velocities (WHSV, the carbon mass of reactant per mass of the catalyst) of 0.54, 0.60, 0.43 and 0.42 h^{-1} for LO, LRS, LCR and LHC, respectively. The effluent liquid that had passed through the cooling system was finally sent to a gas-liquid separator, where the entire portion of gaseous product was purged with 20 mL min^{-1} nitrogen flow away from the system and then collected in a gasbag. The gas composition was analyzed by gas chromatography. The effluent liquid was analyzed for measuring total concentrations of organic and inorganic carbons, TOC and IC, respectively.

3.3. Results and Discussion

3.3.1. Properties of aqueous phase of bio-oil

Biomass pyrolysis oils are unstable due to high content of oxygen functionalities that undergo aging during storage or handling. [1] GC/MS chromatograms of fresh LO and that after two weeks were compared in **Figure 3.2**. In both cases, GC/MS detected more than 88 compounds with carbon number ≤12, including acids, alcohols, ketones, phenols, aldehydes,

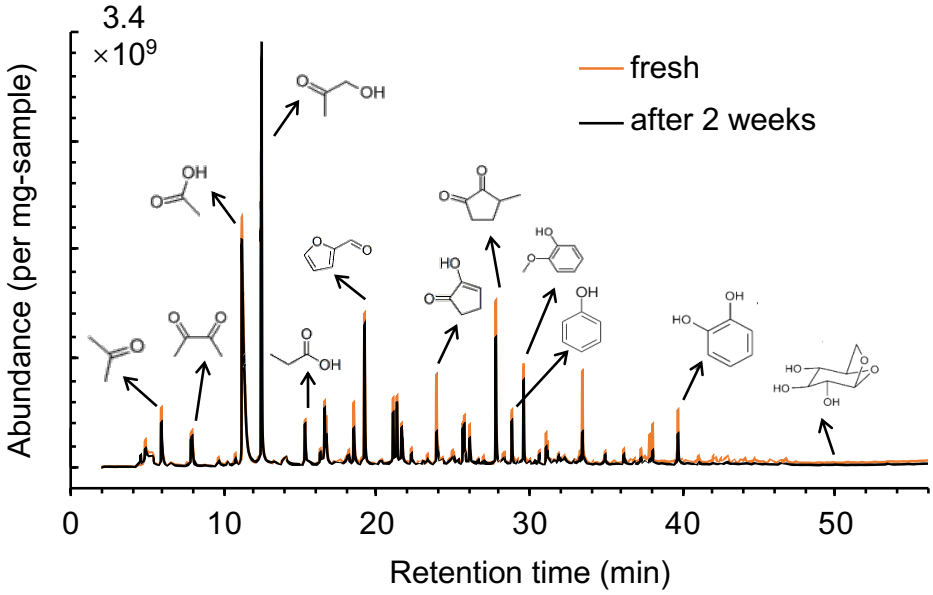

Figure 3.2. *GC/MS chromatograms of fresh LO and that after two-week storage at 5°C.*

carbohydrates and furans, most of which are typical ones and reported in the literature. The abundance (peak intensity) of those compounds, in particular, that of ketones, phenols and aldehydes, clearly shows a more or less decrease after storage. Although the thermochemical mechanism of the aging is not understood well, it is believed that ketones, phenols and sugars are involved in polymerization and condensation to form the water insolubles. [26] As a result of the aging, the TOC decreased by about 1% and fine brownish flakes formed in the storage. Considering the chemical evolution with time, the experiments are performed within 2 weeks since the preparation of LO.

Table 3.2 summarizes changes in pH, TOC, and concentrations of organic acids and AAEMs after the leaching. The low pH value of LO, 2.84, is primarily attributed to the presence of organic acids. Acetic and formic acids are the most abundant ones with individual contents of 361 and 3025 ppm, respectively, and contribute to 19% of TOC in total. The leaching leads to an increase in pH to 3.83 and 5.20 for LRS and LCR, respectively. This suggests the consumption of organic acids. The consumed acids are mainly related to the leaching of AAEMs. Substantial portions of those contained in biomass and its char are in forms of organically-bound cations (20–70% depending on sources). Their removal necessitates an acidic medium. [27] Such acid leaching results in a total of 1,840/4,720 ppm of AAEMs concentrated in LRS/LCR (mainly K species). LHC, as expected, contains no or very little AAEMs and will be a reference of LCR when studying the impact of AAEMs in the following CHTG tests.

Table 3.2. *Properties of LO, LRS, LCR and LHC.*

properties	LO	LRS	LCR	LHC
pH	2.84	3.83	5.20	2.86
TOC (ppm)	18040	21970	14450	14250
organic acid anions (ppm C)				
formate	361	334	341	337
acetate	3025	3252	3460	3006
AAEM species (ppm)				
Na	-	100	90	-
K	-	1460	4150	110
Mg	-	130	290	-
Ca	-	150	190	-

Results of quantification of AAEMs in the solid are presented in **Figure 3.3**, showing the percentages of the individual species leached from RS and char. LO removes 95% K, 87% Na, 80% Mg and 45% Ca from RS. The removal rates are comparable to previous studies that employed aqueous solutions of HCl and organic acids. [28,29] More than 90% of the K species in the char is removed, while the removal rate of Ca is much lower, only 37%. Nonetheless, the LO is still promising as a leaching agent because it exhibits the capability almost equivalent to the aqueous solution of HCl.

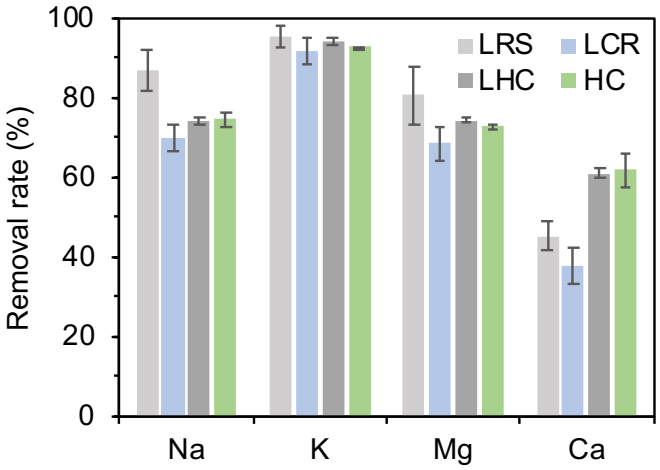

Figure 3.3. *Removal rates of AAEMs of RS or char with LO.*

Leaching of RS caused TOC of LO increased by 22%, indicating that a portion of organic matter was extracted by LO. Although not in-depth studied, acid-hydrolysis might be responsible for the extraction of some organic matter. On the contrary, TOC of LCR and LHC decreased by 20–21%. This reduction is reasonable in view of the high sorption (adsorption or/and absorption) capacity of biochar. [30] The leached char was later subjected to extraction with methanol and then GC/MS for back extraction of sorbed organic matter in LO. A chromatogram is provided in the **Supporting information**. The abundance of phenolic compounds elucidates their sorption by the char matrix. **Figure 3.4** displays the concentrations (in a unit of ppm C) of some representative compounds. Other types of compounds such as ketones and furans also decreased in the leaching with LCR/LHC. Besides, the quantified compounds accounted for only 36% of the total carbon of LO, and the remainder consisted mainly of not-quantified compounds and GC/MS-undetectable lignin and carbohydrate di/oligomers. [31] The GPC profiles shown in **Figure 3.5** confirmed the presence of di/oligomers with molecular weight ranging 200–1000. The abundance of such di/oligomers was significantly lower in LCR/LHC than in LO or LRS. It is in general

believed that the di/oligomers are thermally unstable and involved in catalyst deactivation in aqueous phase reforming. [12]

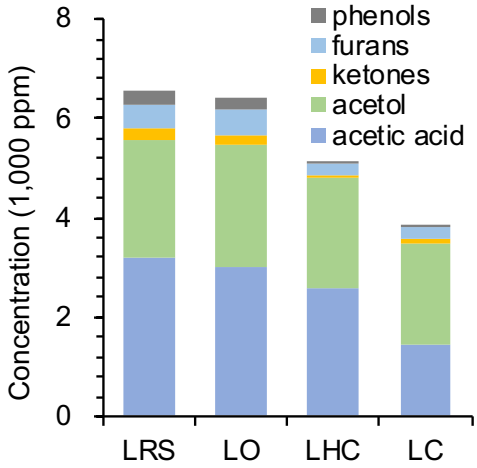

Figure 3.4. *Concentrations of the major compounds identified in GC/MS analysis of LOs.*

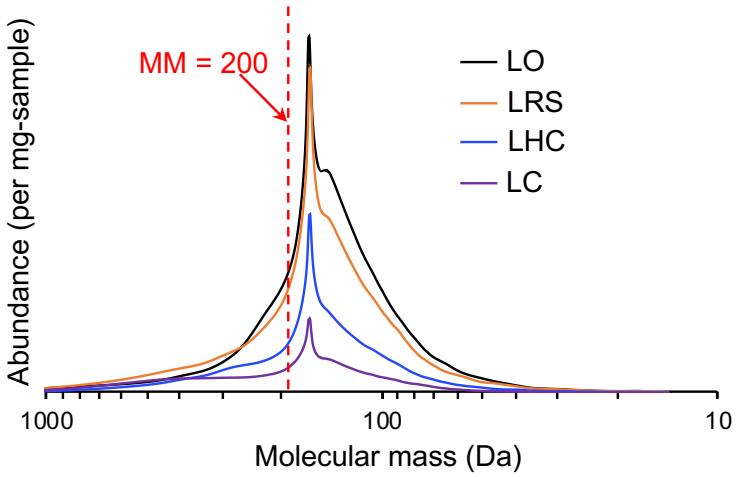

Figure 3.5. *Molecular mass distribution of LOs analyzed by GPC.*

3.3.2. Catalytic hydrothermal gasification of aqueous phase

Figure 3.6 shows the total carbon conversion, gas yields (on a carbon basis) and TOC of effluent liquid among four different feedstocks. CHTG with Ru/C converted the feedstocks to gases (H_2, CO_2, CH_4 and a small amount of C_2H_6 and C_3H_8) near completely leaving TOC as low as 20–150 ppm. The total carbon conversions to gas (C-gas) were around 99% for LO and LHC while slightly lower for LRS and LCR at 93% and 96%, respectively. The remaining carbon (3–6%) was probably due to the formation of carbonate species from CO_2 and Mg/Ca species.

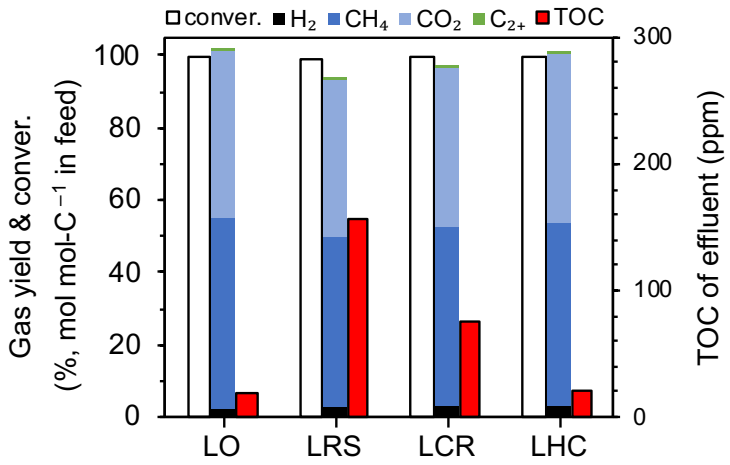

Figure 3.6. *Variations of carbon conversion, gas yields and TOC of effluent liquid among four feedstocks. Reaction conditions: 350°C, 20 MPa and reaction time; 40 min.*

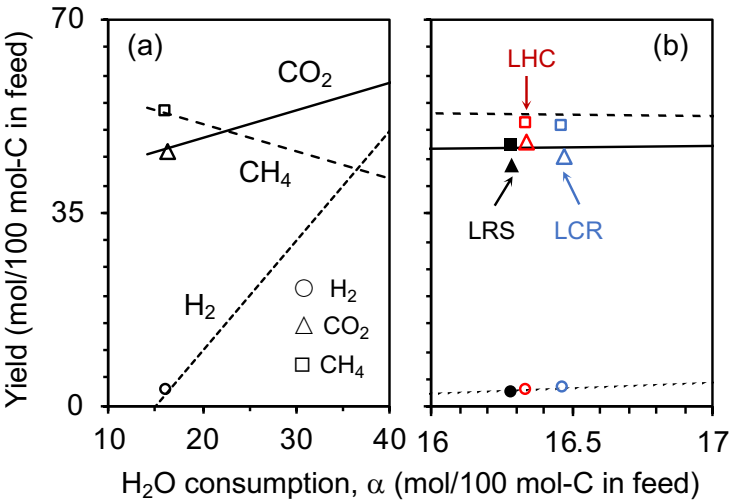

Figure 3.7. *Equilibrium gas yields calculated by eq. 1 for CHTG of (a) fresh LO and (b) spent LOs as a function of a. Open and closed symbols in each figure represent experimental yields.*

Davda et al. [32] concluded that CHTG of oxygenated hydrocarbons mainly involved the following reactions occurring in series and/or parallel; endothermic reforming to CO/H_2, water-gas shift to CO_2/H_2 and exothermic hydrogenation (methanation) reactions to CH_4. The product gas is determined largely by thermodynamics and therefore CHTG at low temperature (< 400°C) produces more CH_4 than H_2. The resulting gas compositions, shown in **Figure 3.6**, were as follows: 2.5–3.1% H_2, 47–53% CH_4 and 44–48% CO_2. Assuming that LO ($C_{100}H_{185.0}O_{77.7}$) was completely converted following the stoichiometry as represented by Equation (1), the theoretical gas yields can be calculated and drawn in **Figure 3.7(a)**, as

a function of *a*, chemical consumption of H_2O. As expected, the measured gas compositions fitted well to the calculated ones. It seems that regardless of the discrepancies between the feedstocks, the conversions of LRS, LCR and LHC roughly followed the stoichiometry, as seen in **Figure 3.7(b)**.

$$C_{100}H_{185.0}O_{77.7} + aH_2O \leftrightarrow\rightarrow xH_2 + yCO_2 + zCH_4 \qquad (1)$$

Figure 3.8 gives changes in carbon conversion and gas yield with the run number in sequential runs. The carbon conversions of LO, in Runs 1–4, were well above 95% but later decreased to around 73%. Such insufficient removal of TOC was apparent as the color of the effluent liquid gradually turned to yellow as shown in **Figure 3.9**. This evidenced catalyst deactivation resulting in a significant decrease in the C-gas from 95% to 61%. Meanwhile, the coke formation was found with a yield of 5.7% and 12.3% C (by difference) in Runs 4 and 5, respectively. The catalyst deactivation was also observed for LRS. The formation of more coke was presumably caused by more amounts of di/oligomers that were extracted from acid-catalyzed hydrolysis of RS. [12,15]

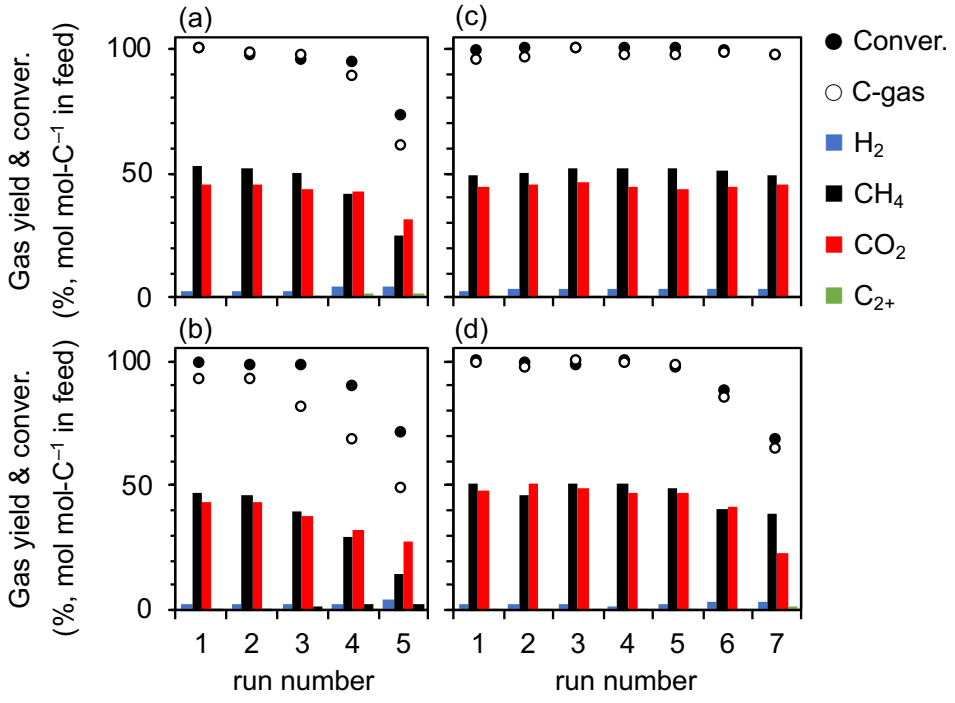

Figure 3.8. *Changes of carbon conversion and gas yield in CHTG of (a) LO, (b) LRS, (c) LCR, and (d) LHC as a function of run number. Reaction conditions; 350°C, 20 MPa and time on stream; 200–280 min.*

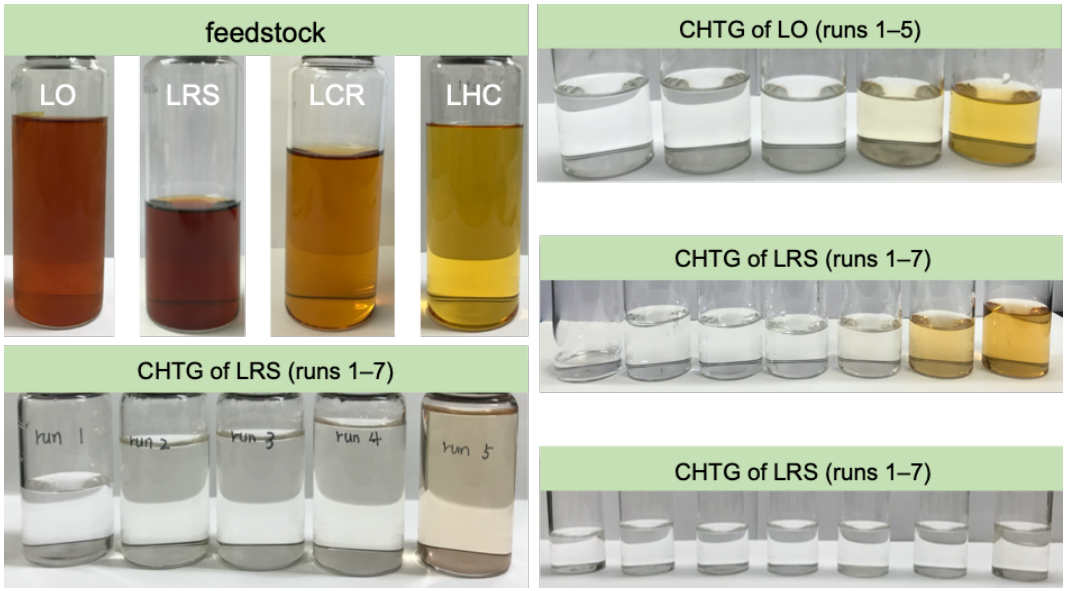

Figure 3.9. *Images of feedstocks and effluent liquids.*

The GC/MS analysis of the liquid effluent from Run 5 revealed the abundance of some particular oxygenated compounds including acetone, acetic acid, acetol, 2-methylcyclopentanone and cyclopentanone (see the **Supporting information**). The cyclopentanones are often key intermediates in the hydrothermal decomposition of glucose. [33,34] The deactivated Ru/C could hardly afford to the reforming of even these low-molecular sugar-compounds. To probe the catalyst activity, an aqueous solution of simulated APB was prepared by employing representative chemicals and used as a feedstock with a TOC of around 20,000 ppm. The Results in **Figure 3.10** clearly demonstrated the activity and durability of the Ru/C, which gasified the GC/MS-detectable compounds with almost

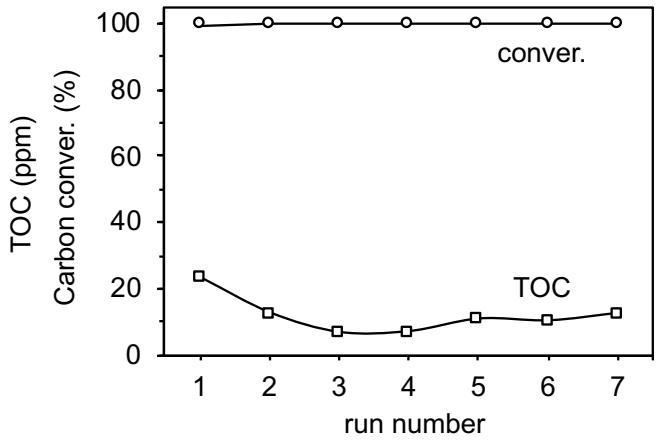

Figure 3.10. *Temporal changes in carbon conversion and TOC of effluent in CHTG of simulated LO. TOC; 20000 ppm, WHSV; 0.60 h^{-1}, and time on stream; 280 min.*

completely giving the colorless effluent liquid with TOC below 30 ppm. Earlier studies [35,36] reported that the deactivation of Pt/Ru catalysts is often in CHTG of model oxygenates such as AcOH. The high activity of Ru/C in this study is mainly due to the resistance of carbon support against phase change and its high surface area (1570 m^2/g).

On the other hand, the Ru/C maintained its the activity for at least 7 runs for CHTG of LCR in sequence. The carbon conversion and C-gas yield were both near steady around 99 and 97%, respectively. The improved performances as compared to LO/LRS was presumably contributed by multiple positive effects regarding the characteristics of LCR. The nature of the char (still abundance in oxygen functionalities) enabled interactions with -OH groups of phenolic compounds or sugar di/oligomers, forming hydrogen bonds and thereby inducing their adsorption. [30] This reduces the coke/char formation from the aqueous phase and catalyst deactivates in CHTG. The LO after using for the char leaching, *i.e.*, LCR, had a higher pH than initial and was also rich in AAEMs that stabilize molecules containing acidic -COOH and -OH groups as $-COO^-$ and $-O^-$. It is well known that phenolate and carboxylate have less tendency toward chemisorption onto the carbonaceous surface of the carbon support and also depolymerization into coke. [37] In addition, a lower feedstock TOC means smaller WHSV, which is generally favorable for a longer lifetime of the catalyst.

To reveal the role played by AAEMs played in CHTG of LCR, LHC that was freed from free from AAEMs was subjected to CHTG. It was believed that LHV had near identical organic compositions with LCR. As illustrated in **Figure 3.8(d)**, the carbon conversion maintained at 97% till Run 5 but decreased to 68% and further to 64% in the subsequent 2

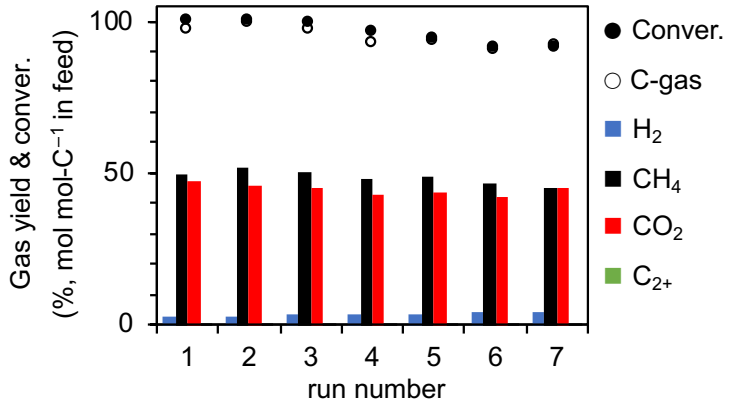

Figure 3.11. *Changes of carbon conversion and gas yield in CHTG of LHC/Na-K as a function of run number. Reaction conditions; 350°C, 20 MPa and time on stream; 200–280 min. Properties of feedstock solution; 120 ppm Na, 4100 ppm K, and pH, 4.61.*

runs. This evidences the catalyst deactivation. The catalyst performances are better that with LO but not so good as LCR. The positive role of AAEMs is thus demonstrated. CHTG runs of LHC, which employed CH_3COOK/CH_3COONa as alkali additives, were carried out. The results were displayed in **Figure 3.11**, clearly demonstrating a more stable catalytic activity by adding the alkali promoters. It is, however, noteworthy that CHTG of LHC occurs with no or very little coke even in Runs 5–7, in which coke-induced deactivation, if any, hardly occurred.

3.3.3. Catalyst characterization

In general, the activity loss of carbon-based catalyst is related to leaching/sintering/phase transformation of active metal or loss of catalyst surface area by coke deposition. The above-developed discussion suggests another deactivation mechanism in addition to coke deposition under the present conditions. This section provides characterizations of the fresh and spent Ru/C catalysts. **Table 3.3** lists Ru loadings and texture properties of the catalysts. The metal leaching is a common contributor to the activity loss but not a major one under the present conditions because the loss of Ru was not significant. The spent catalyst from CHTG of LRS shows the decrease in S_{BET} and V_p by 31% and 34%, respectively, which are mainly due to the coke deposition. The decrease of S_{BET} is ascribed to the insoluble carbonate species formed during CHTG. XRD patterns of the catalysts revealed neither phase change of the support nor significant change of crystallite sizes of Ru (**Figure 3.12**). An extra peak at 38° is noticed in the spent Ru/C after used for CHTG of LCR. The peak is assigned to calcite.

Table 3.3. *Texture properties of fresh and spent Ru/C.*

	S_{BET} (m^2/g)	W_p [a] (nm)	V_t (cm^3/g)	V_{micr} (cm^3/g)	metal (wt%)
fresh	1467	1.78	0.65	0.58	4.6
LO	1217	1.83	0.56	0.48	4.3
LRS	971	1.87	0.45	0.38	4.5
LCR	1200	1.79	0.53	0.47	4.2
LHC	1361	1.75	0.59	0.54	4.6

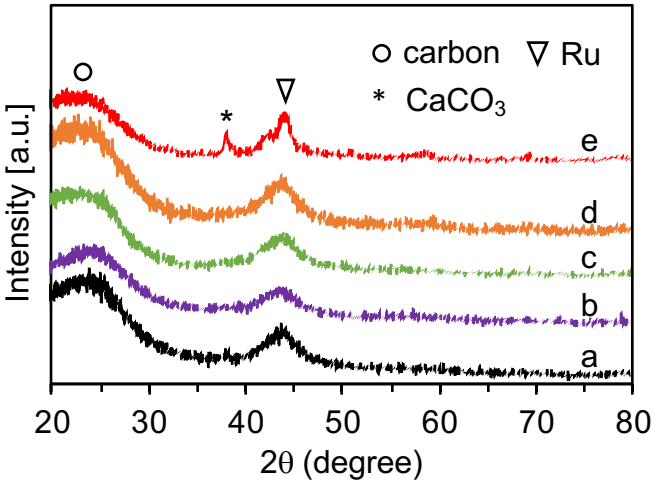

Figure 3.12. *XRD patterns of (a) fresh Ru/C and spent Ru/C catalysts in time-on-stream CHTG of (b) LO, (c) LRS, (d) LHC and (e) LCR.*

Representative TEM images of spent catalysts are presented in **Figure 3.13**. The size distributions of Ru particles were determined by measuring the sizes of more than 200 particles. The results in panels are different from those of XRD analysis, and this suggests changes in the size of Ru particles in CHTG. The fresh Ru/C had Ru nanoparticles (seen as dark grains) with sizes in a narrow range of 1.2–3.5 nm and a mean size (MS) of 2.3 nm.

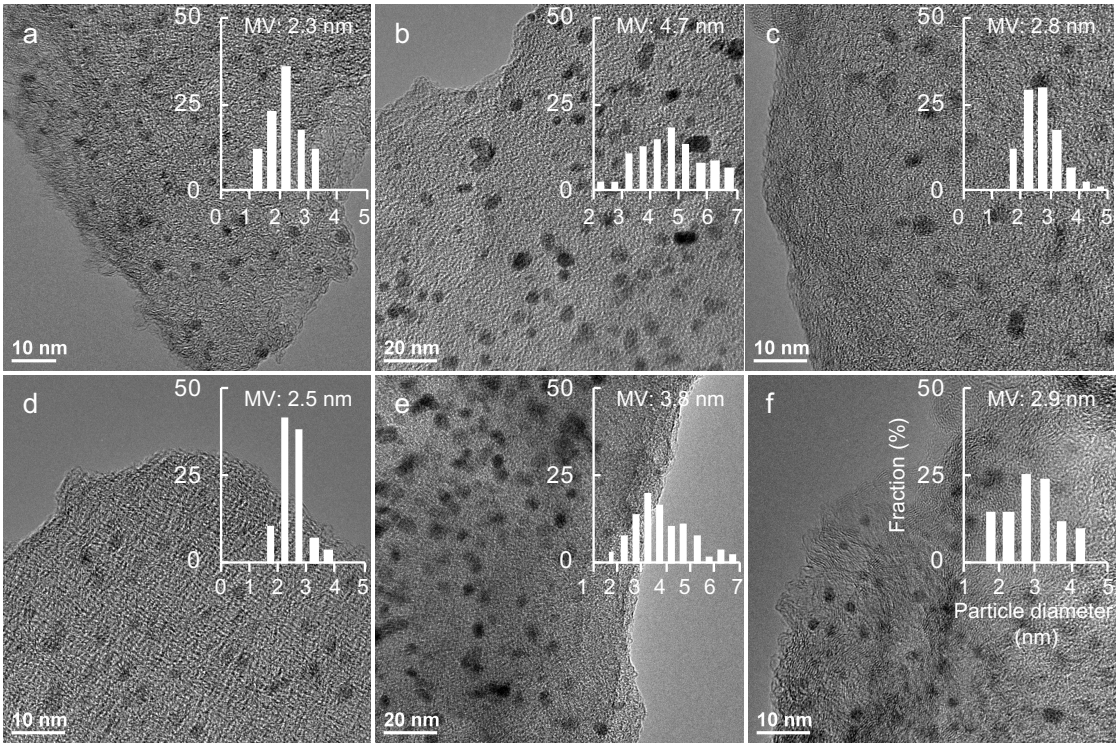

Figure 3.13. *TEM images and metal particle size distribution of (a) fresh Ru/C and spent Ru/C for time-on-stream CHTG of (b) LO, (c) LRS, (d) LCR, (e) LHC and (f) LHC/Na-K.*

Particle growth in size and agglomeration are observed in the spent catalysts from CHTG of LO and that of LHC with broad size distribution ranging up to 7.0 nm. Whereas, the increase in the size of Ru particles is insignificant for the other catalysts, with a MS of 2.5–2.9 nm. It is known that the activity of a catalyst (at a given metal loading) is inversely proportional to the active metal particle size, unless it is extremely small. [20] This explains well the lower activity of Ru/C in CHTG of LO/LHC, and also suggests another deactivation mechanism, *i.e.*, metal particle growth. AAEMs supposedly helped the Ru/C maintain its activity by suppressing agglomeration/growth of Ru particles. van Haasterecht et al. [38] investigated the activity of Pt or Ni supported on carbon nanofiber catalyst that was used for reforming of ethylene glycol. They attributed the catalyst deactivation to the growth in size of metal particles. They also showed that the deactivation was suppressed as pH approached 7. [39] In their opinion, during CHTG in acidic water, the metal undergoes oxidation, leaching and subsequent particles' growth via Ostwald ripening (particle coarsening). In the present work, the AAEMs may inhibit such particle growth by increasing the pH of feedstock liquid, but such a mechanism needs further confirmation and is left in the future study.

3.3.4. Evaluation of the process

Cold gas efficiency (CGE, in gross) is here defined as the ratio of higher heating value (HHV) of cold producer gas to that of the feed. According to Dulong's formula, HHV of the APB and LO, are 20.9 and 17.1 MJ kg^{-1} on a water-free basis, respectively, estimated from their elemental compositions (**Table 3.1**). The precipitation of little oil phase by the addition of water lowers the HHV by around 18%. CHTG of LO achieves 107% of CGE in the first

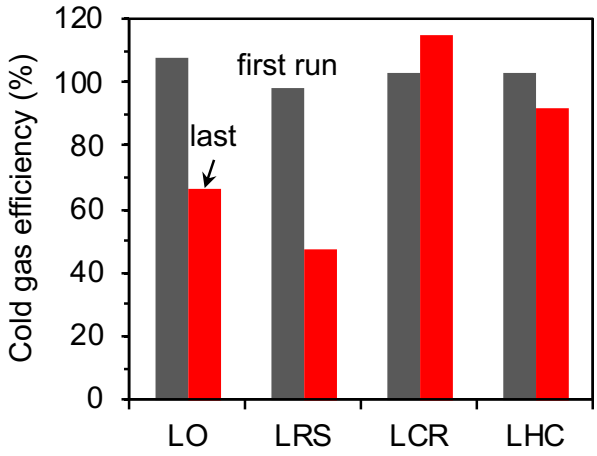

Figure 3.14. *Cold gas efficiencies of CHTG of LOs in the first and last runs.*

run, in good agreement with that expected from the stoichiometry of full conversion of LO (106.6%), but decreases to as low as 60% (Run 5). Assuming that the leaching causes little change in HHV, the CGEs for LRS, LCR and LHC are obtained and compared in **Figure 3.14**. The CGE obtained from LCR maintains the highest CGE of 104% in the last run among the four feedstocks. This efficiency is significantly greater than those with conventional gasification or catalytic steam reforming, in a range of 40–78%. [40-42]

3.4. Conclusions

LO is an excellent substitute for mineral acid such as HCl for leaching of AAEMs from RS and its char owing to the abundance of organic acids. Among the four feedstocks, CHTG with Ru/C converts LCR into CH_4-rich syngas with a CGE as high as 104%, which is maintained for seven runs in sequence. The catalyst deactivation in CHTG of LO is caused by the coke deposition and growth in size of Ru particles. AAEMs suppresses the particle growth, most probably by increasing the pH of LO. The proposed process enables removal of AAEMs and conversion of water-soluble pyrolytic organics into a fuel gas and clean water, providing a new method for utilizing biorefinery wastewaters.

3.5. References

[1] Mohan D., Pittman Jr C. U., Steele P. H. Pyrolysis of wood/biomass for bio-oil: A critical review. *Energy & Fuels* **2006,** 20, 848–889.

[2] Kan T., Strezov V., Evans T. J. Lignocellulosic biomass pyrolysis: A review of product properties and effects of pyrolysis parameters. *Renewable and Sustainable Energy Reviews* **2016,** 57, 1126–1140.

[3] Vitasari C. R., Meindersma G. W., De Haan A. B. Water extraction of pyrolysis oil: The first step for the recovery of renewable chemicals. *Bioresource Technology* **2011,** 102, 7204–7210.

[4] Sanna A., Vispute T. P., Huber G. W. Hydrodeoxygenation of the aqueous fraction of bio-oil with Ru/C and Pt/C catalysts. *Applied Catalysis B: Environmental* **2015,** 165, 446–456.

[5] Choudhary T. V., Phillips C. B. Renewable fuels via catalytic hydrodeoxygenation. *Applied Catalysis A: General* **2011,** 397, 1–12.

[6] Kruse A. Supercritical water gasification. *Biofuels, Bioproducts and Biorefining* **2008,** 2, 415–437.

[7] Peterson A. A., Vogel F., Lachance R. P., Fröling M., Antal J. M. J., Tester J. W. Thermochemical biofuel production in hydrothermal media: A review of sub- and supercritical water technologies. *Energy & Environmental Science* **2008,** 1, 32–65.

[8] Modell M., Reid R. C., Amin S. I. Gasification process. U.S. Patent 4,113,446, **1978.**

[9] Elliott D. C., Sealock Jr L. J., Baker E. G. Chemical processing in high-pressure aqueous environments. 2. Development of catalysts for gasification. *Industrial & Engineering Chemistry Research* **1993,** 32, 1542–1548.

[10] Elliott D. C., Phelps M., Sealock Jr L. J., Baker E. G. Chemical processing in high-pressure aqueous environments. 4. Continuous-flow reactor process development experiments for organics destruction. *Industrial & Engineering Chemistry Research* **1994,** 33, 566–574.

[11] Guan Q., Wei C., Savage P. E. Hydrothermal Gasification of *Nannochloropsis* sp. with Ru/C. *Energy & Fuels* **2012,** 26, 4575–4582.

[12] Vispute T. P., Huber G. W. Production of hydrogen, alkanes and polyols by aqueous phase processing of wood-derived pyrolysis oils. *Green Chemistry* **2009,** 11, 1433–1445.

[13] Behnia I., Yuan Z., Charpentier P., Xu C. Supercritical water gasification of aqueous fraction of pyrolysis oil in the presence of a Ni-Ru catalyst. *AIChE Journal* **2016,** 62, 2786–2793.

[14] Idesh S., Kudo S., Norinaga K., Hayashi J-i. Catalytic hydrothermal reforming of water-soluble organics from the pyrolysis of biomass using a Ni/carbon catalyst impregnated with Pt. *Energy & Fuels* **2012,** 26, 67–74.

[15] Chakinala A. G., Chinthaginjala J. K., Seshan K., van Swaaij W. P., Kersten S. R., Brilman D. W. Catalyst screening for the hydrothermal gasification of aqueous phase of bio-oil. *Catalysis Today* **2012,** 195, 83–92.

[16] Benson S. A., Sondreal E. A. Ash-related issues during combustion and gasification. In: Impact of mineral impurities in solid fuel combustion. *Springer* **2002**, 1-21.

[17] Karnowo, Zahara Z. F., Kudo S., Norinaga K., Hayashi J-i. Leaching of alkali and alkaline earth metallic species from rice husk with bio-oil from its pyrolysis. *Energy & Fuels* **2014,** 28, 6459–6466.

[18] Muangrat R., Onwudili J. A., Williams P. T. Influence of alkali catalysts on the production of hydrogen-rich gas from the hydrothermal gasification of food processing waste. *Applied Catalysis B: Environmental* **2010,** 100, 440–449.

[19] Onwudili J. A., Williams P. T. Hydrogen and methane selectivity during alkaline supercritical water gasification of biomass with ruthenium-alumina catalyst. *Applied Catalysis B: Environmental* **2013,** 132–133, 70–79.

[20] Azadi P., Afif E., Azadi F., Farnood R. Screening of nickel catalysts for selective hydrogen production using supercritical water gasification of glucose. *Green Chemistry* **2012,** 14, 1766–1777.

[21] Azadi P., Farnood R. Review of heterogeneous catalysts for sub- and supercritical water gasification of biomass and wastes. *International Journal of Hydrogen Energy* **2011,** 36, 9529–9541.

[22] Xiong H., Pham H. N., Datye A. K. Hydrothermally stable heterogeneous catalysts for conversion of biorenewables. *Green Chemistry* **2014**, 4627–4643.

[23] Yang H., Kudo S., Kuo H. P., Norinaga K., Mori A., Mašek O., Hayashi J-i. Estimation of enthalpy of bio-oil vapor and heat required for pyrolysis of biomass. *Energy & Fuels* **2013,** 27, 2675–2686.

[24] Kudo S., Goto N., Sperry J., Norinaga K., Hayashi J-i. Production of levoglucosenone and dihydrolevoglucosenone by catalytic reforming of volatiles from cellulose

pyrolysis using supported ionic liquid phase. *ACS Sustainable Chemistry & Engineering* **2017,** 5, 1132–1140.

[25] Yip K., Tian F., Hayashi J-i., Wu H. Effect of alkali and alkaline earth metallic species on biochar reactivity and syngas compositions during steam gasification. *Energy & Fuels* **2009,** 24, 173–181.

[26] Oasmaa A., Kuoppala E. Fast pyrolysis of forestry residue. 3. Storage stability of liquid fuel. *Energy & Fuels* **2003,** 17, 1075–1084.

[27] Zevenhoven M., Yrjas P., Skrifvars B. J., Hupa M. Characterization of ash–forming matter in various solid fuels by selective leaching and its implications for fluidized–bed combustion. *Energy & Fuels* **2012,** 26, 6366–6386.

[28] Wigley T., Yip A. C., Pang S. The use of demineralisation and torrefaction to improve the properties of biomass intended as a feedstock for fast pyrolysis. *Journal of Analytical and Applied Pyrolysis* **2015,** 113, 296–306.

[29] Zhang S., Su Y., Xu D., Zhu S., Zhang H., Liu X. Effects of torrefaction and organic–acid leaching pretreatment on the pyrolysis behavior of rice husk. *Energy* **2018,** 149, 804–813.

[30] Liu W. J., Zeng F. X., Jiang H., Zhang X. S. Preparation of high adsorption capacity bio-chars from waste biomass. *Bioresource Technology* **2011,** 102, 8247–8252.

[31] Vispute T. P., Zhang H., Sanna A., Xiao R., Huber G. W. Renewable chemical commodity feedstocks from integrated catalytic processing of pyrolysis oils. *Science* **2010,** 330, 1222–1227.

[32] Davda R., Shabaker J., Huber G., Cortright R., Dumesic J. A. A review of catalytic issues and process conditions for renewable hydrogen and alkanes by aqueous-phase reforming of oxygenated hydrocarbons over supported metal catalysts. *Applied Catalysis B: Environmental* **2005,** 56, 171–186.

[33] Williams P. T., Onwudili J. Composition of products from the supercritical water gasification of glucose: a model biomass compound. *Industrial & Engineering Chemistry Research* **2005,** 44, 8739–8749.

[34] Yin J., Cheng Z., Guo L., Li S., Jin H. Products distribution and influence of nickel catalyst on glucose hydrothermal decomposition. *International Journal of Hydrogen Energy* **2017,** 42, 4642–4650.

[35] de Vlieger D. J. M., Lefferts L., Seshan K. Ru decorated carbon nanotubes–a promising catalyst for reforming bio-based acetic acid in the aqueous phase. *Green Chemistry* **2014,** 16, 864–874.

[36] De Vlieger D., Mojet B., Lefferts L., Seshan K. Aqueous Phase Reforming of ethylene glycol–Role of intermediates in catalyst performance. *Journal of Catalysis* **2012,** 292, 239–245.

[37] Muangrat R., Onwudili J. A., Williams P. T. Influence of NaOH, Ni/Al_2O_3 and Ni/SiO_2 catalysts on hydrogen production from the subcritical water gasification of model food waste compounds. *Applied Catalysis B: Environmental* **2010,** 100, 143–156.

[38] Van Haasterecht T., Ludding C., De Jong K., Bitter J. Stability and activity of carbon nanofiber-supported catalysts in the aqueous phase reforming of ethylene glycol. *Journal of Energy Chemistry* **2013,** 22, 257–269.

[39] Van Haasterecht T., Ludding C., De Jong K., Bitter J. Toward stable nickel catalysts for aqueous phase reforming of biomass-derived feedstock under reducing and alkaline conditions. *Journal of Catalysis* **2014,** 319, 27–35.

[40] Zheng J. L., Zhu M. Q., Wen J. L., Sun R. C. Gasification of bio-oil: Effects of equivalence ratio and gasifying agents on product distribution and gasification efficiency. *Bioresource Technology* **2016,** 211, 164–172.

[41] Ghezelchi M. H., Wu H. Modelling of bio-oil steam gasification in a fluidized bed reactor. *Fuel* **2018,** 220, 575–585.

[42] Wang Z., Pan Y., Dong T., Zhu X., Kan T., Yuan L., Torimoto Y., Sadakata M., Li Q. Production of hydrogen from catalytic steam reforming of bio-oil using C12A7–O^--based catalysts. *Applied Catalysis A: General* **2007,** 320, 24–34.

Supporting information

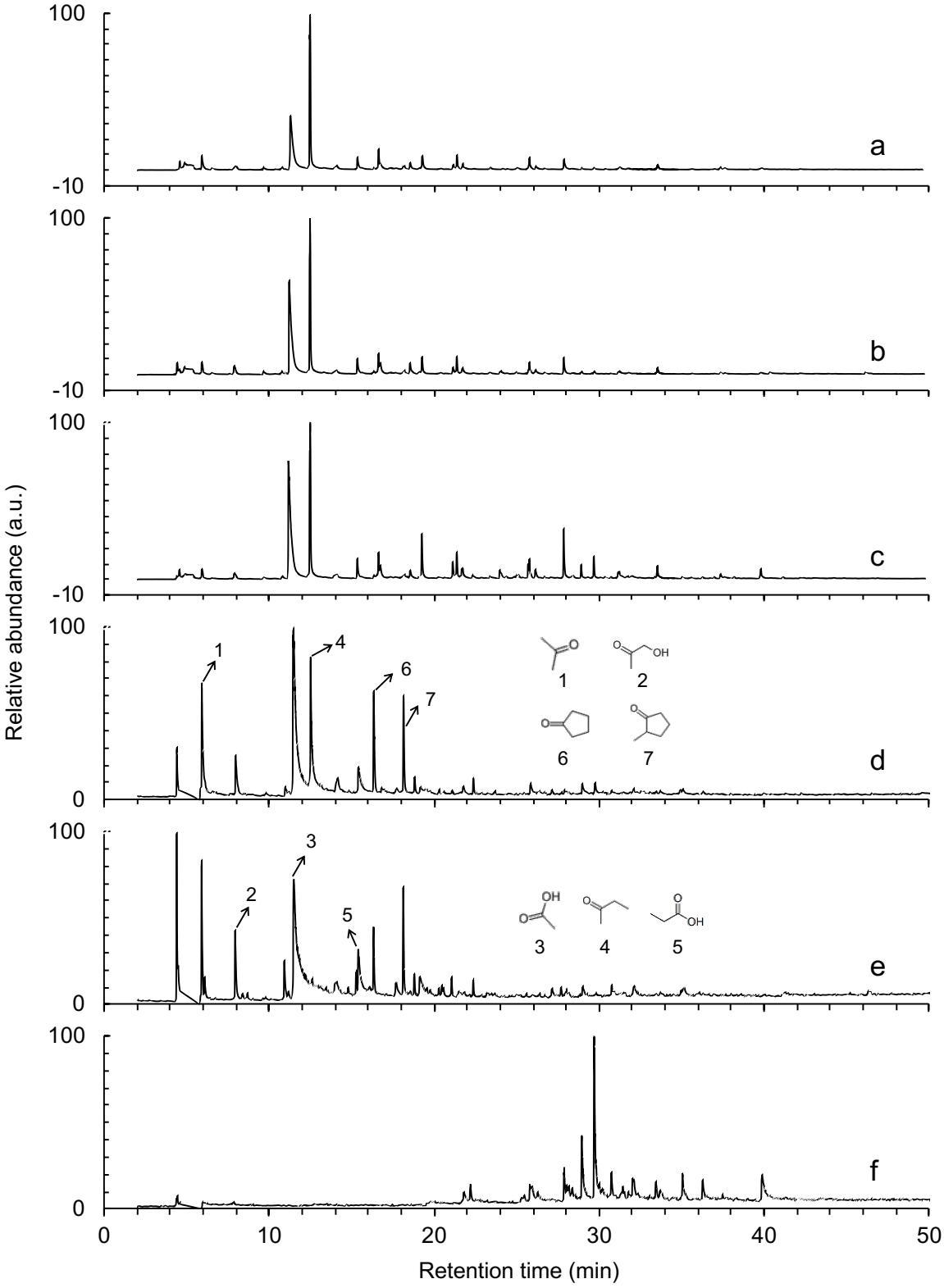

GC/MS chromatograms of (a) LCR, (b) LHC, (c) LRS, (d) effluent liquids in CHTG of LO (Run 5), (e) effluent liquids in CHTG of LRS (Run 5) and (f) methanol extract from the char after LO leaching.

CHAPTER 4

LEACHING OF CHAR WITH FULL RECYCLING OF PYROLYTIC AQUEOUS PHASE

4.1. Introduction

In response to greenhouse emission and depleting fossil fuel reserves, biomass and bio-based charcoal, as renewable energy sources, have been successfully tested with facilities and technologies ever developed for power/electricity generation from coal. [1] The inherent inorganic species in those solid fuels, in particular, alkali and alkaline earth metallic species (AAEMs), can be problematic in operating combustion and gasification, leading to agglomeration, deposition, corrosion and fine particulate matter emission. [2,3] To mitigate the ash-related problems, the removal of AAEMs is often required prior to the combustion or gasification. Numerous works [4–7] thus far have developed effective leaching approaches with an acidic medium such as mineral acids (*e.g.*, HCl and H_2SO_4) or organic acids (*e.g.*, AcOH). Use of these agents is technically feasible but not necessarily advantageous from both practical and economic perspectives, for example, with respect to the carryover of Cl or S that will end up in flue gas or/and char. The present authors [8] recently applied an aqueous phase of bio-oil from the pyrolysis of rice husk to the leaching of the parent biomass, which removed the majority of AAEMs. This leaching process has the advantage of no employment of additional agents external to the pyrolysis. Unlike mineral acids, the acidic aqueous phase is expected to be less corrosive to the used equipment, especially at elevated temperatures. A recent techno-economic study [9] evaluated the feasibility of using pyrolytic acid leaching as a pretreatment step in a biomass fast pyrolysis plant and revealed the potential of increasing pyrolytic sugar and heating oil yields and thereby the net economic value of the overall process.

Despite the above-mentioned benefits of using pyrolytic aqueous phase, there are still barriers associated with the leaching of biomass in several particular aspects. Typical drawbacks of biomass, as summarized in the literature, [10–12] are low bulk density, high hydrophilicity and poor grindability that necessitate power/energy-intensive steps for size reduction and moisture evaporation prior to and after leaching, respectively. A smaller size is favored by a lower intraparticle diffusion resistance during leaching, whereas the biomass grind is also time-consuming. In addition, a portion of organics is prone to migrate from biomass into the leachate during leaching with even water, which, to a more or less extent, increases the burden for wastewater treatment. In a process directed towards charcoal, the removal of AAEMs from biomass is far from desired due to their positive roles in the biochar formation via the catalyzed cross-linking reactions. [13,14] All these key issues hinder the

demineralization of raw biomass as a solid fuel for combustion or/and gasification. Alternatively, use of biochar instead of its parent for leaching may be a solution to the above issues. The biochar, a primary product of slow pyrolysis, is a promising solid fuel with high volumetric carbon and energy densities. [15] The excellent grindability of biochar overcomes the constraint of large particles. The hydrophobic nature enables a moisture content of less than 10 wt% by simple mechanical dewatering after leaching, significantly lower than that in biomass. It was also found that only a negligible amount of organic matter (< 0.2% of biochar carbon) was washed out by water because the pyrolysis transforms the organic structure of raw biomass into robust forms that are recalcitrant to water leaching. [16] On the other hand, biochar as a sorbent for inorganic and organic contaminant reduction in soil and water has been critically reviewed. [17,18] It is thus expected that the leaching of biochar with pyrolytic aqueous phase will ab/adsorb portions of organic compounds and thereby reduce the total organic carbon (TOC) of the solution.

While considerable efforts have been devoted to biomass leaching, only very limited studies are available on the leaching of AAEMs in biochar. A simple water wash [16, 19, 20] was reported to effectively remove AAEMs from various biomass feedstocks but less effective for biochar. In a series of studies on bioslurry fuels prepared from a woody biomass by suspending fast pyrolysis fine biochar particles in bio-oil, Wu et al. [21, 22] investigated the leaching characteristics of AAEMs from the biochar to the bio-oil during 29 days of stationary storage at room temperature. Substantial quantities of AAEMs was leached out following two-step reaction kinetics, *i.e.*, a rapid leaching step in the first 24 h and then a slow leaching step. The results suggested that the leaching of AAEMs was mostly attributed to the water-soluble fraction of the bio-oil, such as organic acids and phenolic compounds. Their further investigation on the adsorption behaviour of the bio-oil on the biochar showed that the latter selectively adsorbed heavy organic compounds, particularly those containing fused aromatics. [23] Caprariis et al. [24] performed batch leaching tests using pyrolysis wastewater and biochar produced from poplar biomass but with different temperatures and demonstrated the high sorption capacity of the biochar for organic carbons. The existing studies are in-detail but not necessarily applicable to a practical process in which a pyrolytic bio-oil (or its aqueous phase) is dedicatedly designed for washing char. More systematic research work is needed to take into account the real mass ratio of biochar and bio-oil produced in a plant and the recyclability of the bio-oil has also been scantly discussed in the literature.

In this study, we proposed a process that integrates pyrolysis, multistage condensation and leaching, as illustrated in **Scheme 4.1**. We, for the first time, systematically investigated the leaching of biochar with pyrolytic aqueous phase without discharge of the both. Once-through leaching and repeated leaching tests were performed focusing on the removal of AAEMs and the uptake of organic compounds onto the char.

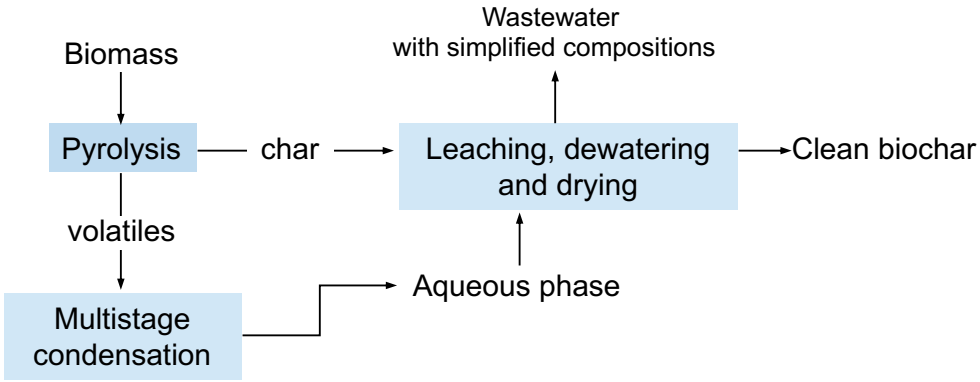

Scheme 4.1. *A flow diagram of the proposed process that leaches char with pyrolytic AP.*

4.2. Experimental Section

4.2.1. Preparation of pyrolytic aqueous phase and char

Chipped wheat straw with an average length of 1 cm was used as the starting biomass for the preparation of pyrolytic aqueous phase and char in a horizontal screw-conveyer (auger) reactor. The details of the reactor are described elsewhere. [25] Briefly, the chips had been dried overnight at 105°C and then, was fed into the pyrolyzer at a constant rate of 3.3 g min^{-1}, together with a nitrogen flow at 1.0 L min^{-1}. The heating rate and peak temperature were 5.3 °C min^{-1} and 450°C, respectively. The condensable liquids were collected at the reactor downstream with an aerosol filter (180°C) and three cold traps (0, –40, and –70°C) in series. As shown in **Table 4.1**, the pyrolysis enables a total recovery of the products of 103.2% on a dry-feedstock-mass basis.

Table 4.1. *Product yields from pyrolysis of wheat straw at 450°C (wt% of dry feedstock).*

	condensable liquid [a]			non-condensable gases						sum [b]
char	AP	LO	HO	H_2	CH_4	CO	CO_2	C_2H_4	C_2H_6	
30.8	33.4	8.1	11.1	0.03	0.27	5.40	13.92	0.08	0.10	103.2

[a] Condensable liquid was collected in a series of an aerosol filter (150°C) and three cold condensers (0, –40, and –70°C) located downstream of the reactor. [b] Sum of all the pyrolytic products.

The condensate at 0°C is a mixture of aqueous phase and oil phase that were separated from each other by centrifugation and then careful decantation. The oil (bottom phase), together with that deposited on the aerosol filter, was defined as heavy oil (HO) while those collected at –40 and –70°C were termed light oil (LO). The aqueous phase (AP), a water-thin liquid with a Karl–Fischer moisture and a pH value of 54 wt% and 2.3, respectively, was used for the leaching of char without dilution or enrichment. The yield of AP is higher than that of char by *ca.* 1.1 times. It was later suggested that such a proportion enables an internal recycle of the products, in other words, with neither discharge of AP nor that of char during the leaching.

4.2.2. Preparation of synthetic aqueous phase

Due to the unavailability of large-scale production of pyrolytic AP, an aqueous solution of representative components of that was prepared at the same concentrations as in AP and used for the leaching as the synthetic aqueous phase. The fifteen components are listed in **Table 4.2**. These compounds accounting for 74 wt% of AP (including water) were identified

Table 4.2. *Concentrations of the 12 compounds contained in pyrolytic AP,* synthetic *AP and aqueous solution of organic acids.*

compounds	concentration (wt%)		
	pyrolytic AP	synthetic AP	organic acids
HCOOH	3.40	3.40	3.30
AcOH	12.00	12.70	12.70
phenol	0.09	0.08	
o-cresol	0.03	0.02	
4-ethylphenol	0.02	0.02	
guaiacol	0.24	0.20	
creosol	0.08	0.06	
4-ethylguaiacol	0.05	0.05	
furfural	0.70	0.60	
5-methylfurfural	0.09	0.08	
2(*5H*)-furanone	0.34	0.36	
2,3-butanedione	0.70	0.50	
acetol	2.20	1.90	
2-methyl-2-cyclopentenone	0.06	0.05	
water	53.98	79.98	84.00
total	73.98	100.00	100.00

by gas chromatography-mass spectrometry on a PerkinElmer mode (Clarus SQ 8) and further quantified using a gas chromatograph coupled to a flame ionization detector (GC-FID, Nexis GC-2030, Shimadzu) while the HCOOH was analysed with a high-performance liquid chromatograph (LC-20 prominence, Shimadzu). A capillary column, TC-1701 (GL Science Inc., i.d. 0.25 mm, length 60 mm), was used for the gas chromatography. The conditions were as follows: carrier gas, helium (purity > 99.9999 vol%); carrier gas flow rate, 1.0 mL min^{-1}; split ratio, 20; temperature of injection port, 250°C; temperature program, holding at 40°C for 5 min, heating at 4 °C min^{-1} to 270°C, holding at 270°C for 20 min, and then cooling. The major compounds were calibrated by using individual standard samples.

4.2.3. Leaching of char with aqueous phase

Prior to leaching tests, the char was pulverized to a particle size of 53–212 μm for minimizing the intraparticle diffusion resistance. The water-soluble and HCl-soluble AAEMs of the char were first determined. The char was washed with ultrapure water (resistivity > 18.2 MΩ.cm) or an aqueous solution of HCl (0.1 M) under the following conditions: temperature, 25°C; liquid/solid mass ratio, 250; time, 24 h. The contents of AAEMs in solid chars were then measured. [26] A total of about 10 mg of the solid was heated at a very slow rate of 1 °C min^{-1} to 600°C. The ashed sample was digested in an equivolume mixture of HF/HNO_3 (1:1, mol/mol) solution at 60°C for 12 h and then evaporated to dryness and finally dissolved in a known volume of 2 mM methanesulfonic acid solution. The solution was analysed with an ion chromatograph (IC, LC-10A, Shimadzu), on a Shim-pack IC-C4 column and detected with a conductivity detector (CDD 10Avp, Shimadzu).

Once-through leaching of the char with pyrolytic AP, synthetic AP or ultrapure water (as a blank reference) was carried out at ambient temperature in a batch mode. An aqueous solution of HCOOH and AcOH, the major organic acids contained in AP, was also prepared for the leaching, which aims to illustrate the role of other organic components. The concentrations are available in **Table 4.2**. Typically, a given amount of the solution and the char (approximately 0.5 g) were charged into an airtight glass bottle with a liquid-to-solid of 20, the lowest mass ratio for a homogenous slurry. The mixture was agitated in a thermostatic water-bath shaker (SN-60SD, Nissin) for a period of 0.25–24 h, and then filtrated through a 0.45 μm PTFE membrane filter to separate the residual solid from the leachate. The leachate was subjected to analyses by IC and GC-FID for the concentrations of AAEMs and the major

compounds, respectively. The concentration of total organic carbon (TOC) was measured using a Shimadzu TOC-V_{CPH} equipment. The removal rates of AAEMs, *i.e.*, the percentages of those leached from the char, were defined as the amounts of AAEMs in the leachate by those in the char.

Repeated leaching of the char serves to investigate the durability of synthetic AP. This set of tests was performed by recycling synthetic AP up to ten times under the same conditions as once-through leaching but for a fixed period of 1 h. It has been demonstrated that the leaching process almost reaches equilibrium within 1 h, that is to say, no further increase in the contents of TOC and AAEMs of leachate. To start with the sequential ten runs, fresh synthetic AP was used in the first run. After filtration, the used synthetic AP was employed in the next run for leaching fresh char. In each run, the leached char and a very small fraction of the used synthetic AP were subjected to analysis.

4.3. Results and Discussion

4.3.1. Once-through leaching of char

4.3.1.1. Removal of AAEM species from char

Figure 4.1 compares the removal rates of AAEM species leached by pyrolytic and synthetic APs for 24 h at a liquid-to-solid mass ratio of 20. The total concentration of organic acids contained in synthetic AP is as high as 16.1 wt%, which was out of the measurement range of a general pH electrode. The pH value of the pyrolytic AP, calculated following a previous method, [8] is 1.9, slightly lower than that of synthetic AP. Both APs exhibited near-equivalent leaching performance regardless of the differences in both pH values and chemical compositions. Major portions of Na, K, Mg and Ca were washed out in both cases with a rate of *ca.* 94, 76, 68 and 78%, respectively. The comparable leachability of synthetic AP was thus evidenced, demonstrating its validation as a counterpart of pyrolytic AP for leaching char. It was, therefore, decided to use the synthetic AP as the alternative leaching agent that was referred to as “pyrolytic AP” through the following sections. Because the char has an extremely low fraction of Na (5% of total AAEM species) and the removal of that reaches a high rate of 93% (by synthetic AP) within 0.25 h merely, the results on Na species will not be involved in later discussion.

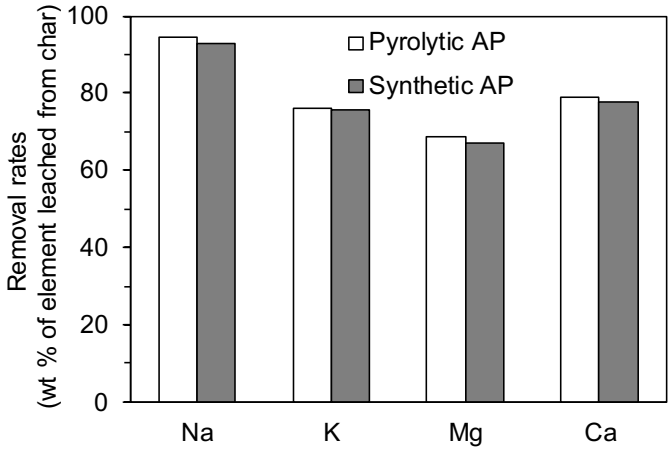

Figure 4.1. *Removal rates of AAEM species leached by pyrolytic AP and synthetic AP for 24 h at a liquid-to-solid mass ratio of 20.*

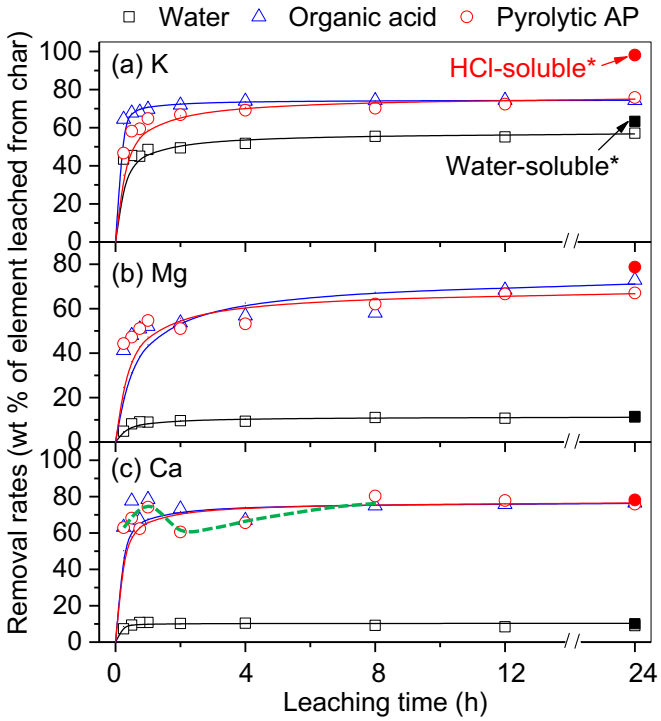

Figure 4.2. *Time-dependent changes in the removal rates of (a) K, (b) Mg, and (c) Ca by leaching with water, organic acid, and pyrolytic AP at a liquid-to-solid mass ratio of 20. Scatter points represent experimental data while the solid lines are derived from fitting with pseudo-second order model (kinetic parameters shown in* ***Table 4.3****). *Solid red circle and black square indicate HCl-soluble and water-soluble AAEM species, as determined by leaching with 0.1 M HCl solution and water, respectively (liquid-to-solid mass ratio: 250; leaching time: 24 h).*

Table 4.3. *Fitted pseudo-second-order kinetic parameters for the removal of K, Mg, and Ca from char via leaching with water, organic acid, and pyrolytic AP.*

kinetic parameters	water			organic acid			pyrolytic AP		
	K	Mg	Ca	K	Mg	Ca	K	Mg	Ca
C_s (g/L)	0.753	0.010	0.021	0.98	0.065	0.155	0.998	0.06	0.156
k_1 (L/g/h)	5.503	280.054	946.174	19.852	22.89	49.165	3.458	37.764	38.828
h_1 (g/L/h)	3.120	0.028	0.414	19.048	0.097	1.184	3.441	0.138	0.945
R^2	1.000	0.999	1.000	1.000	0.994	1.000	0.999	0.998	0.998

C_s: equilibrium concentration in leachate; k_1: second-order leaching rate constant; h_1: initial leaching rate at ~0 h; and R^2: correlation coefficient.

Once-through leaching of char for a duration of 24 h was performed to study the leaching kinetics with pyrolytic AP as well as water and organic acid. It was found in **Figure 4.2** that the removal of AAEM species leached by the three agents is rapid in the first hours and then becomes slow towards equilibrium. This trend coincides well with the reduction in the concentration of acetic acid. As shown in **Figure 4.3**, the acetic acid quickly decreased the concentrations within the first hour from 137 to 85 g/L and remains almost unchanged at 4–24 h with an average of 74 g/L. Taking into consideration the total amount of AAEM species leached by pyrolytic AP, such a consumption as much as 46% of initial acetic acid is most probably involved in not only the stabilization of those species but also the carryover of char. By fitting the experimental data to pseudo-second-order model, a good fit was observed for individual species, suggesting that the model well describes the leaching kinetics expect for Ca leached by pyrolytic AP. The fitted kinetic parameters were summarized in **Table 4.3**. Clearly, the non-acid compounds contained in pyrolytic AP has a more or less effect on the

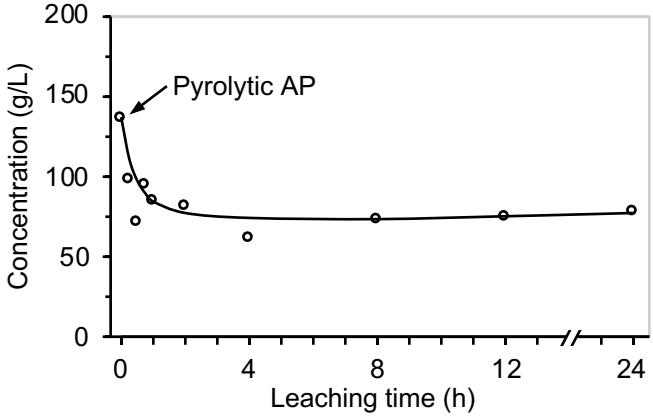

Figure 4.3. *Time-dependent changes in the concentration of AcOH in leachate during pyrolytic AP leaching.*

overall leaching rate constants (k_1) and initial leaching rates (h_1) of AAEMs while leads to negligible changes in equilibrium concentrations (C_s) of those species. This will be in detail discussed for each species.

K is the most abundant AAEM species in raw char. Under equilibrium, the rates of K species leached by acid media (*i.e.*, organic acid/pyrolytic AP) are significantly higher than that by water (74/76 *versus* 57%, **Figure 4.2**). This is attributed mainly to the leaching of organically associated species that are ion-exchanged to acidic oxygen functionalities, in addition to those in water-soluble form. [27, 28] From the parameters presented in **Table 4.3**, k_1 and h_1 of pyrolytic AP are significantly lower than those of organic acid, and a longer time is needed to reach equilibrium for the former, indicating a negative role of non-acidic compounds on the leaching of K. Zhang et al. [22] investigated the leachability of bio-oil model compounds and found that phenolic compounds promoted the leaching of AAEM species while the low-dielectric-constant compounds such as ketones and alcohols hindered AAEM leaching. In the case of K, the hindering effects dominates. However, such an adverse impact seems to diminish with time. It should also be noted that the equilibrium removal of K by pyrolytic AP is far less than the HCl-soluble amount of that (98%). This is a result of the smaller liquid-to-solid mass ratio employed for leaching (20 for pyrolytic AP *versus* 250 for HCl solution). Under such a low ratio, K that had been leached out may re-deposit onto the char surface. [29]

As is the case with K, the leaching of Mg by the agents shows similar trends, levelling off within the first hour. Pyrolytic AP removes majority portions of Mg from char, the rate of which almost approaches the HCl-soluble Mg species. As comparison to the leaching characteristics with organic acid, no specific impacts of other organic compounds were identified on the leaching of Mg. This is confirmed by the roughly same kinetic parameters for pyrolytic AP and organic acid. A similar phenomenon, *i.e.*, leaching kinetics and little influence by non-acidic organic compounds, was also observed for Ca. It is, however, found that the Ca removal shows an apparent reduction after 1 h for both pyrolytic AP and organic acid. Although not investigated in detail, it is believed that some organic matter such as oxalate was leached out from char and in turn, resulted in the redeposition of Ca species as oxalates onto the char surface. [30] In terms of leaching kinetics of K, Mg and Ca, the time for pyrolytic AP leaching was optimized at 1 h.

4.3.1.2 uptake of water-soluble organics by char

The porous structures and abundant surface functional groups offer the possibility of biochar as a modification-free sorbent for the removal of organic pollutants. [15] **Figure 4.4** displays the uptake of the representative organics contained in pyrolytic AP, as a function of leaching time. These compounds show a common trend which is initially rapid and followed by a slower uptake toward equilibrium. The pseudo-second-order model reasonably described the uptake kinetics. **Table 4.4** listed the fitted kinetic parameters, proving a new

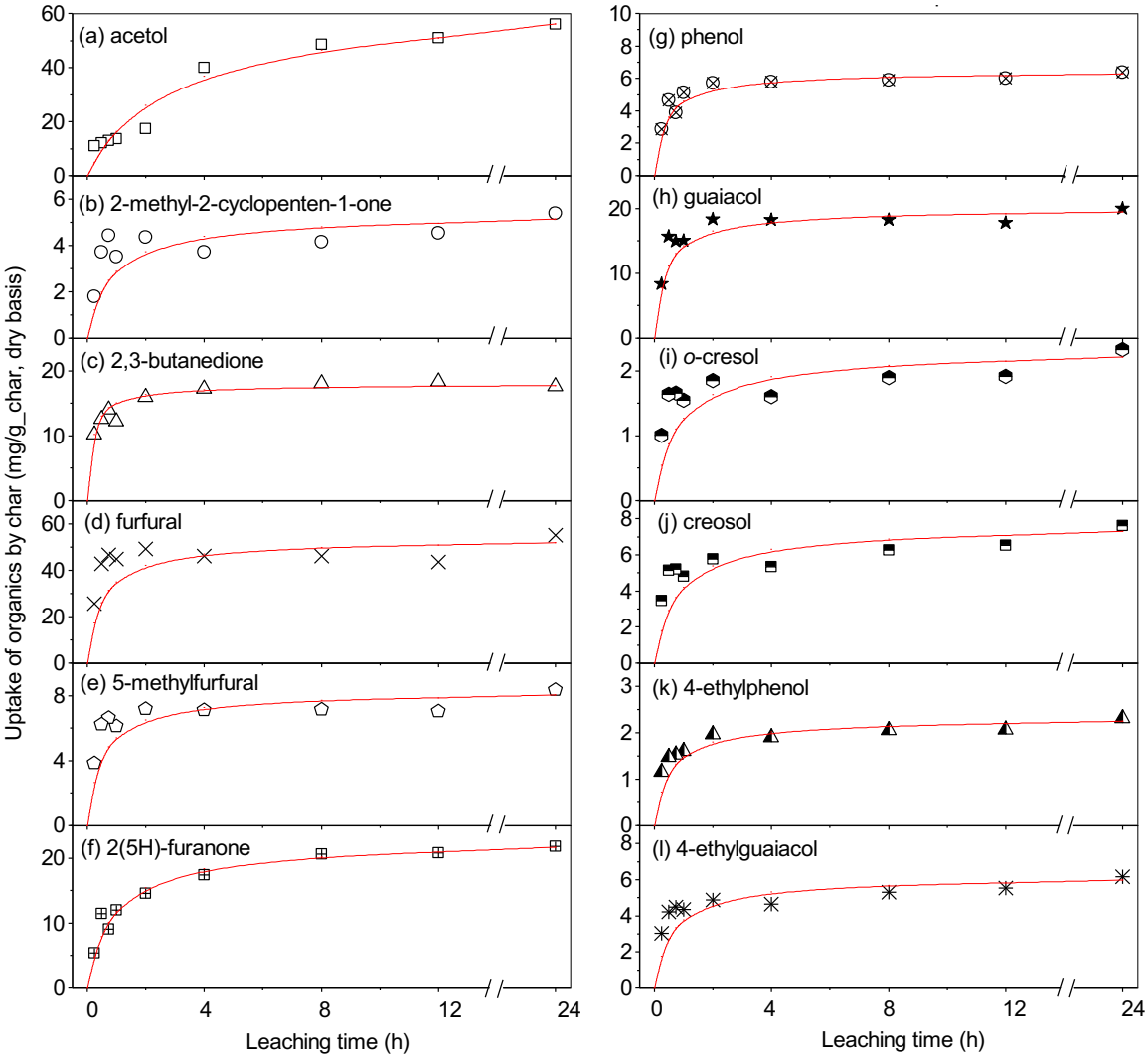

Figure 4.4. *Time-dependent changes in the uptake of (a) acetol, (b) 2-methyl-2-cyclopenten-1-one, (c) 2,3-butanedione, (d) furfural, (e) 5-methylfurfural, (f) 2(5H)-furanone, (g) phenol, (h) guaiacol, (i) o-cresol, (j) creosol, (k) 4-ethylphenol, and (l) 4-ethylguaiacol by biochar. Scatter points represent experimental data while the solid lines are derived from fitting with pseudo-second order model (kinetic parameters shown in* ***Table 4.4****).*

information on this kind of complex leaching system. As seen, acetol, 2-methyl-2-cyclopenten-1-one and 2(*5H*)-furanone have a small k_2 (i.e., overall uptake rate constant) and therefore take 4 h or more to reach equilibrium, whereas other compounds, in particular, phenolic compounds, within less than 2 hours. The equilibrium uptakes of phenols, guaiacols and furfurals are 11, 34 and 85 mg/g-char, respectively, corresponding to 40–58% of their initial contents. Liu *et al.* [31] studied the adsorption of phenol onto rice husk/corncob-derived chars and proposed the adsorption mechanism by which the oxygen-containing functional groups (*e.g.*, –OH and –COOH) interacted with phenol *via* hydrogen bonding. The solution pH is one of the major factors influencing the adsorption capacity of phenolic compounds. At acidic pH values, phenols chiefly exist as not phenolate anions but molecules that are preferentially adsorbed on the char surface. [32, 33]

Table 4.4. *Fitted pseudo-second-order kinetic parameters for the uptake of organics by char.*

compounds	kinetic parameters			
	q_e (mg g^{-1})	k_2 (g mg^{-1} h^{-1})	h_2 (mg g^{-1} h^{-1})	R^2
acetol	62.893	0.006	22.422	0.980
2-methyl-2-cyclopentenone	5.322	0.224	6.357	0.987
2,3-butanedione	17.921	0.299	96.154	0.999
furfural	53.191	0.036	103.093	0.986
5-methylfurfural	8.217	0.235	15.873	0.992
2(*5H*)-Furanone	22.573	0.049	24.752	0.999
phenol	6.394	0.408	16.694	0.999
guaiacol	19.841	0.130	51.020	0.997
o-cresol	2.294	0.545	2.869	0.987
creosol	7.576	0.166	9.506	0.991
4-ethylphenol	2.307	0.796	4.237	0.997
4-ethylguaiacol	6.154	0.261	9.901	0.995

q_e: equilibrium uptake of organic compound ad/absorbed by char; k_2: pseudo-second-order rate constant, h_2: initial uptake rate at ~0 h; and R^2: correlation coefficient.

4.3.2. A new process for leaching char with aqueous phase

In practice, both percolation leaching systems and countercurrent extractors [13] are applicable for leaching char with pyrolytic AP. These two options however require a considerable amount of process water due to the low mass ratio of pyrolytic AP and char (~1.1 as shown in **Table 4.1**), increasing both water consumption and the burden for wastewater treatment. Here, we propose a new system that consists of two continuous

stirred-tank reactors (CSTRs): one for leaching and the other for rinsing (**Figure 4.5**). The system can be operated in two modes: mode A for repeated leaching and rinsing; and mode B for draining wastewater as well as diluting both leaching and rinsing agents. To start up mode A, pyrolytic AP is first accumulated in the leaching reactor, without adding char in. The char produced at this stage is not leached, the quantity which is negligible compared to that generated from subsequent steady-state operation. The newly produced char with mass flow of m_{char} (t/h, dry basis) is fed into the leaching reactor when the accumulated pyrolytic AP reaches a certain quantity that enables homogeneous mixing of AP/char slurry. When the desired leaching time is reached, the slurry is delivered to a dewatering unit for phase separation, after which liquid is recycled back to the leaching reactor and dewatered wet char is subjected to the rinsing reactor (pre-filled with water) to further remove the inorganic

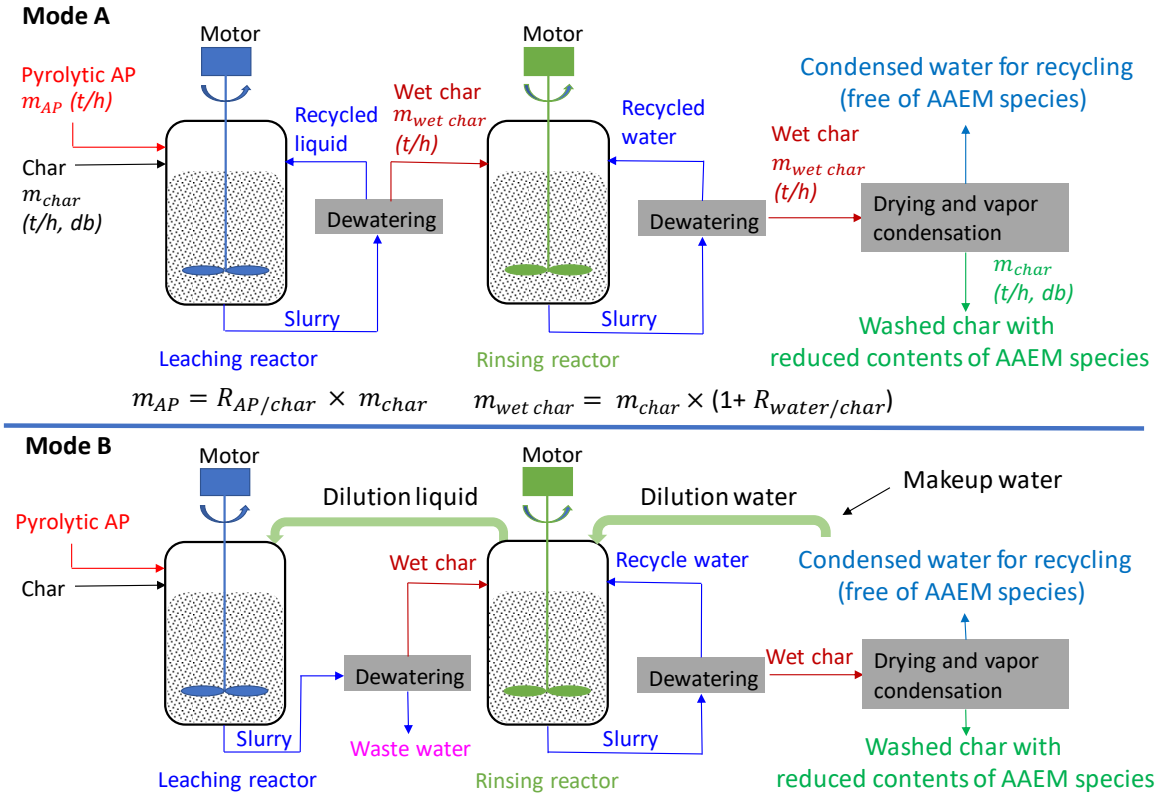

Figure 4.5. *Schematic diagram of the proposed system for leaching char with pyrolytic AP. For the simplicity of concept explanation, mass flow of dry char, m_{char}, is assumed to be unchanged before and after leaching. $R_{AP/char}$ represents mass ratio of pyrolytic AP and char, as determined by pyrolysis process. $R_{water/char}$ stands for the mass ratio of water retained in char after dewatering to dry char. The number of rinsing reactor may be more than one, depending on the desired AAEM concentrations in the washed char.*

species dissolved in the water retained in char. The mass of water retained after vacuum filtration is equal to 1.1 times the mass of char. This exactly matches the mass ratio of pyrolytic AP and char, as determined from pyrolysis. In other words, the liquid-to-solid ratio in the leaching reactor is maintained and thus continuous operation is achieved. Similar to that for the leaching reactor, the water/char slurry is dewatered, with surplus water being recycled back to the rinsing reactor and dewatered wet char being subjected to drying. After drying, the dry char with reduced contents of AAEMs is obtained. The water vapor is condensed to recover water, which is free of AAEMs, for further recycling.

Repeated leaching or rinsing may lead to the concentrations of AAEMs (in particular K) in the being saturated and thereby the failure of further removal of these inorganic elements. This condition triggers mode B operation, in which wastewater with saturated concentrations of AAEMs is drained from the leaching reactor. Same amount of dilution liquid is taken from the rinsing reactor to reduce the AAEM concentrations and maintain the liquid-to-solid ratio in the leaching reactor. The water lost in the rinsing reactor is compensated by the condensed water and makeup water (if the former is insufficient). In this way, both process water consumption and wastewater discharge are minimized.

4.3.3. Proof of concept *via* leaching of char with spent aqueous phase

To experimentally demonstrate the proposed leaching process, repeated leaching of "fresh" char with leachate from the last run was carried out. To leach char with mass flow of m_{char} using pyrolytic AP with mass flow of $1.1 \times m_{char}$ (as determined by the pyrolysis process), ~18 runs are required at the liquid-to-solid mass ratio of 20. However, due to the constrains on both time and available sample size, we performed 10 repeated leaching runs to answer two essential questions. One is the ability of leaching agent to remove AAEMs during repeated leaching. The other is to assess how much water-soluble organics can be captured by char.

Figure 4.6 presents the concentrations of AAEMs in the leachates from repeated leaching runs. Interestingly, the concentrations of K, Mg, and Ca increase linearly (with R^2 of 0.999) from 880, 40, and 137 mg/L in the leachate from run 1 to 8451, 393, and 1242 in that from run 10, respectively. There are no reductions in the slopes for all the elements, indicating that even the leachate from run 9 is as effective as the fresh pyrolytic AP in removing AAEMs from char. This is further confirmed by **Figure 4.7**, in which the removal rates of K, Mg, and Ca in char are plotted as a function of the concentrations of these elements in

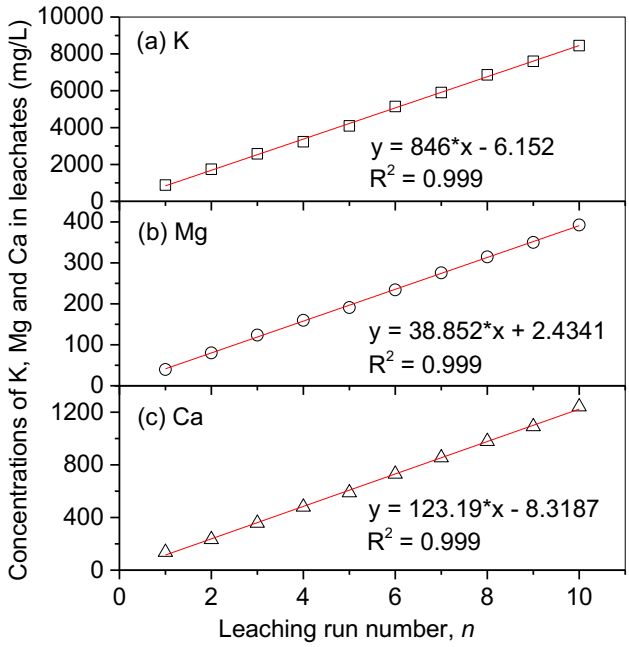

Figure 4.6. *Concentrations of AAEMs in the leachates from repeated leaching runs as function of run number and concentration, respectively.*

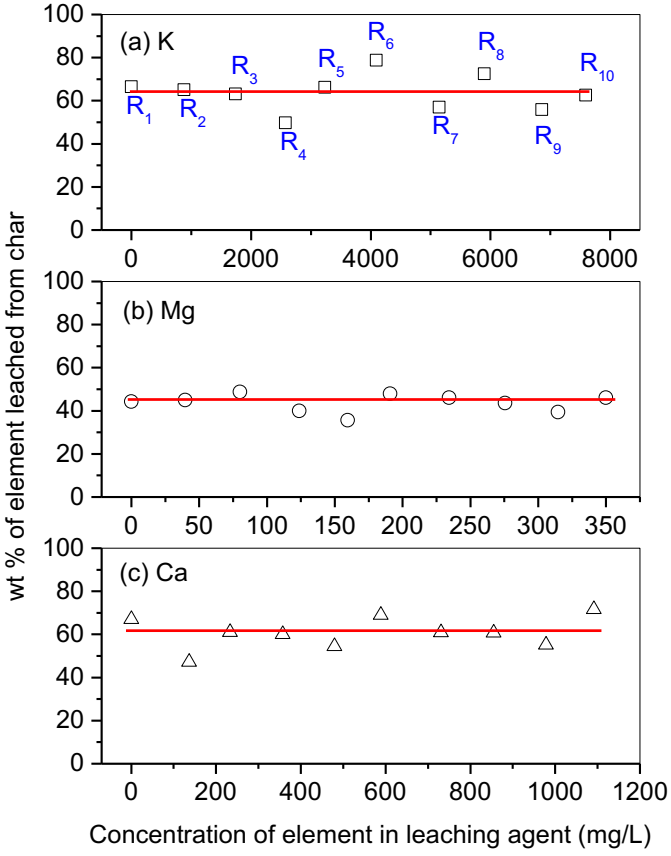

Figure 4.7. *Removal rates of AAEMs in the leachates from repeated leaching runs as function of run number and concentration, respectively.*

the corresponding leaching agent. Indeed, the removal rates of K, Mg, and Ca in char broadly remain unchanged with increasing the concentrations of these elements in the leaching agents. The average removal rates for K, Mg, and Ca are 63.7, 43.7, and 60.7 wt %, respectively, which coincide well with the corresponding values shown in **Figure 4.1** for the leaching time of 1 h.

The near-linear correlations between the run number and the concentrations of K, Mg and Ca encourage us to predict the concentrations of these elements in the leachates up to run 18 (the last one required to complete leaching), using the equations shown in **Figure 4.7**. The results are depicted in **Figure 4.8**, benchmarking against the concentrations of these elements calculated from the real scenario described below. Assuming 1 kg of char being leached with 1.1 kg, the concentrations of K, Mg, and Ca are estimated as 15.6, 0.7, and 2.3 g/L, respectively, when the average removal rates of these elements illustrated in **Figure 4.7** are considered. These concentrations exactly match with the predicted values for the leachate from run 18, which are far lower than the saturated concentrations of K, Mg, and Ca species estimated from the solubility of possible salts (*e.g.*, formate, acetate, and chlorides) in water.

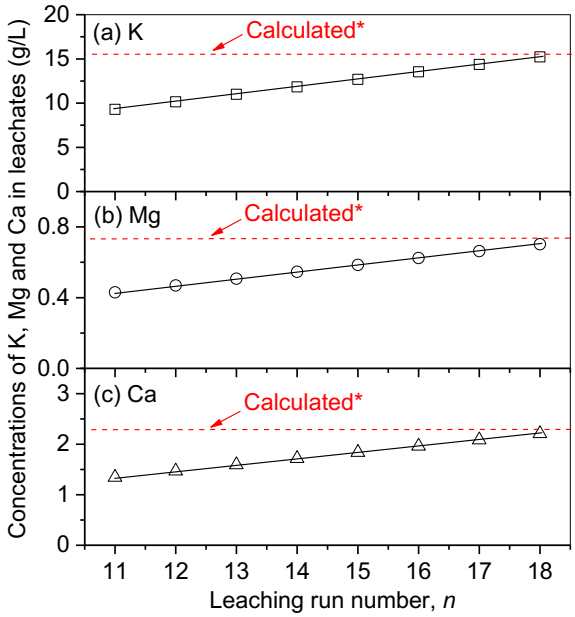

Figure 4.8. *Concentrations of (a) K, (b) Mg, and (C) Ca in the leachates from repeated leaching runs 11–18 predicted from the equations shown in Figure 8, benchmarking against the concentrations that are calculated* based on leaching 1 kg of char (dry basis) with 1.1 kg of pyrolytic AP (density: 1.025 g/mL) at removal rates of 63.7 wt % for K, 43.7 wt % for Mg, and 60.7 wt % for Ca.*

Thus, it is plausible to conclude that the pyrolytic AP produced from pyrolysis of wheat straw at 450 °C is sufficient for leaching the char from the same run, achieving the removal rates of ~63.7 wt % for K, ~43.7 wt % for Mg, and ~60.7 wt % for Ca when the leaching time is 1 h.

The strong ability of pyrolytic AP in removing AAEMs (particularly K) from char can be attributed to two reasons. One is the acidic nature of the spent leachate from repeated leaching runs. As shown in the **Figure 4.9**, the concentration of AcOH drops significantly from ~130 g/L in the raw pyrolytic AP to ~61 g/L in the leachate from run 1, and then flattens out at ~28 g/L with further increasing the repeated leaching run numbers to 10. The substantial reduction in AcOH concentration after run 1 is most likely due to its adsorption on char (because of its high concentration in the pyrolytic AP), rather than consumption by char. This is because that the AcOH concentration remains nearly unchanged in runs 2–10, although the amount of "fresh" char leached is identical to that used for run 1. Insignificant consumption of AcOH has also been reported in a previous study that leached wood with an organic acid. In practice, the AcOH carried by char in run 1 can be effectively recovered and recycled back to leaching after drying washed char (with vapor condensation), as recycled

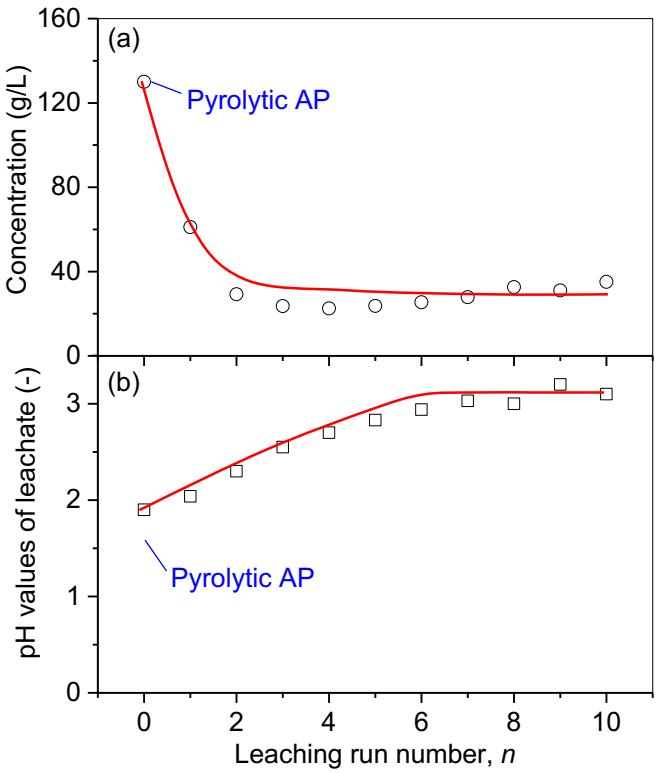

Figure 4.9. *(a) Concentrations of AcOH in leachates and (b) pH values of leachates in repeated runs.*

back to leaching after drying the washed char (with vapor condensation), as illustrated in **Figure 4.6**. The acetic nature of the leachates from repeated leaching runs is further confirmed by the pH values (see **Figure 4.9**). The pH values of the leaching agents increase steadily from ~1.9 in the pyrolytic AP to ~3.0 in the run 6 leachate and then level off with further increasing the run numbers. The increase of pH values in the leachate up to run 6 does not match exactly with the reduction profile of the concentrations of AcOH. This is explained by the consumption of HCOOH during repeated leaching, which cannot be quantified by the GC-FID. The other reason is believed to be the superior solubilities of potassium formate and potassium acetate in water. Converting K in char from other forms (*e.g.*, hydroxide and carbonate) into formate and acetate by the organic acids is beneficial for its removal during repeated leaching.

It is further confirmed that rinsing the washed char with water (i.e., the rinsing reactor in **Figure 4.6**) is essential to remove the inorganics that have been dissolved in leachate but carried over with the liquid retained in the pores of char and its surface after dewatering and drying. For instance, the content of K in the char collected from the repeated leaching run 10 is 2.175 wt % (dry basis, db), which is only ~19% lower than that (2.628 wt %, db) in the raw char. Rinsing the char from run 10 with water for 1 h at a liquid-to-solid mass ratio of 20 successfully reduced the K content to 0.784 wt % (db), ~70% lower than that in the raw char. Up to now, it is experimentally demonstrated that leaching 1 kg of char with 1.1 kg of pyrolytic AP (as determined by pyrolysis) for 1 h could achieve the removal rates of ~63.7 wt % for K, ~43.7 wt % for Mg, and ~60.7 wt % for Ca, and rinsing is required to yield char with reduced contents of AAEMs.

4.4. Conclusions

We have demonstrated that the repeated leaching with aqueous phase produced near AAEM-free char with a liquid-to-solid ratio of 1.1. A major portion of alkali and alkaline earth metal species (AAEMs) was leached from the char following a pseudo-second-order model while some non-acidic compounds such as ketones and alcohols had negative effects on the leaching. Repeated leaching char up to 18 times enables the internal recycling of the pyrolysis products.

4.5. References

[1] Gao X., Wu H. Biochar as a fuel: 4. Emission behavior and characteristics of PM_1 and PM10 from the combustion of pulverized biochar in a drop-tube furnace. *Energy & Fuels* **2011,** 25, 2702–2710.

[2] Lin W., Dam-Johansen K., Frandsen F. Agglomeration in bio-fuel fired fluidized bed combustors. *Chemical Engineering Journal* **2003,** 96, 171–185.

[3] Benson S. A., Sondreal E. A., Ash-related issues during combustion and gasification. In: Impact of mineral impurities in solid fuel combustion, *Springer* **2002**, 1–21.

[4] Jiang L., Hu S., Sun L., Su S., Xu K., He L., Xiang J. Influence of different demineralization treatments on physicochemical structure and thermal degradation of biomass. *Bioresource Technology* **2013,** 146, 254–260.

[5] Liu X., Bi X. T. Removal of inorganic constituents from pine barks and switchgrass. *Fuel Processing Technology* **2011,** 92, 1273–1279.

[6] Eom I. Y., Kim K. H., Kim J. Y., Lee S. M., Yeo H. M., Choi I. G., Choi J. W. Characterization of primary thermal degradation features of lignocellulosic biomass after removal of inorganic metals by diverse solvents. *Bioresource Technology* **2011,** 102, 3437–3444.

[7] Davidsson K., Korsgren J., Pettersson J., Jäglid U. The effects of fuel washing techniques on alkali release from biomass. *Fuel* **2002,** 81, 137–142.

[8] Karnowo, Zahara Z. F., Kudo S., Norinaga K., Hayashi J. Leaching of alkali and alkaline earth metallic species from rice husk with bio-oil from its pyrolysis. *Energy & Fuels* **2014,** 28, 6459–6466.

[9] Oudenhoven S., van der Ham A. G., van den Berg H., Westerhof R. J. M., Kersten S. R. Using pyrolytic acid leaching as a pretreatment step in a biomass fast pyrolysis plant: Process design and economic evaluation. *Biomass & Bioenergy* **2016,** 95, 388–404.

[10] He C., Tang C., Li C., Yuan J., Tran K. Q., Bach Q. V., Qiu R., Yang Y. Wet torrefaction of biomass for high quality solid fuel production: A review. *Renewable Sustainable Energy Review* **2018,** 91, 259–271.

[11] Bach Q. V., Skreiberg Ø. Upgrading biomass fuels via wet torrefaction: A review and comparison with dry torrefaction. *Renewable Sustainable Energy Review* **2016,** 54, 665–677.

[12] Alonso D. M., Wettstein S. G., Dumesic J. A. Bimetallic catalysts for upgrading of biomass to fuels and chemicals. *Chemical Society Review* **2012,** 41, 8075–8098.

[13] Teng H., Wei Y. C. Thermogravimetric studies on the kinetics of rice hull pyrolysis and the influence of water treatment. *Industrial & Engineering Chemistry Research* **1998,** 37, 3806–3811.

[14] Yip K., Tian F., Hayashi J-i., Wu H. Effect of alkali and alkaline earth metallic species on biochar reactivity and syngas compositions during steam gasification. *Energy & Fuels* **2009,** 24, 173–181.

[15] Manyà J. J. Pyrolysis for biochar purposes: A review to establish current knowledge gaps and research needs. *Environmental Science & Technology* **2012,** 46, 7939–7954.

[16] Wu H., Yip K., Kong Z., Li C. Z., Liu D., Yu Y., Gao X. Removal and recycling of inherent inorganic nutrient species in mallee biomass and derived biochars by water leaching. *Industrial & Engineering Chemistry Research* **2011,** 50, 12143–12151.

[17] Mohan D., Sarswat A., Ok Y. S., Pittman Jr C. U. Organic and inorganic contaminants removal from water with biochar, a renewable, low cost and sustainable adsorbent–a critical review. *Bioresource Technology* **2014,** 160, 191–202.

[18] Huang Q., Song S., Chen Z., Hu B., Chen J., Wang X. Biochar-based materials and their applications in removal of organic contaminants from wastewater: state-of-the-art review. *Biochar* **2019,** 1, 45–73.

[19] Mourant D., Wang Z., He M., Wang X. S., Garcia-Perez M., Ling K., Li C. Z. Mallee wood fast pyrolysis: effects of alkali and alkaline earth metallic species on the yield and composition of bio-oil. *Fuel* **2011,** 90, 2915–2922.

[20] Jensen P. A., Sander B., Dam-Johansen K. Removal of K and Cl by leaching of straw char. *Biomass & Bioenergy* **2001,** 20, 447–457.

[21] Zhang M., Liaw S. B., Wu H. Bioslurry as a fuel. 5. Fuel properties evolution and aging during bioslurry storage. *Energy & Fuels* **2013,** 27, 7560–7568.

[22] Zhang M., Wu H. Bioslurry as a fuel. 6. leaching characteristics of alkali and alkaline earth metallic species from biochar by bio-oil model compounds. *Energy & Fuels* **2015,** 29, 2535–2541.

[23] Zhang M., Shen Q., Wu H. Adsorption characteristics of bio-oil on biochar in bioslurry fuels. *Energy & Fuels* **2017,** 31, 9619–9626.

[24] de Caprariis B., De Filippis P., Hernandez A. D., Petrucci E., Petrullo A., Scarsella M., Turchi M. Pyrolysis wastewater treatment by adsorption on biochars produced by poplar biomass. *Journal of Environmental Management* **2017,** 197, 231–238.

[25] Yang H., Kudo S., Kuo H. P., Norinaga K., Mori A., Mašek O., Hayashi J-i. Estimation of enthalpy of bio-oil vapor and heat required for pyrolysis of biomass. *Energy & Fuels* **2013,** 27, 2675–2686.

[26] Yip K., Tian F., Hayashi J-i., Wu H. Effect of alkali and alkaline earth metallic species on biochar reactivity and syngas compositions during steam gasification. *Energy & Fuels* **2009,** 24, 173–181.

[27] Zevenhoven M., Yrjas P., Skrifvars B. J., Hupa M. Characterization of ash-forming matter in various solid fuels by selective leaching and its implications for fluidized-bed combustion. *Energy & Fuels* **2012,** 26, 6366–6386.

[28] Khazraie Shoulaifar T., DeMartini N., Zevenhoven M., Verhoeff F., Kiel J., Hupa M. Ash-forming matter in torrefied birch wood: Changes in chemical association. *Energy & Fuels* **2013,** 27, 5684–5690.

[29] Zhou S., Hosseini T., Zhao J., Zhang X., Wu H., Zhang L. Selective removal of sodium from low-rank Xinjiang coal upon multistage countercurrent water washing: experimental investigation and kinetics modeling. *Energy & Fuels* **2019,** 33, 2142–2152.

[30] Werkelin J., Skrifvars B.-J., Zevenhoven M., Holmbom B., Hupa M. Chemical forms of ash-forming elements in woody biomass fuels. *Fuel* **2010,** 89, 481–493.

[31] Liu W. J., Zeng F. X., Jiang H., Zhang X. S. Preparation of high adsorption capacity bio-chars from waste biomass. *Bioresource Technology* **2011,** 102, 8247–8252.

[32] Laszlo K., Szűcs A. Surface characterization of polyethyleneterephthalate (PET) based activated carbon and the effect of pH on its adsorption capacity from aqueous phenol and 2, 3, 4-trichlorophenol solutions. *Carbon* **2001,** 39, 1945–1953.

[33] Liu Q.S., Zheng T., Wang P., Jiang J.P., Li N. Adsorption isotherm, kinetic and mechanism studies of some substituted phenols on activated carbon fibers. *Chemical Engineering Journal* **2010,** 157, 348–356.

CHAPTER 5

APPLICATION OF CATALYTIC HYDROTHERMAL GASIFICATION TO LIGNITE-TO-SYNGAS CONVERSION

5.1. Introduction

In the near future, coal continues as an important energy resource due to abundant reserves worldwide. The BP statistical review of world energy [1] reveals that coal is the fastest increasing fossil fuel, constituting 27% of global energy consumption in 2018. However, current technologies, such as gas-solid gasification and combustion, for coal utilization are uneconomical or environmentally unfriendly. A major and common disadvantage is the necessity of feeding dry solid with less than 10 wt% moisture, whereas wet coal that contains high water up to 60 wt% represents a large portion of the available resources. Sub/supercritical water gasification is a modern technology worth devoting great attention because of particular features, such as no need of either drying or steam generation, moderate operating temperatures and high theoretical cold gas efficiency. Comprehensive reviews on catalytic and non-catalytic gasification in sub/supercritical water are available. [2,3] It is well known that water near the thermodynamic critical point (374.3°C and 22.1 MPa) behaves like a nonpolar solvent having unique properties concerning the diffusivity, ionic product and dielectric constant. It has been widely accepted as an attractive and potential medium for dissolution, degradation and conversion of solid fuels. [4,5]

The gasification of coal in hydrothermal environments has been investigated with/without a catalyst since the first report by Modell in 1978. [6] It was found that non-catalytic processes were insufficient for a desired gasification efficiency because of the recalcitrant nature of coal. [7] To improve the efficiency, Ge et al. [8] investigated partial oxidation of coal in supercritical water using H_2O_2 as the oxidant in a batch reactor. The results demonstrated complete gasification into H_2-rich gases with no char formation, but the temperature is up to 900°C. Hydrothermal gasification using a catalyst (*i.e.*, CHTG) has the potential to gasify coal efficiently at a lower temperature. Several studies [9–11] employed alkaline catalysts such as NaOH, K_2CO_3 and $Ca(OH)_2$ that improved the gasification efficiency significantly. Yu et al. [12] prepared a ruthenium catalyst for CHTG of a lignite in a batch reactor and obtained 86% carbon conversion with a 21-fold enhancement of H_2 yield compared to that in the non-catalytic case at 500°C. Despite the significant progress by using catalysts, there have are still barriers to those strategies in two particular aspects. The temperature for the complete conversion of coal is still as high as 700°C. In addition, the majority of the attempts are hardly translated into commercial practice owing to the technical obstacle of delivering solid coal into highly pressurized reactors continuously.

The organic portion of coal is a macromolecular network with plenty of aromatic clusters highly cross-linked by bridge bonds. Early studies [13–15] reported complete gasification of organic compounds (*e.g.*, benzene and phenols) in subcritical water using heterogeneous catalysts such as Ni, Ru and Rh supported by TiO_2, ZrO_2 or carbon. As such, it is possible to realize high or even full conversion of coal near the critical regime using active metal catalysts if the coal is preliminarily decomposed and solubilized in an aqueous medium. Unfortunately, few studies have pertained to such a dissolution-gasification strategy. Miura et al. [16,17] proposed sequential extraction of a lignite and CHTG of the extract with a carbon-supported nickel catalyst and reported the extract yield and its conversion to gas of 46 wt% and 97%, respectively, in subcritical and neutral water (350°C and 18 MPa). This may be a reasonable way to gasify a portion of the lignite, but also difficult to overcome the drawback such as low concentration of the soluble matter due to very low solubility as well as low degree of solubilization.

It is known that alkali-oxygen/air oxidation is effective for coal depolymerization by eliminating aromatic clusters. [18] Many studies have applied the method to the production of lower carboxylic acids from coal because air/oxygen is the least inexpensive oxidant. [19,20] It is expected that a substantial portion of coal is soluble in alkaline water after the liquid-phase oxidation. The basicity is important to both degradation and dissolution. [21] This study proposes to use an aqueous solution of NaOH, resulting in a high dissolution rate of a lignite and then CHTG of the dissolved lignite. Although an alkaline environment has been reported to suppress the char formation in CHTG, the presence of alkali leads to catalyst deactivation and low reactivity of compounds having carboxylic groups that are in a stable ionic form (*e.g.*, $-COO^-Na^+$). [22–24] The choice of catalyst is thus important. The most frequent options are metal catalysts such as Ni, Pt and Ru, which exhibit high activities for C-C bond cleavage, water-gas shift and methanation reactions. [25] The support for metal is another crucial factor for its activity and stability. Elliott et al. [26] identified α-Al_2O_3, monoclinic ZrO_2, and carbon as stable supports in subcritical but neutral water at 350°C. The main motivation of employing carbon in this study was the superior stability in hot alkaline water. Metal oxide supports, such as, Al_2O_3 and SiO_2, are reactive with alkalis under hydrothermal conditions. [27,28] Besides, higher specific area of carbon well above 1,000 $m^2\ g^{-1}$ is preferred for a higher metal dispersion. Use of carbon support, which can be burned-off, is also advantageous in recovery of precious metals.

Our recent study has demonstrated near-complete gasification of a bamboo lignin in an aqueous solution of Na_2CO_3 by applying a Ru/C catalyst. [29] We expected conversion of coal into syngas by a sequence of hydrolysis/oxidation in alkaline water and CHTG with a highly active catalyst, and therefore investigated it with the targets of (i) completely solubilizing lignite into the medium and (ii) converting the solubilized lignite into CH_4-rich gas in subcritical water, and (iii) taking carbon and chemical energy balances to evaluate the process feasibility.

5.2. Experimental Section

5.2.1. Preparation of lignite sample

A Victorian lignite, Loy Yang, was employed as the starting sample. It had an ash content of 0.8 wt% on a dry basis and C, H, N and O+S contents of 66.9, 4.8, 0.6 and 27.7 wt% on a dry-ash-free basis, respectively. The lignite was ground into sizes smaller than 500 μm and vacuum-dried at 85°C for 24 h before use.

5.2.2. Solubilization of lignite in alkaline water

The lignite solubilization was performed in a SUS316-made autoclave (Taiatsu Techno Co., TVS-1-100) with a volume capacity of 500 mL. Briefly, given amounts of aqueous solution of NaOH and the lignite were charged into the autoclave with a volume-to-mass ratio of 20. The concentration of NaOH (C_{NaOH}) was within a range of 0.5–2.0 M. The autoclave was pressurized with N_2 at 2.0 MPa (in HT mode) or O_2 at the same pressure (in OX mode) unless otherwise noted. The suspension was stirred for 20 min at ambient temperature, and then heated to the prescribed temperature, 250°C (HT) or 100°C (OX). In HT mode, the slurry was heated up to 250°C at a nominal heating rate of 7.6 °C min^{-1}. The holding periods at peak temperatures were zero and 6–40 h for HT and OX, respectively. HT and OX were also performed in sequence. The sequence of HT and OX and that of OX and HT are hereafter referred to as HT-OX and OX-HT, respectively. The chemical consumption of O_2 was measured for OX directly from the decrease in its volume. After the solubilization, the suspension was separated into the solid (insoluble portion of the lignite) and liquid (the solution of 'solubilized' lignite) by centrifugation, filtration and repeated washing with deionized water in series. The solid was finally dried at 60°C under vacuum. The solution was measured using a total organic carbon analyzer (Shimadzu, TOC-V_{CPH}) for concentrations of total organic and inorganic carbons (*i.e.*, TOC and IC).

5.2.3. Fractionation of solubilized lignite

Stepwise fractionation of the solubilized lignite was achieved by acidification of the solution. An aliquot of 5 M HCl aq. was dropped into the solution until neutralization. The precipitated solid, termed F1, was collected after neutralization by cycles of centrifugation, filtration and washing with deionized water, and finally dried. The filtrate was acidified to pH of 1.0, and then the precipitate was recovered as another fraction, F2, in the same way as F1. It was found that the filtrate at pH = 1 contained lower organic acids such as oxalic, malonic, succinic, glycolic, acetic and formic acids. These acids were quantified with a high-performance liquid chromatograph (Shimadzu, LC-20 prominence) equipped with a refractive index detector. A BioRad Aminex 87H column was used for the chromatography under the following conditions: column temperature; 55°C, mobile phase; 5 mM H_2SO_4, flow rate; 0.6 mL min^{-1}. Liquid-liquid extraction with 2-butanone was employed to recover the organic matter except oxalic acid from the pH = 1 solution. The extract, F3, was recovered by evaporation of the solvent at 60°C and then vacuum-drying at 40°C. Molecular mass (MM) distributions of F1, F2 and F3 were measured by laser desorption mass spectrometry on a JEOL model (JMS-S3000) that was equipped with a Nd:YLF laser operated at 394 nm in wavelength. The spectra over *m/z* ranges of 100–10,000 were obtained in a linear mode at an acceleration voltage of 20 KV. No matrix reagent was necessary because all the fractions adsorbed the laser light.

The above fractions and the insoluble solid were subjected to ultimate analysis for determining carbon, hydrogen and nitrogen contents while that of oxygen was calculated by difference. Besides, the carbon type distribution was analyzed and quantified by solid-state ^{13}C-NMR. A JEOL model (ECA-400) was employed for the NMR analysis by applying the following method and conditions: method; depth2, repetition time; 20 s, frequency; 150 MHz, rotor spinning rate; 15 kHz, accumulation number; 4,000. Each spectrum was analyzed for classifying the carbon into aliphatic carbon (chemical shift; 0–90 ppm), aromatic carbon (90–170 ppm) and carboxyl/carbonyl carbon (170–210 ppm).

5.2.4. Catalyst preparation and characterization

The carbon-based Ru, Pt and Ni catalysts were prepared by wetness impregnation using acetone as a solvent. [30] The metal precursors are ruthenium (III) chloride, hydrogen hexachloroplatinate (IV) and nickel (II) nitrate. Activated charcoal (AC) was used as a common support of those metals. All the chemicals were purchased from Wako Pure

Chemical Industry. Prior to the preparation, AC was ground to sizes within a range of 0.50–1.10 mm, sonicated in water to remove fines and dried at 105°C. The AC-supported metal precursor was transformed into the metal by heating at 400°C for 3 h in a flow of equivolume mixture of H_2 and N_2. The as-prepared Ru, Pt and Ni catalysts are hereafter referred to as Ru/C, Pt/C and Ni/C, respectively. The metal content was determined gravimetrically by combustion in air at 800°C for 1 h. Brunauer−Emmett−Teller surface area (S_{BET}) and total pore volume (V_P) of each catalyst were estimated from N_2 adsorption/desorption isotherms measured at –196°C on a Quantachrome NOVA 3200e. Before the measurement, the catalyst was outgassed at 200°C for 3 h under high vacuum. Transmission electron micrography (TEM) was observed with a JEOL JEM-2100F microscope operating at a voltage of 200 kV. X-ray diffraction analysis was carried out on a Rigaku TTR-III X-ray diffractometer with Cu Kα radiation at a voltage of 50 kV and a current of 300 mA.

5.2.5. Catalytic hydrothermal gasification and product analysis

The continuous flow reactor system has been schematically illustrated in **Chapter 3**. For a typical CHTG, a known mass of catalyst was packed into the SUS 316 tubular reactor. The solution of solubilized lignite was diluted by deionized water so that the TOC was 1500, 2500 and 3500 ppm prior to use as the feedstock, unless otherwise stated. The temperature at the reactor exit was monitored with a SUS-sheathed K-type thermocouple, of that tip had been inserted into the catalyst bed. Prior to the run, the catalyst was reduced in an atmospheric flow of 25 vol% H_2/N_2 through the reactor at 400°C for 1 h. A flow of degassed water was first supplied to the reactor at a rate of 0.5 mL min^{-1} for 2 h to flush the catalyst bed at temperature and pressure of 350°C and 20 MPa, respectively. Then, the solubilized lignite solution was fed to the reactor for a duration of 1–10 h at the same flow rate, temperature and pressure of 0.5 mL min^{-1}, 350°C and 20 MPa, respectively. The corresponding weight hourly space velocity (WHSV) was in a range of 0.05–0.20 h^{-1} [g-C/g-cat]. The effluent stream was sent to the gas/liquid separator via the cooler, SUS-made filter plate and backpressure regulator. At the end of the run, the flow of the lignite solution was replaced by that of degassed water and after a 30 min duration, the reactor was air-cooled to ambient temperature. The entire portion of product gas was purged with 20 mL min^{-1} N_2 flow and collected in a gasbag and analyzed by gas chromatography on an Agilent 490 Micro-GC. The effluent liquid product was subjected to TOC/IC measurements.

During the flushing, very small amounts of CO_2 and CH_4 were collected at the reactor downstream. However, those were not added to the CO_2/CH_4 yield due to the following reasons. First, it was difficult to distinguish CO_2/CH_4 remaining in the reactor at the end of the flushing from those formed during the flushing. Second, the amount of CO_2/CH_4 collected during the flushing was less than 0.1% of that during the run. One possibility of the gas formation was that from the support. Elliot et al. [26] reported very slow gasification of active carbon that supported a Ru catalyst under a similar hydrothermal condition of this study. They estimated the lifetime of that support as 542 days. In the flowing tables and figures, we reported results within errors (in the product yields) of ±3% on the basis of feedstock. Some runs were repeated at least three times until the reproducibility is within the above-mentioned errors.

5.3. Results and Discussion

5.3.1. Solubilization and low-temperature degradation of lignite in alkaline water

5.3.1.1. Rate of lignite solubilization

Solubilization in an aqueous medium is the primary step of coal conversion by CHTG. HT, OX, HT-OX and OX-HT were the candidates for the degradation and dissolution of lignite in alkaline water. **Table 5.1** summarizes conditions and results of runs in these modes and demonstrates solubilization of major portions of the lignite into alkaline water. The solubilization rate on the lignite mass basis, X_M, depended on the mode and conditions but within a range of 82–95%. Such high X_M enabled to prepare lignite solutions with TC of 27,000–32,000 ppm. Though not shown in the table, it was found that the carbon-based solubilization rate, X_{TC}, was correlated with X_M linearly and very well (slope ≈ 1.04, r^2 = 0.992). It was initially expected that X_M was higher than X_{TC} because molecules richer in oxygen is normally more soluble into alkaline water. X_M and X_{TC}, however, are near equivalent to each other. The solubilization degree was thus not so sensitive or selective to the type or abundance of oxygen functionalities. It was rather suggested that the degradation/solubilization was promoted by formation of fragments with a smaller MM.

HT causes solubilization of coal/lignite mainly by base-catalyzed hydrolysis of ether bonds and other types of inter-aromatic-unit linkages. [4, 31] It is seen from R1–R3 that X_M and X_{TC} increase with C_{NaOH} up to 1.0 M, and level off. Formation of CO_2 with a yield of 4–6% on the lignite carbon basis was probably due to thermal decomposition of carboxylic

groups. In spite of such loss of the acidic groups, pH after R1 was as low as 10.2. This suggests the formation of other acidic groups such as phenolic -OH and carboxylic groups and supports the base-catalyzed hydrolysis. It is, however, noted that a higher pH of the aqueous solution has a more or less positive effect on the solubility as far as the lignite components are weak acids. OX gives X_M/X_{TC} equivalent to HT (R4 and R5). A positive effect of O_2 pressure on X is consistent with the mechanism of oxidative degradation; oxidation of aromatic rings and resulting in their opening and breaking, in other words, not breakage of inter-aromatic-unit linkages but decomposition of aromatic units. [32] The positive O_2 pressure effect supports oxidative degradation (R5 *vs* R4). The pH after R5 is much lower than that after R4, and this implies the formation of more carboxylic groups. X_{IC} of 5–7% was due to CO_2 formation by the oxidation. More detailed discussion of the oxidative degradation will be developed later.

Table 5.1. *Mass and carbon-based dissolution rate (X_M and X_C) of lignite.*

Run ID	process mode	C_{NaOH} (M)	O_2 pressure (MPa) [a]	pH [b]	X_M (wt%)	X_{TC} (%)	X_{IC} (%)
R1	HT	0.5	–	10.24	83.5	82.4	4.0
R2	HT	1.0	–	13.88	93.3	92.9	5.4
R3	HT	2.0	–	13.75 [c]	91.0	90.2	5.7
R4	OX	1.0	1.0	12.91	88.8	89.0	5.3
R5	OX	1.0	2.0	9.36	93.4	93.4	6.9
R6	HT-OX	1.0	1.0	11.35	93.2	92.9	6.1
R7	HT-OX	1.0	2.0	9.34	95.1	94.7	8.0
R8	HT-OX	2.0	2.0	13.96	95.2	94.7	8.9
R9	OX-HT	2.0	2.0	13.95	93.5	93.0	13.1

[a] The oxidation time was 6 h for R4–R9. [b] pH was measured after separating solid residue from the slurry after the processing. [c] pH was measured after dilution with deionized water by twice in volume.

Table 5.1 also shows that OX subsequent to HT increases X_M/X_{TC} slightly, forming CO_2 due to the oxidation (R6–R8). As far as the solubilization is concerned, X_M/X_{TC} of around 95% seems to be upper limits of solubilization. The ^{13}C-NMR analysis of solid residues revealed that those were very rich in aliphatic carbon with fractions of 60–67% (see **Table S5.1**). The lignite contained a small portion of aliphatic-rich components that were not only thermally stable at 250°C but also refractory to the oxidation at 100°C. OX-HT was not effective for further increasing X_M/X_{TC}. One of the reasons was that X_M/X_{TC} had already approached 95% in OX. This sequence caused CO_2 formation, as evinced by X_{IC} as much as

13%. This was attributed to the fact that HT decomposed carboxylic groups that had been introduced by OX. Loss of carboxylic groups could have a negative impact on the lignite solubility in alkaline water.

5.3.1.2. Changes in chemical structure of lignite associated with solubilization

This section characterizes the solubilized lignites by HT, HT-OX and OX-HT that correspond to R3, R8 and R9, respectively. **Figure 5.1** shows the fractions of different types of carbon; f_{al} (aliphatic carbon), f_{ar} (aromatic carbon), $f_{C=O}$ (carbonyl/carboxyl carbon) and f_{CO2} (CO_2 from the lignite carbon). These fractions distribute over the solubilized lignite (F1–F3), insoluble residue and CO_2. It was unexpected for HT that a portion of the original aromatic carbon was transformed into aliphatic carbon to a significant degree (by 7.8%), and also to carbonyl/carboxyl carbon. Liu et al. [33] treated a lignite hydrothermally in the absence of alkali and found the transfer of hydrogen from water to lignite contributed to the degradation. However, a portion of the original aliphatic carbon was lost regardless of the temperature within a range of 200–300°C. In consideration of the net formation of carbonyl/carboxyl carbon probably from aromatic carbon in R3 ($f_{C=O}$ [HT] + f_{CO2} [HT] – $f_{C=O}$ [No treatment] = 6.7% + 5.7% – 5.0% = 7.4%), the formation of aliphatic carbon seemed to be associated with that of carbonyl or carboxyl carbon in the presence of the alkali. The

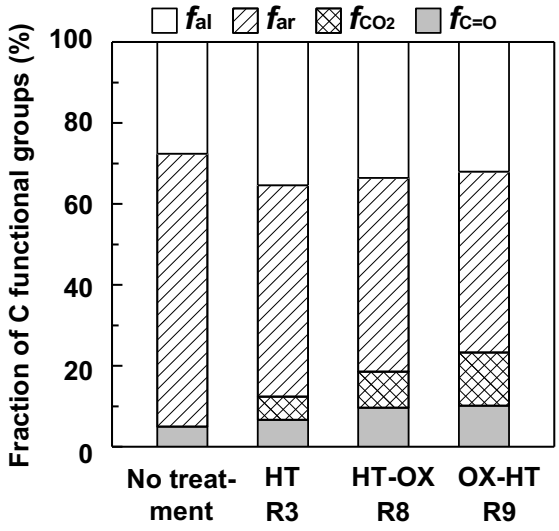

Figure 5.1. *Fractions of different types of carbon in the lignite after HT, OX-HT or HT-OX with 2.0 M NaOH, 2.0 MPa O_2 and 6 h oxidation time (only for OX). f_{al}; fraction of aliphatic carbon, f_{ar}; fraction of aromatic carbon, $f_{C=O}$; fraction of carbonyl/carboxyl carbon, f_{CO2}; yield of CO_2 formed during processing. The carbon type distributions for insoluble matter, F1, F2 and F3 are available in* ***Table S5.1****.*

concentrations of hydroxyl ions under the present conditions were higher by orders of magnitude than those in hydrothermal conditions without alkali. It was suspected that oxygen and hydrogen of hydroxyl ions were used for the oxidation and hydrogenation of aromatic carbon, respectively. An examination of such a reaction mechanism is left for future study.

It is also seen in **Figure 5.1** that OX following HT oxidized a portion of remaining aromatic carbon, converting it mainly into CO_2 and carbonyl/carboxyl carbon, while maintaining f_{al}. This is in broad agreement with the authors' previous report. [34] On the other hand, the sequence of OX and HT produced maximum amounts of CO_2 and carbonyl/carboxyl carbon with a total yield of 23%. HT decomposed carboxyl groups that had been introduced by OX. **Figures. 5.2** and **5.3** show carbon-based product compositions and MM distributions of F1, F2 and F3, respectively. The vertical axis of **Figure 5.3** indicates not molar but mass-based relative abundance. It was confirmed that the average MM was in the order of F1 > F2 > F3. MM of F1 ranges from 100 to even up to 5,000. HT solubilized about 90% of the lignite while giving F1 as the major product. OX after HT caused further degradation, converting F1 to F2 and F3 with a lower MM, and decreasing the number-average MM of F1 from 1,040 to 770. The OX-HT sequence gave more F2/F3 than HT but less than HT-OX. It was believed that the solubilized lignite with a smaller MM was a better feedstock for CHTG, and HT-OX was therefore chosen as the mode of pre-conversion.

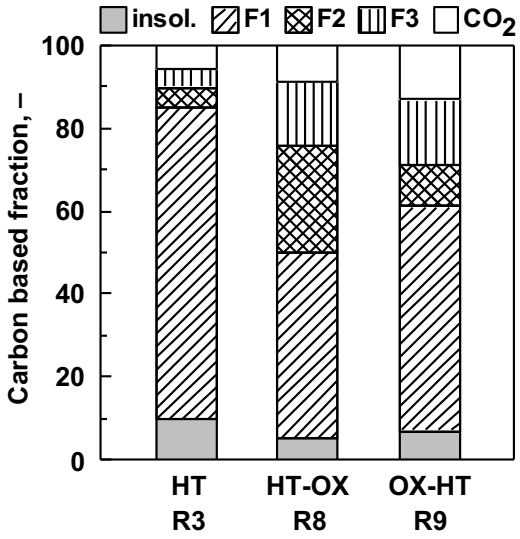

Figure 5.2. *Compositions of solubilized lignite in HT, OX-HT and HT-OX under the same conditions as shown in* ***Fig. 5.1****.*

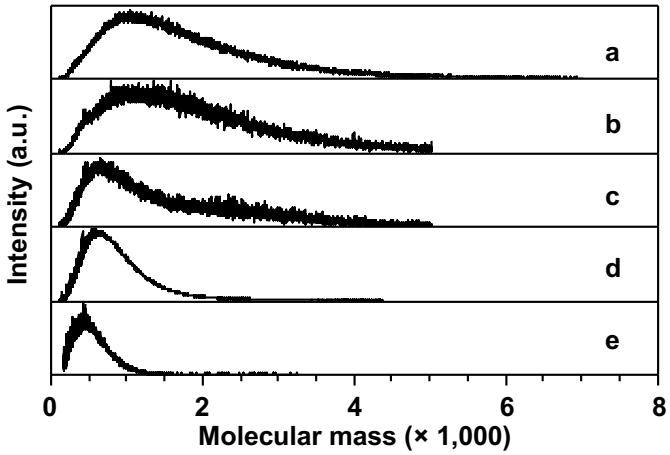

Figure 5.3. *Molecular mass distributions of F1, F2 and F3. The vertical axis indicates the intensity based on not number of molecules (molar amount) but mass. Fractions (a), (b) and (c); F1 from HT (R3), OX-HT (R9) and HT-OX (R8), respectively. Fractions (d) and (e); F2 and F3 from HT-OX (R8). The number-average MM for fractions (a)–(e) is 1,024, 1,040, 770, 630, and 434, respectively.*

5.3.1.3. Solubilization of lignite with oxidation time

The effect of oxidation time on the product composition was investigated for HT-OX. The conditions for HT was fixed at C_{NaOH}; 2 M, temperature; 250°C, and holding time; 0, while the oxidation time was varied from 6 to 40 h at a fixed temperature of 100°C. The results are shown in **Figure 5.4**, displaying the variation in oxygen consumption, pH of suspension, composition of solubilized lignite and yields of carboxylic acids with oxidation time. It is seen that the O_2 consumption continuously increases up to 12.5 mmol/g-lignite in 20 h, and further at 20–40 h but by only 0.6 mmol. On the other hand, pH decreases monotonously. This is attributed to the formation of lower monoacids and diacids. In terms of the O_2 consumption and acid formation, the oxidation continued up to 40 h.

Figure 5.4 also shows the time-dependent changes in the carbon-based composition of the product in a cumulative manner. The changes in F1 and F3 yields are monotonous, whereas the F2 yield changes through a maximum at 6 h. The CO_2 yield increases gradually but systematically. The yield of insoluble matter decreases but very slowly at 10–40 h. The changes in the F1–F3 yields indicate that the oxidative degradation occurred consecutively, *i.e.*, from F1 to F3 *via* F2. It is noted that the degradation of F1 to F2 is quick up to 10 h but much slower at 10–40 h, during which the rate of F1 conversion is only 18% of that in 0–10 h. The prolonged oxidation resulted in more production of smaller MM components, *i.e.*, F2

and F3, but the rate of F1 conversion was very slow. Moreover, increasing O_2 consumption caused more degree of degradation at the expense of more loss of chemical energy of the lignite. The time for OX was then optimized at 10 h.

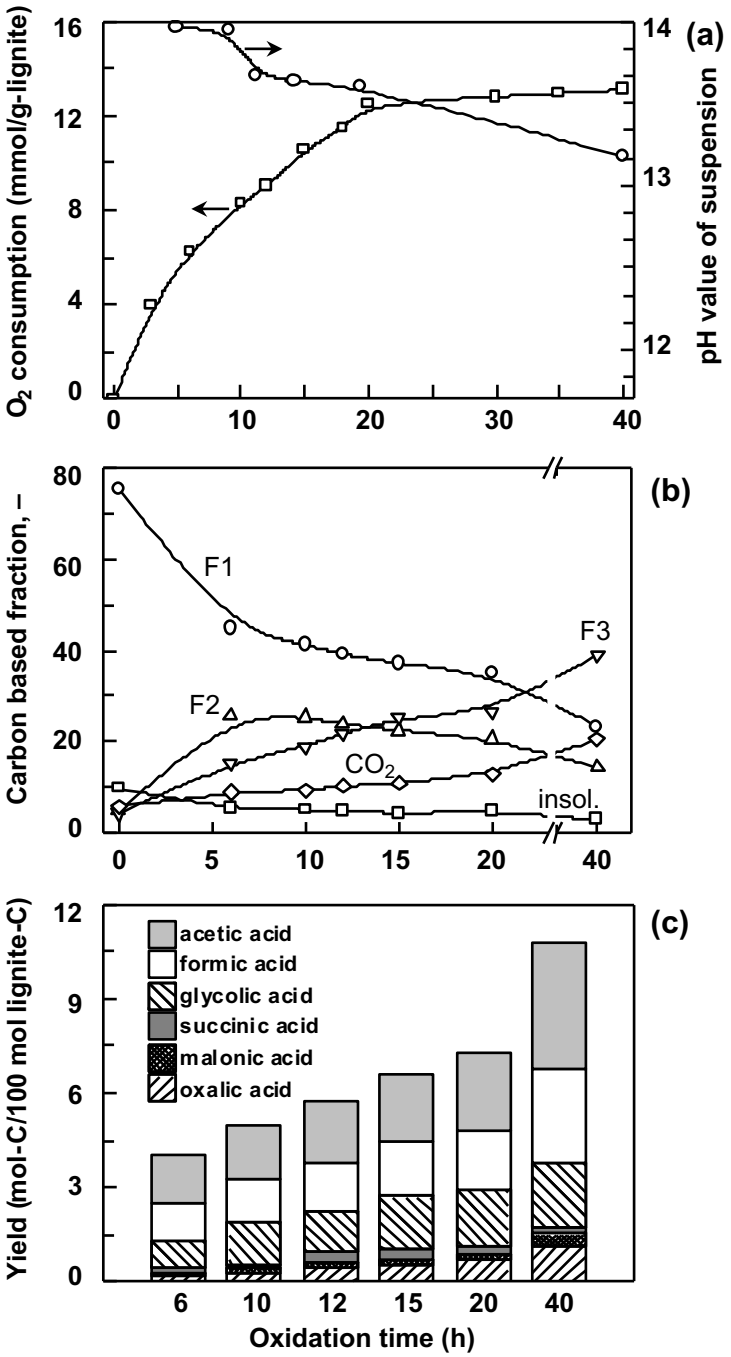

Figure 5.4. *Variation in (a) oxygen consumption and pH of suspension, (b) composition of solubilized lignite and (c) yields of carboxylic acids with oxidation time.*

5.3.2. Catalytic hydrothermal gasification of solubilized lignite

Here are presented CHTG characteristics of HT-OX-solubilized lignite focusing on combined effects of catalyst, WHSV, concentration, and Ru loading on the gas yield, composition and carbon conversion. The gas yields are given in a common unit of mol per 100-mol-C of the solubilized lignite. The carbon conversion is shown in a unit of [(total amount of C feed − amount of C in liquid product)/total amount of C feed]. As a consensus [25], sub/supercritical water gasification is a process containing reactions occurring in series and parallel; hydrothermal reforming [$CH_xO_y + (1 - y)\ H_2O \leftrightarrow CO + (1 - y + x/2)\ H_2$], water-gas shift [$CO + H_2O \leftrightarrow CO_2 + H_2$] and methanation [$CO + 3H_2 \leftrightarrow CH_4 + H_2O$]. Reactions such as cracking, dehydration and polymerization leading to coke formation may also take place in competition with the above-mentioned major reactions. The underlying reaction networks are interesting, but the focus of this study was rather to identify the process feasibility.

5.3.2.1. Effect of catalyst type

Figure 5.5 compares the gas yields, total carbon conversion, and TOC of the effluent liquid among four catalysts. The carbon conversion in the non-catalytic case was only 9% including the CO_2 yield of 8.4%. The gasification also produced H_2 (2.2%) but neither CH_4 nor CO. NaOH could play a role of catalyst for the water-gas shift reaction, producing CO_2 and H_2 from CO and H_2O. [35] Either Ni/C (loading; 6.8 wt%) or Pt/C (loading; 4.7 wt%)

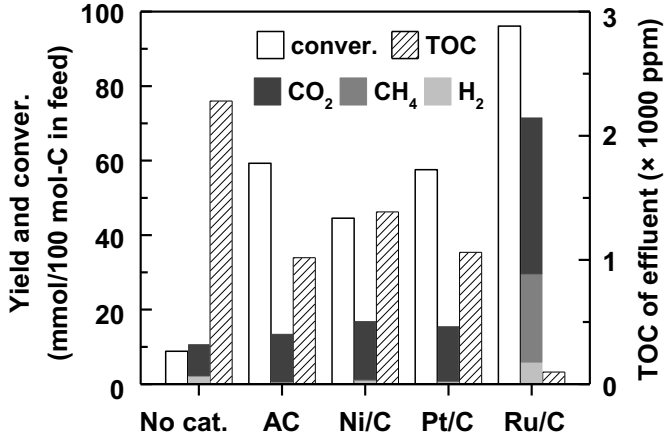

Figure 5.5. *Variation with catalyst of carbon conversion, gas yields and TOC of effluent liquid product. Feedstock; HT-OX-solubilized lignite with oxidation for 10 h, TOC of feedstock; 2500 ppm, pH; 12.6, temperature; 350°C; pressure; 20 MPa; WHSV; 0.10 h^{-1}, time on stream, 1 h.*

gave a negligibly low CH_4 yield. CO_2 yields were higher than that in the absence of catalyst, but this was probably due to a catalytic role of AC that promoted decarboxylation. The carbon conversions achieved by AC, Ni/C and Pt/C were 59, 58 and 44%, respectively, indicating that a substantial portion of the solubilized lignite underwent coking over AC. It was also implied that the presence of Pt suppressed the coke deposition to some extent.

On the other hand, Ru/C (loading; 5.7 wt%) gave 96% carbon conversion, 42% CO_2, 24% CH_4 and 6% H_2. CO was not detected while trace C_{2+} alkanes (< 0.1%) were found in the product gas but not shown here because of the extrememly low yield. Numerous studies [36–38] reported the higher activity of Ru than Pt/Ni for CHTG of biomass or its derived oxygenates. Nevertheless, the composition of CH_4 was far less than that of CO_2, suggesting the deactivation of methanation sites. A most plausible reason was coke deposition onto the Ru/C. Assuming the deposited coke had an elementary composition of $CH_{0.5}$, the conversion of the solubilized lignite ($C_{100}H_{86.8}O_{62.9}$) into gases was described well by the following stoichiometry:

$$0.96C_{100}H_{86.8}O_{62.9} + 20.7H_2O \leftrightarrow 41.8CO_2 + 23.7CH_4 + 5.9H_2 + 30.5CH_{0.5}$$

Regardless of the near-complete carbon conversion, the Ru/C with 5.7 wt% metal loading was insufficient for CH_4 production due to the coke formation as much as 30.5% on the feedstock carbon basis.

5.3.2.2. Effect of weight hourly space velocity

CHTG runs were performed at WHSV ranging from 0.05 to 0.20 h^{-1} by packing different weights of Ru/C catalyst. The other conditions were the same as those for **Figure 5.5**. As illustrated in **Figure 5.6(a)**, the conversion and gas yield decrease with higher WHSV, in analogy with the results by Lee et al. [39] The difference between the conversion and total yield of C-containing gas, the major portion of which was attributed to coke, increases from 17 to 31% as WHSV increases from 0.05 to 0.10 h^{-1}, while it is roughly steady at 0.10–0.20 h^{-1}. This result seems impossible if the flow through catalyst bed was an ideal plug flow or similar one because WHSV was decreased by packing more catalyst. The average velocity of liquid was as small as 0.17 mm s^{-1} in consideration of water density, 0.6 g cm^{-3}, at 350°C and 20 MPa. It is known that mixing of liquid in axial direction is significant inside packed bed when the liquid velocity is extremely small. [40] Assuming such mixing in the Ru/C catalyst bed, the trend of coke deposition is understood qualitatively by hypothesizing the followings; (i) The conversion into gas over Ru/C and that into coke over AC (*i.e.*, the

support of Ru) occurred in parallel and therefore in competition. In other words, more amount of Ru gave higher product selectivity to gas, suppressing that to coke. (ii) Ru underwent deactivation due to coke deposition and others. (iii) The loss of activity of AC (toward coke deposition), if any, was slower than that of catalytic activity of Ru. (iv) The carbon conversion was not stable due to deactivation of Ru and its support.

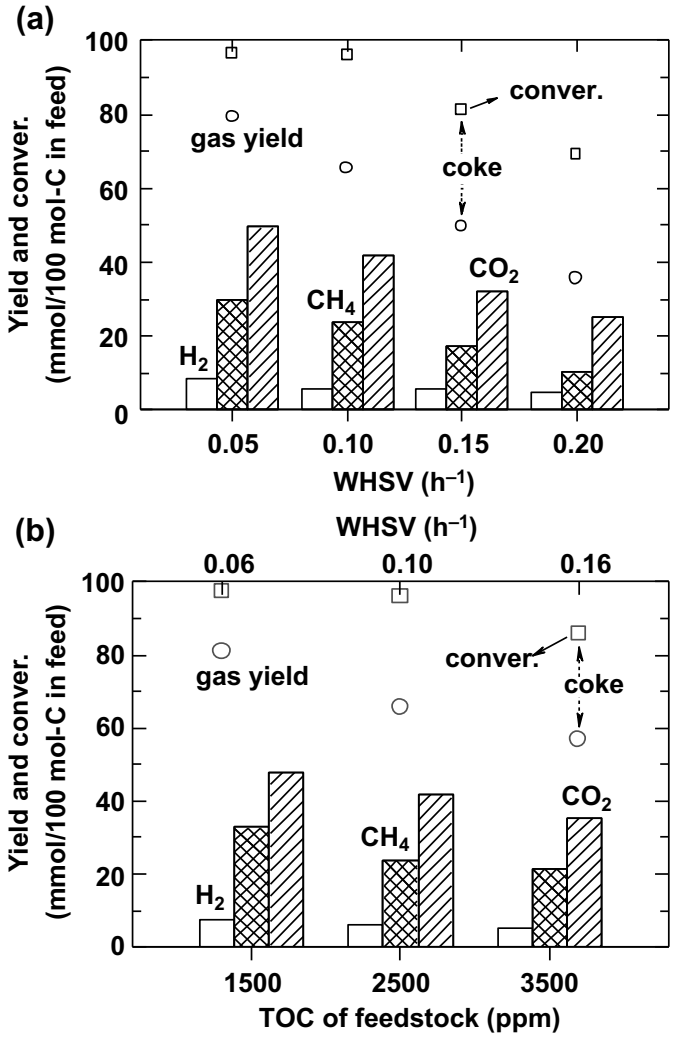

Figure 5.6. *CHTG performances as a function of (a) WHSV and (b) lignite concentration. Feedstock; HT-OX-solubilized lignite with oxidation for 10 h, TOC; (a) 2500 ppm and (b) 1500–3500 ppm, catalyst; Ru/C (5.7 wt% Ru), temperature; 350°C, pressure; 20 MPa, time on stream; 1 h.*

5.3.2.3. Effect of solubilized lignite concentration

Figure 5.6(b) also shows the influence of lignite concentration on the gasification under identical conditions. The concentrations of 1500–3500 ppm correspond to the initial pHs of

12.3–12.8 and WHSVs of 0.06–0.14 h^{-1}, respectively. The changes in pH were insignificant, if any, having negligible effects on the catalyst performances. It is that the decrease in the initial TOC from 1500 to 3500 ppm caused the conversion decrease from 96 to 86% while increasing the coke yield from 17 to 30%. In other words, the increased initial concentration deactivated the catalyst more rapidly. The catalyst deactivation will be discussed in more detail late.

5.3.2.4. Time-on-stream gasification of solubilized lignite

Figure 5.7 shows the results from time-on-stream runs, which were performed over Ru/C with 5.7 wt% Ru loading. The carbon conversion was 96% in the first hour but was finally decreased to 55% with a rate of 9.8% h^{-1}. The deactivation of Ru/C was thus evident. The catalyst deactivation also decreased the gas yield from 66 to 35%, while the coke yield more gradually from 31 to 20%. These trends are consistent with the mechanism hypothesized in the previous section. It is noted that the H_2 yield was near steady over the 5 h but the CH_4 and CO_2 yields continuously decreased. This is an indication of loss of catalysis for methanation. [41] Wambach et al. [42] characterized a commercial Ru/C catalyst after gasification of biomass in supercritical water and found a thin 'carbonaceous' layer covering the ruthenium clusters that caused the deactivation.

The catalyst deactivation by another mechanism [43], *i.e.*, leaching of active metal, was examined. As listed in **Table 5.2**, the metal content of spent Ru/C was lower by about 10%

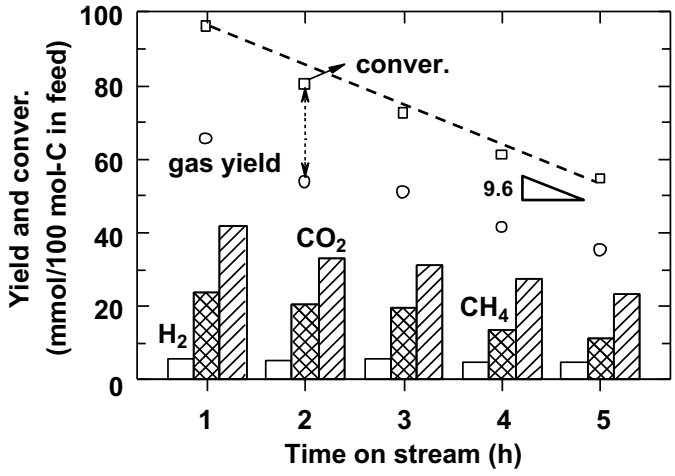

Figure 5.7. *Changes with time of gas yield and carbon conversion. Feedstock; HT-OX-solubilized lignite with oxidation for 10 h, TOC; 2500 ppm, pH; 12.6, catalyst; Ru/C (5.7 wt% Ru), temperature; 350°C, pressure; 20 MPa, WHSV; 0.10 h^{-1}.*

catalyst was subjected to a post-run period (*i.e.*, flushing). The metal weakly bound to AC surface had already been leached out by water flushing. [44] It is thus implausible to attribute the deactivation to metal leaching. The catalysts were further analyzed by XRD. As shown in **Figure 5.8**, the spent Ru/C reveals no significant growth in the Ru crystallite size during CHTG. It was hence concluded that the catalyst deactivation occurred due to neither leaching nor sintering/agglomeration of Ru, but mainly the coke deposition. **Table 5.2** shows that S_{BET} and V_t of the spent Ru/C were both smaller than those of the fresh one, supporting this discussion, and also the activity loss of the AC surface by the coke deposition.

Table 5.2. *Properties of fresh and spent catalysts.*

	fresh				spent				
catalyst	S_{BET} [a] (m^2/g)	W_p [b] (nm)	V_t [c] (cm^3/g)	metal [d] (wt%)	S_{BET} (m^2/g)	W_p (nm)	V_t (cm^3/g)	metal (wt%)	mass change [e] (wt%)
AC	1567	1.73	0.68	–	1456	1.76	0.64	–	4.1
Ni/C	1509	1.77	0.67	6.8	1259	1.75	0.55	6.8	3.4
Pt/C	1057	1.78	0.47	5.0	1032	1.72	0.44	4.7	1.7
Ru/C [f]	1467	1.78	0.65	5.7	1300	1.73	0.56	5.4	1.3
Ru/C [g]					1147	1.77	0.51	5.1	5.3
Ru/C [h]	1243	1.79	0.56	16.2	1278	1.79	0.57	15.7	0.4

[a] Calculated by the BET equation. [b] Average pore width (= $4V_t/S_{BET}$). [c] Total pore volume at $p/p_0 = 0.99$. [d] Metal content of catalyst. [e] Mass change between fresh and spent catalysts. [f] Ru/C with 5.7 wt% Ru loading was used in 1 h CHTG of solubilized lignite by HT-OX with oxidation for 10 h. [g] Ru/C (5.7 wt% Ru) was used in 5 h CHTG of solubilized lignite by HT-OX with oxidation for 10 h. [h] Ru/C (16.2 wt% Ru) was used in 10 h CHTG of solubilized lignite by HT-OX with oxidation for 10 h.

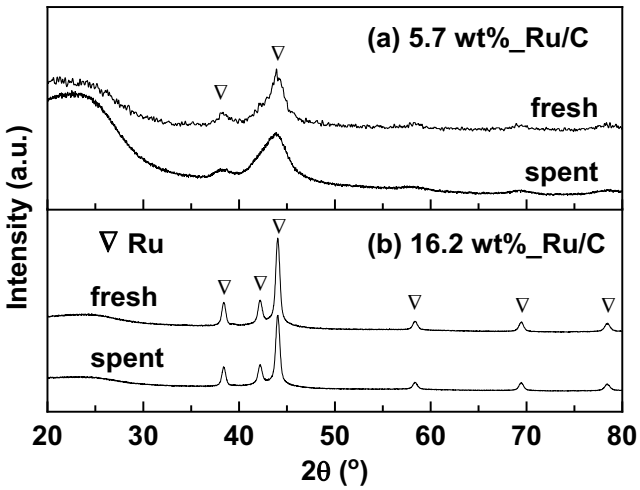

Figure 5.8. *XRD patterns of fresh and spent Ru/C from time-on-stream CHTG under the conditions of (a)* ***Fig. 5.7*** *and (b)* ***Fig. 5.10****.*

5.3.2.5. Time-on-stream gasification of solubilized lignite fractions

Further investigation was carried out for the catalyst performance in CHTG of individual fractions of the solubilized lignite. **Figure 5.9** displays the results. The Ru/C (Ru loading; 5.7 wt%) maintains stable activities for F3 conversion under near-neutral and alkaline conditions, while the carbon conversion (≈ 98%) and gas yield (≈ 94%) were both near steady. It is also seen that pH = 12.6 gave slightly higher conversion and gas yield than pH = 8.0. This would be a result from three positive/negative effects of the alkalinity of aqueous solution. Higher pH favors the stabilization of molecules having acidic -COOH and -OH groups as $-COO^-$ and $-O^-$, which could suppress their chemisorption onto the carbonaceous surface and subsequent transformation into coke. In addition to this, higher pH could enhance the gasification of coke if abundant alkali metal ions (*i.e.*, Na^+ under the present conditions) plays a role of catalyst. On the other hand, the reactivity toward the gasification of molecules with acidic -COOH and -OH groups could become lower as pH increased at the expense of stabilization as mentioned above. [23]

The gasification behaviors of F1 and F2 were much different from that of F3. The carbon conversions of F1 and F2 were about 80% in the first hour but decreased later to 55 and 58%,

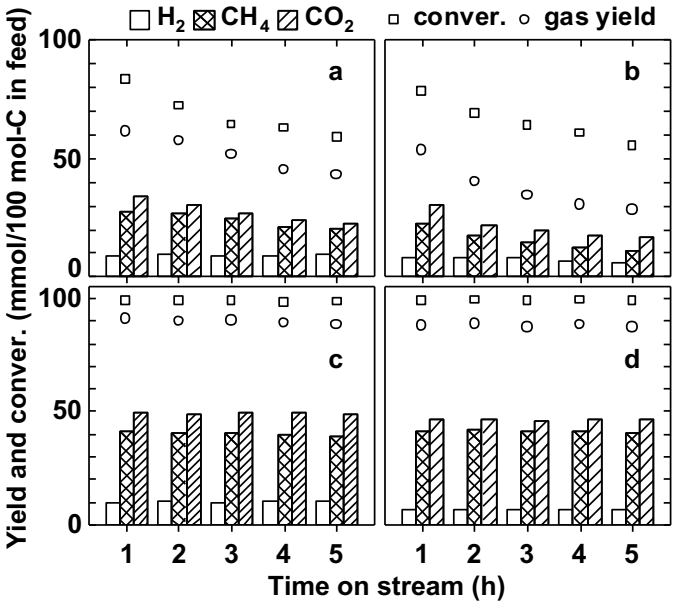

Figure 5.9. *Changes in carbon conversion and gas yield for CHTG of fractions of HT OX-solubilized lignite with 10 h oxidation. (a) F1 (pH = 12.6), (b) F2 (pH = 12.6), (c) F3 (pH = 12.6), (d) F3 (pH = 8.0). TOC of feedstock solution; 2,500 ppm, catalyst; Ru/C (5.7 wt% Ru), temperature; 350°C; pressure; 20 MPa, WHSV; 0.10 h^{-1}.*

respectively. F1 had the lowest gas yield and the highest coke yield. Comparing the conversion characteristics of the three fractions, it is simply said that achieving higher carbon conversion and also gas yield is more difficult for the fraction with a greater MM. This is reasonable because high-mass molecules generally undergo adsorption onto the catalyst surface and subsequent transformation into coke more easily than lower-mass molecules unless chemical structural units are much different from each other.

5.3.2.6. Effect of ruthenium loading

The discussion developed in the previous sections suggested employing Ru/C with higher Ru loading as a solution to the problems of coke deposition and catalyst deactivation. It was expected that higher Ru concentration, in other words, higher frequency of catalytic reactions would suppress coke deposition and resultant deactivation of Ru. The Ru/C with 16.2 wt% Ru loading was prepared for CHTG of the solubilized lignite. **Figure 5.10** shows the time-dependent changes in the carbon conversion and gas yield. In the first 2 h, the Ru/C gave carbon conversion of 99%, total CH_4/CO_2 yield of 98% (43–44%/54–55%) and H_2 yield of 10 mol-H_2/100 mol-C, while the coke yield was negligibly low. The conversion and gas yield gradually decreased, but the former remained over 90% even at 10 h. As shown in **Table 5.2**, the spent Ru/C had S_{BET} even greater than the fresh one, and also similar V_t. In other words, the coke formation, if any, caused no or little loss of micro/mesopores of AC. It was confirmed that Ru crystallite size was maintained for 10 h, as revealed by **Figure 5.10**.

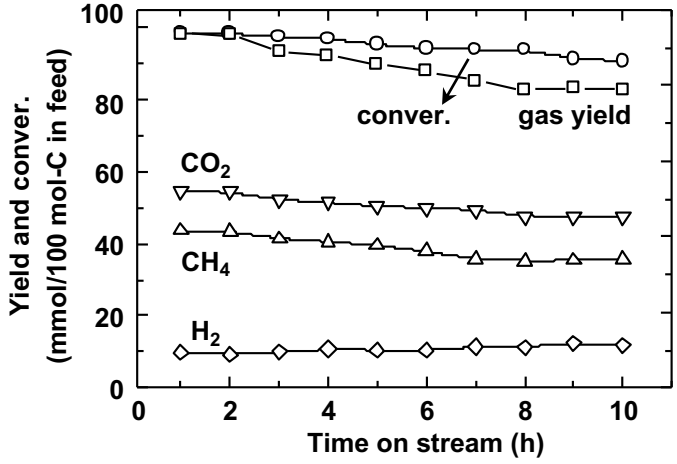

Figure 5.10. *Changes in carbon conversion and gas yield for CHTG of HT-OX-solubilized lignite with 10 h oxidation. Catalyst; Ru/C (16.2 wt% Ru), TOC; 2500 ppm, pH; 12.6, temperature; 350°C; pressure; 20 MPa, WHSV; 0.10 h^{-1}.*

5.3.3. Evaluation of overall process

Carbon and chemical energy balances were analyzed for the CHTG run over Ru/C with 16.2% Ru loading. **Table 5.3** summarizes the distributions of carbon and high heating value (HHV) over the ranges of products as averages for 0–10 h. The total HHV of CH_4, H_2 (from CHTG) and the insoluble matter (from HT-OX) accounts for 80% of the lignite HHV. The HHV recovery as CH_4/H_2 was 74%. Though not yet achieved, if CHTG gasifies the solubilized lignite completely without forming coke, the total HHV recovery will be 88%. However, further improvement of the catalyst performance is necessary for increasing the gas yield. Another important improvement is minimization of O_2 consumption in OX. Chemical introduction of oxygen into the lignite is effective for degradation and solubilization but associated with the loss of chemical energy and decrease in the CH_4/H_2 yields in the subsequent CHTG. Further improvements of the lignite dissolution process and CHTG are thus needed in future studies.

The efficiency achieved here is much higher than those by the existing gasification in sequence of steam-air or steam-O_2 gasification and CO/CO_2 methanation with H_2, 53–70% HHV. [45,46] In theory, the lignite can be converted into CH_4-rich syngas with an energy efficiency around 100% because of the thermal neutrality resulting from endothermic H_2/CO

Table 5.3. *Carbon and energy balances over the range from the lignite to CHTG products.*

feedstock or product	amount of C (mol)	energy (MJ-HHV)
Loy Yang lignite	100	43.9
HT-OX of lignite		
CO_2	8.9	0
insolubles (i) [a]	4.7	2.61
solubles	85.8	–
CHTG of solubles		
CH_4 (ii)	33.3	29.7
H_2 (iii) [b]	9.3	2.6
CO_2	43.3	0
unconverted	4.3	–
coke (by difference)	4.9	–
Total product HHV, (i)+(ii)+(iii)	–	34.9

[a] *Calculated by the Dulong's equation based on the elemental compositions that are available in* ***Table S5.2****.*
[b] *Unit of amount: mol-H_2/100 mol-lignite C.*

formation and its exothermic conversion into CH_4. However, the low-temperature CHTG needs materials 'dissolved in water' for their complete conversion. The present study thus proposes the sequence of oxidative degradation with O_2 in alkaline water, resulting in dissolution of lignite and CHTG of the dissolved lignite. The advantage over supercritical water gasification of solid coal is obviously high energy recovery at a moderate temperature. Matsumura [47] evaluated supercritical water gasification to CH_4 for a wet biomass at 600°C and 34.5 MPa and estimated the energy efficiency to be 65%, which was the highest value reported for supercritical water gasification. Though the yield of CH_4 and energy efficiency are not yet equivalent to the theoretical ones, the present study has demonstrated potential of the proposed sequential process and also shown works to be done in the future.

5.4. Conclusions

The present authors investigated the sequence of the lignite solubilization in alkaline water and CHTG of the solubilized matter and have demonstrated the followings within the ranges of experimental conditions.

(1) All the processes for solubilization, *i.e.*, HT at 250°C, OX at 100°C and with pressurized O_2, HT-OX and OX-HT, solubilize 84–95% portion of the lignite, leaving aliphatic-rich solids.

(2) HT converts a portion of aromatic carbon into CO_2, carbonyl/carboxyl carbon and aliphatic carbon, while OX converts that into CO_2 and carbonyl/carboxyl carbon.

(3) HT-OX depolymerizes the lignite most extensively, producing the solubilized lignite with number-average MM no greater than 770.

(4) Among the catalysts prepared, only the Ru/C catalysts effectively convert the solubilized lignite into CH_4, CO_2 and H_2.

(5) The Ru/C with 5.7 wt% Ru loading undergoes deactivation that is primarily brought about by the coke deposition onto the catalyst and its accumulation. The heavier portion of the solubilized lignite, of that MM ranges up to 5,000, is responsible for the significant coke deposition and resulting catalyst deactivation. The coke deposition also occurs from the lighter portion of the solubilized lignite but causing no significant catalyst deactivation.

(6) The Ru/C with 16.2 wt% Ru loading converts 97–98% of the solubilized lignite into gas with little or no coke formation. The catalyst deactivation occurs but very slowly for 10 h. The gas yield becomes near steady around 83%.

5.5. References

[1] Dudley B. BP statistical review of world energy. *BP Statistical Review of World Energy,* London, accessed June **2019**.

[2] Kruse A. Supercritical water gasification. *Biofuels, Bioproducts and Biorefining* **2008,** 2, 415–437.

[3] Kruse A., Dinjus E. Hot compressed water as reaction medium and reactant: Properties and synthesis reactions. *The Journal of Supercritical Fluids* **2007,** 39, 362–380.

[4] Kashimura N., Hayashi J-i., Chiba T. Degradation of a Victorian brown coal in sub-critical water. *Fuel* **2004,** 83, 353–358.

[5] Zheng Q., Morimoto M., Sato H., Takanohashi T. Molecular composition of extracts obtained by hydrothermal extraction of brown coal. *Fuel* **2015,** 159, 751–758.

[6] Modell M., Reid R. C., Amin S. I. Gasification process. U.S. Patent 4,113,446, **1978.**

[7] Yamaguchi D., Sanderson P. J., Lim S., Aye L. Supercritical water gasification of Victorian brown coal: Experimental characterisation. *International Journal of Hydrogen Energy* **2009,** 34, 3342–3350.

[8] Ge Z., Guo S., Guo L., Cao C., Su X., Jin H. Hydrogen production by non-catalytic partial oxidation of coal in supercritical water: Explore the way to complete gasification of lignite and bituminous coal. *International Journal of Hydrogen Energy* **2013,** 38, 12786–12794.

[9] Kumabe K., Nishimura Y., Kambara S., Moritomi H. Kinetic study of subcritical steam gasification of coal using calcium-based carbon dioxide sorbent. *Industrial & Engineering Chemistry Research* **2014,** 53, 2183–2188.

[10] Ge Z., Jin H., Guo L. Hydrogen production by catalytic gasification of coal in supercritical water with alkaline catalysts: Explore the way to complete gasification of coal. *International Journal of Hydrogen Energy* **2014,** 39, 19583–19592.

[11] Lan R., Jin H., Guo L., Ge Z., Guo S., Zhang X. Hydrogen production by catalytic gasification of coal in supercritical water. *Energy & Fuels* **2014,** 28, 6911–6917.

[12] Yu J., Lu X., Shi Y., Chen Q., Guan Q., Ning P., Tian S., Gu J. Catalytic gasification of lignite in supercritical water with Ru/CeO_2–ZrO_2. *International Journal of Hydrogen Energy* **2016,** 41, 4579–4591.

[13] Huber G. W., Shabaker J. W., Dumesic J. A. Raney Ni-Sn catalyst for H_2 production from biomass-derived hydrocarbons. *Science* **2003,** 300, 2075–2077.

[14] Elliott D. C., Phelps M., Sealock Jr L. J., Baker E. G. Chemical processing in high-pressure aqueous environments. 4. Continuous-flow reactor process development experiments for organics destruction. *Industrial & Engineering Chemistry Research* **1994,** 33, 566–574.

[15] Elliott D. C., Hart T. R., Neuenschwander G. G. Chemical processing in high-pressure aqueous environments. 8. Improved catalysts for hydrothermal gasification. *Industrial & Engineering Chemistry Research* **2006,** 45, 3776–3781.

[16] Nakagawa H., Namba A., Böhlmann M., Miura K. Hydrothermal dewatering of brown coal and catalytic hydrothermal gasification of the organic compounds dissolving in the water using a novel Ni/carbon catalyst. *Fuel* **2004,** 83, 719–725.

[17] Morimoto M., Nakagawa H., Miura K. Hydrothermal extraction and hydrothermal gasification process for brown coal conversion. *Fuel* **2008,** 87, 546–551.

[18] Hayashi J-i., Matsuo Y., Kusakabe K., Morooka S. Depolymerization of lower rank coals by low-temperature O_2 oxidation. *Energy & Fuels* **1997,** 11, 227–235.

[19] Wang W., Hou Y., Wu W., Niu M., Liu W. Production of benzene polycarboxylic acids from lignite by alkali-oxygen oxidation. *Industrial & Engineering Chemistry Research* **2012,** 51, 14994–15003.

[20] Li W., Hou Y., Yang F., Wu W. Production of benzene carboxylic acids and small-molecule fatty acids from lignite by two-stage alkali-oxygen oxidation. *Industrial & Engineering Chemistry Research* **2017,** 56, 1971–1978.

[21] Miller J., Evans L., Littlewolf A., Trudell D. Batch microreactor studies of lignin and lignin model compound depolymerization by bases in alcohol solvents. *Fuel* **1999,** 78, 1363–1366.

[22] Muangrat R., Onwudili J. A., Williams P. T. Influence of alkali catalysts on the production of hydrogen-rich gas from the hydrothermal gasification of food processing waste. *Applied Catalysis B: Environmental* **2010,** 100, 440–449.

[23] Elliott D. C., Sealock L. J. J., Baker E. G. Chemical processing in high-pressure aqueous environments. 3. Batch reactor process development experiments for organics destruction. *Industrial & Engineering Chemistry Research* **1994,** 33, 558–565.

[24] Onwudili J. A., Williams P. T. Hydrogen and methane selectivity during alkaline supercritical water gasification of biomass with ruthenium-alumina catalyst. *Applied Catalysis B: Environmental* **2013,** 132–133, 70–79.

[25] Davda R., Shabaker J., Huber G., Cortright R., Dumesic J. A. A review of catalytic issues and process conditions for renewable hydrogen and alkanes by aqueous-phase reforming of oxygenated hydrocarbons over supported metal catalysts. *Applied Catalysis B: Environmental* **2005,** 56, 171–186.

[26] Elliott D. C., Sealock Jr L. J., Baker E. G. Chemical processing in high-pressure aqueous environments. 2. Development of catalysts for gasification. *Industrial & Engineering Chemistry Research* **1993,** 32, 1542–1548.

[27] Ravenelle R. M., Copeland J. R., Kim W. G., Crittenden J. C., Sievers C. Structural changes of γ-Al_2O_3-supported catalysts in hot liquid water. *ACS Catalysis* **2011,** 1, 552–561.

[28] Muangrat R., Onwudili J. A., Williams P. T. Influence of NaOH, Ni/Al_2O_3 and Ni/SiO_2 catalysts on hydrogen production from the subcritical water gasification of model food waste compounds. *Applied Catalysis B: Environmental* **2010,** 100, 143–156.

[29] Kudo S., Hachiyama Y., Takashima Y., Tahara J., Idesh S., Norinaga K., Hayashi J-i. Catalytic hydrothermal reforming of lignin in aqueous alkaline medium. *Energy & Fuels* **2014,** 28, 76–85.

[30] Liu T. L., Cao J. P., Zhao X. Y., Wang J. X., Ren X. Y., Fan X., Zhao Y. P., Wei X. Y. *In situ* upgrading of Shengli lignite pyrolysis vapors over metal-loaded HZSM-5 catalyst. *Fuel Processing Technology* **2017,** 160, 19–26.

[31] Penninger J. Selectivity effects in aqueous supercritical fluid extraction of subbituminous coal. *Fuel* **1989,** 68, 983–989.

[32] Hayashi J-i., Aizawa S., Kumagai H., Chiba T. Evaluation of macromolecular structure of a brown coal by means of oxidative degradation in aqueous phase. *Energy & Fuels* **1999,** 13, 69–76.

[33] Liu P., Wang L., Zhou Y., Pan T., Lu X., Zhang D. Effect of hydrothermal treatment on the structure and pyrolysis product distribution of Xiaolongtan lignite. *Fuel* **2016,** 164, 110–118.

[34] Hayashi J-i., Chiba T. Quantitative description of oxidative degradation of brown coal in aqueous phase on the basis of Bethe Lattice statistics. *Energy & Fuels* **1999,** 13, 1230–1238.

[35] Kruse A., Dinjus E. Hydrogen from methane and supercritical water. *Angewandte Chemie International Edition* **2003,** 42, 909–911.

[36] Idesh S., Kudo S., Norinaga K., Hayashi J-i. Catalytic hydrothermal reforming of water-soluble organics from the pyrolysis of biomass using a Ni/carbon catalyst impregnated with Pt. *Energy & Fuels* **2012,** 26, 67–74.

[37] Chakinala A. G., Chinthaginjala J. K., Seshan K., van Swaaij W. P., Kersten S. R., Brilman D. W. Catalyst screening for the hydrothermal gasification of aqueous phase of bio-oil. *Catalysis Today* **2012,** 195, 83–92.

[38] Zhang L., Xu C. C., Champagne P. Activity and stability of a novel Ru modified Ni catalyst for hydrogen generation by supercritical water gasification of glucose. *Fuel* **2012,** 96, 541–545.

[39] Lee I. G., Ihm S. K. Catalytic gasification of glucose over Ni/activated charcoal in supercritical water. *Industrial & Engineering Chemistry Research* **2009,** 48, 1435–1442.

[40] Kawazoe K. Axial dispersion in packed bed wherein mass transfer between fluid and particle exists. *Kagaku Kogaku* **1968,** 32, 1122–1127.

[41] Davda R., Shabaker J., Huber G., Cortright R., Dumesic J. A. Aqueous-phase reforming of ethylene glycol on silica-supported metal catalysts. *Applied Catalysis B: Environmental* **2003,** 43, 13–26.

[42] Wambach J., Schubert M., Döbeli M., Vogel F. Characterization of a spent Ru/C catalyst after gasification of biomass in supercritical water. *CHIMIA* **2012,** 66, 706–711.

[43] Forzatti P., Lietti L. Catalyst deactivation. *Catalysis Today* **1999,** 52, 165–181.

[44] de Vlieger D. J. M., Lefferts L., Seshan K. Ru decorated carbon nanotubes – a promising catalyst for reforming bio-based acetic acid in the aqueous phase. *Green Chemistry* **2014,** 16, 864–874.

[45] Hayashi J-i., Kudo S., Kim H. S., Norinaga K., Matsuoka K., Hosokai S. Low-temperature gasification of biomass and lignite: Consideration of key thermochemical phenomena, rearrangement of reactions, and reactor configuration. *Energy & Fuels* **2014,** 28, 4–21.

[46] van der Meijden C. M., Veringa H. J., Rabou L. P. The production of synthetic natural gas (SNG): A comparison of three wood gasification systems for energy balance and overall efficiency. *Biomass and Bioenergy* **2010,** 34, 302–311.

[47] Matsumura Y. Evaluation of supercritical water gasification and biomethanation for wet biomass utilization in Japan. *Energy Conversion and Management* **2002,** 43, 1301–1310.

Supporting information

Table S5.1. *Distribution of different types of carbon for insoluble solid and F1, F2 and F3.*

carbon type	HT		HT-OX				OX-HT			
	insol.	F1	insol.	F1	F2	F3	insol.	F1	F2	F3
aliphatic	5.9	29.5	3.4	19.7	3.8	6.7	4.7	20.4	4.2	2.8
aromatic	3.6	48.7	1.6	20.9	7.0	18.2	2.0	29.8	7.9	5.0
C=O	0.4	6.3	0.3	4.0	4.5	0.9	0.3	3.9	3.8	2.2
total	9.9	84.4	5.3	44.7	15.3	25.8	7.0	54	15.8	10.0

HT, HT-OX and OX-HT correspond to R3, R8 and R9, respectively. The distribution was indicated on total carbon of the starting lignite. F1 and F2 for HT could not be analyzed due to their insufficient yields and resulting amounts. The carbon distributions of these fractions were then assumed to be the same as that of F3, which was the major product from R3. insol.; alkaline insolubles. C=O; carbonyl/carboxyl.

Table S5.2. *Ultimate analyses (wt.%, dry-ash-free basis) of insoluble solid, F1, F2 and F3.*

	HT				HT-OX				OX-HT			
	C	H	N	O	C	H	N	O	C	H	N	O
insol.	69.8	5.8	0.6	23.7	76.0	8.5	0.3	15.2	81.4	8.3	0.6	8.9
F1	67.1	5.0	0.6	26.8	65.3	4.7	0.7	29.3	66.0	4.9	0.8	28.4
F2	-	-	-	-	60.2	4.1	0.6	35.1	58.0	4.4	0.5	37.1
F3	-	-	-	-	32.2	2.7	0.2	64.9	27.1	2.4	0.3	70.2

HT, HT-OX and OX-HT correspond to R3, R8 and R9, respectively. F1 and F2 for HT are not analyzed due to their insufficient yields (and resulting amounts). insol.; alkaline insoluble matter. The distribution of F1, F2 and F3 in the solubilized lignite (R8) are 36.0, 25.6 and 38.4 wt%, respectively. The molecular formula of the solubilized lignite is thus estimated to be $C_{100}H_{86.8}O_{62.9}$ *for R8.*

CHAPTER 6

GENERAL CONCLUSIONS

Biomass is the only renewable source of energy and organic carbon that has the potential to reduce our overreliance on fossil fuels and mitigate environmental issues. Effective utilization of biomass in the current energy system, which is essential to the establishment of a circular, bio-based economy, necessitates the development of new technologies to overcome the limitations of the structural recalcitrance, low bulk density and high moisture content of the biomass. With this perspective, this thesis has been devoted to the combined hydrothermal and pyrolytic conversion of biomass, the implementation of which is expected to achieve a simple and selective production of light oil, clean biochar or/and fuel gas, with sufficiently high recoveries and relatively low temperatures.

In **Chapters 2 and 3** described the novel processes for the conversion of typical biowastes of modern biorefineries, that is, solid lignin and aqueous streams, respectively. A Japanese cedar lignin prepared by a *Klason* method, *i.e.*, hydrothermal treatment with concentrated sulfuric acid, was selectively converted to phenolic monomers and biochar by a particular type of pyrolysis free from external chemicals/catalysts. The pyrolysis enabled heavier portions of the bio-oil, that is, HO, to be sorbed by the parent lignin and then be repyrolyzed with the lignin. The feasibility of the process was successfully examined in a fix-bed reactor by repeating pyrolysis of HO-loaded lignin up to nine times at a peak temperature of 600°C. As a result, the biochar gained an increase in the production to a more or less extent with near-unchanged elemental composition, volatile matter content, and calorific value. Most importantly, the resultant liquid bio-oil is abundant in phenolic monomers with a molecular mass below 200, in particular, catechol, guaiacol and their derivates. The HO recycling pyrolysis can be technically feasible in industrial practice, such as, a countercurrent moving bed reactor, because the lignin has capabilities of HO capturing in terms of condensation and holding capacity and allows for neither discharge of HO from the system nor accumulation therein. Biomass-derived wastewaters, in general, possess hazardous properties such as corrosivity and high TOC. The conversion strategy that we proposed in **Chapter 3** applied the wastewater as not a by-product but instead a leaching agent to remove AAEMs from biomass and biochar. The leachate was then converted under subcritical conditions (350°C, 20 MPa) to a fuel gas rich in CH_4. An aqueous phase of bio-oil derived from the pyrolysis of rice straw was used as starting feedstock. The pH of the feedstock as low as 2.8 enabled a removal rate of K up to 95% from the biomass/char. The organic compounds were near completely gasified to mainly H_2, CH_4, and CO_2 and particularly, the

AAEMs solubilized in the solution suppressed the growth of Ru particles and thus the deactivation of Ru/C catalyst during CHTG. This proposed process is supposed to be applicable in many biorefineries that generate exhaust liquids. Another feature of the process is the recovery of inorganic mattes such as K and Na in their ionic forms, for recycling into cultivation. **Chapter 4** in-detail investigated once-through leaching and repeated leaching of char with pyrolytic aqueous phase. The leaching of AAEMs roughly follows pseudo-second order reaction kinetics. Repeated leaching of char with AP up to 18 times enables the internal recycling of the pyrolytic products.

In **Chapter 5**, application of CHTG to lignite-to-syngas conversion was investigated and discussed. Additional effort was devoted to achieving a high degree of dissolution of the lignite in an alkaline aqueous medium. A Victorian lignite was subjected to hydrothermal treatment in an aqueous solution of NaOH at 250°C and then oxidation with pressurized O_2 at 100°C. The sequential treatments solubilized 95% of the lignite on mass/carbon bases. The resulting solution was further converted by CHTG in a flow reactor at 350°C for 10 h, employing a Ru/C catalyst (16 wt% Ru). The initial carbon conversion to gas was as high as 98% while CH_4, CO_2 and H_2 were produced. The conversion gradually decreased due to coke deposition over the catalyst but was near steady around 83% at 8–10 h. The solubilized lignite consisted of compounds with molecular mass up to 5,000. The heavier portion (molecular mass > 1,000) was responsible for the coke formation and accumulation that caused the catalyst deactivation. Taking into account the dissolution and CHTG of the lignite, total higher heating value recovery of CH_4/H_2 and insoluble matter was 80%, much higher than those by gas-solid gasification operated at reaction temperatures well above 1000°C.

In conclusion, this work has presented several aspects of combined pyrolytic and hydrothermal conversion of biomass and lignite and it has shown that such technologies are potentially very effective. Nevertheless, it is also quite complex, since there are many aspects to be considered at the same time. Hydrothermal gasification actually needs much more scientific and technical work in order to be fully developed and applied to real scale. First, heterogeneous catalysts are necessary at low temperatures to allow effective gasification. However, continuous or semi-continuous studies with long periods online often show a significant decline in catalyst activity that is, in general, related to changes in the support and active metal (*e.g.*, leaching, loss of surface are by crystallite growth or sintering). Coking is a serious issue with biomass streams as is fixing of sulfate onto catalysts. The degradation

or oxidation of catalyst support is another key issue under hydrothermal conditions. More research works are needed to design and develop superior catalysts and supports to ensure long-term operations of a full-scale plant. Second, the detailed reactions pathways, mechanisms and kinetics are still unknown or not clear for hydrothermal processing owing to the complex of biomass and lignite.

ACKNOWLEDGEMENTS

Nothing is lost, nothing is created, everything is transformed. *Three years have passed since I came to this little city, covered with cherry blossoms, that looks as though it is covered with pink snow, invoking an unforgettable luxuriance in springtime. At the tail end of the Ph. D, I turn back to see what I have lost: a movie ticket, a weekend time with family or a deep-rooted memory? That is as it is. Yet, the life here, no matter how bitter or sweet it tastes, makes it up to me: a time of my own to forget, experience and remember, a night view of the illuminated Tokyo tower, said the prayers at Itsukushima Shinto Shrine, and, of course, felt every depressing and exciting moment with my apparatus.*

At this moment, I would like to express my sincere gratitude to Prof. Jun-ichiro Hayashi, my supervisor, for his great patience, intelligent and careful guidance, and constructive feedback for this research. His willingness to give kindness so generously and share the experience of life has been very much appreciated. I would also like to thank Associate prof. Shinji Kudo, who has been of great help with his feedback, discussions, and opinions and general guidance mostly related to experimental. I was greatly inspired by his rigorous and meticulous attitude. I am also grateful for the help given by Assistant prof. Shusaku Asano in both research and daily life.

Special thanks should be given to all of the lab members, especially Mrs. NaoKo Sudo, Ms. Asuka Mori, Ms. Yasuyo Hachiyama, Mr. Kentaro Shima, Mr. Jingxian Wang and Ms. Phatchada Santawaja, for their kind help and smile. Further thank for keeping the mood up in the laboratory with interesting and fun discussions.

Finally, I wish to thank my parents for their support and encouragement throughout this whole time. Also, I acknowledge the China Scholarship Council with financial support for my study in Japan.

Liu Tianlong

Chikushi Campus

June 16, 2020